**UNIVERSIDAD COMPLUTENSE DE MADRID**
FACULTAD DE CIENCIAS FÍSICAS
Departamento de Física de la Tierra y Astrofísica


# TESIS DOCTORAL

# Modelling glacial abrupt climate changes and their impacts on the Northern Hemisphere glacial ice sheets

# Modelización de los cambios climáticos abruptos glaciales y de su impacto en los mantos de hielo glaciales del hemisferio norte

MEMORIA PARA OPTAR AL GRADO DE DOCTOR

PRESENTADA POR

**Rubén Banderas Carreño**

Directores

**Mª Luisa Montoya Redondo**
**Jorge Álvarez Solas**

Madrid
Ed. electrónica 2019

# Modelling glacial abrupt climate changes and their impacts on the Northern Hemisphere glacial ice sheets

# Modelización de los cambios climáticos abruptos glaciales y de su impacto en los mantos de hielo glaciales del hemisferio norte

*Memoria que presenta*
Rubén Banderas Carreño
*para optar al grado de*
Doctor en Ciencias Físicas
*en el año* 2019


*Directores:*
Dra. Mª Luisa Montoya Redondo
Dr. Jorge Álvarez Solas

Departamento de Física de la Tierra y Astrofísica
Facultad de Ciencias Físicas
Universidad Complutense de Madrid

Katsushika Hokusai, *Under the Wave off Kanagawa* from the series *Thirty-six Views of Mount Fuji*, Edo period (1615-1868), ca. 1831-33.

*Little snail, inch by inch, climb Mount Fuji.*
The Haiku of Kobayashi Issa (1763-1827).

# Contents

# Acknowledgements

This thesis has been conducted during my stay as a PhD student at the Faculty of Physics of the Universidad Complutense (UCM). This work has been supported by a predoctoral fellowship of the UCM and partially funded by the Spanish Ministries for Environment (MARM), for Education, Culture, and Sports (MECD), for Science and Innovation (MICINN), and for Science and Innovation (MINECO) under projects 200800050084028, CGL08-06558-C02-01, CGL2011-29672-C02-01, and CGL2014-59384-R. Simulations included in this Thesis were performed at the Spanish Environmental Research Centre (CIEMAT) and at EOLO, the High Performance Computing Cluster (HPC) of the International Campus of Excellence of Moncloa, funded by MECD and MICINN.

Several people deserve recognition for their contribution to the completion of this thesis. Marisa, thank you for guiding me through this fruitful experience. The value of your patience and support throughout these years is impossible to overestimate. Jorge, you were also instrumental in helping me to reach my goals. Thank you for this amazing opportunity to learn from you. I will always be immensely grateful to both of you.

The completion of this thesis would not have been possible without your strong support, Alex. Your advice were not only essential for my work, but also for my personal scientific development and I will always be immensely grateful to you. I was very lucky for having you by my side.

I would like to thank Kerim Nisancioglu and Camille Li for making me feel at home when I was far away during my reserach stay in Norway. Thank you for helping me to expand my horizons as a scientist. This was a beatiful experience that enriched my life and work.

A heartfelt thanks goes to all of my colleagues at the PalMA group. You made work particularly enjoyable at the lab. Fidel, Elena, Jorge Navarro, Pedro and

Pablo, you were always willing to help and your advice contributed to improve my understanding of science. A warm thank you goes to my friends Laura, Etor and Germán. If I had to start my PhD again I would not do it without you. I will always have you in my mind.

Finally, my greatest gratiude goes to family and to you, Lorena. None of this would have come to be without your support and constant encouragement.

# Summary


## Motivation

During the last glacial period (LGP), the North Atlantic region experienced a series of abrupt climate changes known as Dansgaard-Oeschger (D/O) events which comprised rapid temperature excursions from cold to relatively mild climatic conditions and widespread impacts recurring on millennial time scales. The prevailing paradigm to explain these glacial abrupt climate changes involves reorganisations of the Atlantic meridional overturning circulation (AMOC). Cold climatic conditions in the North Atlantic are thought to be associated to a weak AMOC regime in which the heat transport towards the North Atlantic is strongly diminished, while relatively warm climatic conditions are thought to result from a reinvigoration of this northward heat transport. Freshwater fluxes have been commonly invoked to be responsible for perturbing the AMOC stability, thus promoting these abrupt climate changes. However, there is still a high degree of uncertainty regarding the origin and magnitude of these freshwater fluxes, a factor that challenges the implication of this forcing in glacial abrupt climate changes. Thus, the exact mechanisms that led to glacial abrupt climate changes are unknown. In addition, their impacts on the surrounding ice sheets have not been investigated in depth. The occurrence of abrupt climate events appears to be related to glacial climatic conditions, with global ice volumes varying at intermediate levels. This implies the discharge of meltwater from the ice sheets surrounding the Nordic Seas on millennial time scales. Investigating their contribution is important to constrain freshwater inputs into the North Atlantic ocean in order to improve our understanding of the driving mechanisms of glacial abrupt climate changes.

## Aim of this study and main results

The goal of this thesis is double: on one hand, to investigate the origin of glacial abrupt climate changes; on the other, to assess their impact on the Northern Hemisphere (NH) ice sheets. The first part of this thesis focuses on the first question. A new mechanism consistent with proxy records is proposed in order to explain glacial D/O variability and its global climatic imprint. Paleorecords indicate that $CO_2$ variations during glacial abrupt climate changes were preceded by significant increases of Southern Ocean (SO) upwelling caused by an intensification and/or shift of surface winds over that region. Climate model simulations in combination with proxy records reveal that periods of halted or reduced North Atlantic Deep Water (NADW) formation result in warming of the SO through the so called bipolar seesaw effect, leading to a southward shift of the Intertropical convergence zone (ITCZ) together with a reorganisation of SO winds, and thereby enhanced upwelling and atmospheric $CO_2$ concentration. Here, we investigate, from a modelling perspective, the role of these changes in order to assess whether $CO_2$ variations and SO winds could be part of an internal oscillation which could eventually trigger glacial abrupt climate changes through AMOC reorganisations. Our results indicate that gradual variations of atmospheric $CO_2$ levels and/or wind-stress in the SO are able to trigger millennial-scale climatic fluctuations in response to changes in the AMOC strength. The simulated temperature evolution over Greenland and Antarctica satisfactorily reproduce the phasing and timing of D/O and Antarctic millennial-scale climatic events.

The second part of the thesis focuses on the second question above, i.e., the importance of NH ice sheets in modulating the phasing and timing of millennial-scale climate variability. An efficient way to simulate the paleo-evolution of ice sheets is to force an ice-sheet model offline using an approach in which the temperature and precipitation anomalies relative to the present are calculated by combining a simulated glacial-interglacial climatic anomaly field, interpolated through an index derived from the ice-core record, with present-day climatologies. However, an important drawback of this approach is that it clearly misrepresents climate variability at millennial timescales because the spatial glacial-interglacial anomaly field is associated with orbital climatic variations, while it is scaled following the characteristic time evolution of the index, which includes both orbital and millennial-scale climate variability. Here, a new offline forcing method is developed to investigate the paleo-evolution of the NH ice sheets on millennial time scales. This approach provides a more realistic representation of orbital and millennial-scale climate variability and improves the transient forcing of ice sheets during the last glacial period. This method is specifically applied to investigate the impact of oceanic variations in the evolution of the Eurasian ice sheet (EIS) throughout the last glacial period. Together with the Greenland Ice

Sheet (GrIS), this was the ice sheet that most likely suffered the largest impacts associated with abrupt glacial climate changes. Our results show that the response of the EIS comprises enhanced iceberg discharges occurring in phase with Greenland interstadials. Separating the atmospheric and oceanic effects confirms the major role of the ocean in controlling the dynamics of the EIS on millennial time scales. Together with previous work, our results provide a consistent explanation for the timing of the responses of all NH ice sheets to glacial abrupt climate changes.

## Publications

The main results of this thesis have been published in the following articles:

- Banderas, R., J. Alvarez-Solas, and M. Montoya, 2012: Role of $CO_2$ and Southern Ocean winds in glacial abrupt climate change, *Clim. Past*, 8, 1011–1021,http://doi:10.5194/cp-8-1011-2012.
- Banderas, R., J. Alvarez-Solas, A. Robinson, and M. Montoya, 2015: An interhemispheric mechanism for glacial abrupt climate change. *Clim. Dyn.*, 44, 2897–2908, https://doi:10.1007/s00382-014-2211-8.
- Banderas, R., J. Alvarez-Solas, A. Robinson, and M. Montoya, 2018: A new approach for simulating the paleo evolution of the Northern Hemisphere ice sheets. *Geosci. Model Dev.*, https://doi.org/10.5194/gmd-2017-158.
- Alvarez-Solas, J. R. Banderas, A. Robinson, and M. Montoya, 2018: Oceanic forcing of the Eurasian Ice Sheet on millennial time scales during the Last Glacial Period *Clim. Past*, submitted; online review: https://doi.org/10.5194/cp-2018-89.

# Resumen


## Motivación

Durante el último periodo glacial, la región del Atlántico Norte experimentó una serie de cambios climáticos abruptos conocidos como eventos Dansgaard-Oeschger (D/O), rápidos incrementos de temperatura con impactos climáticos generalizados que se repitieron en escalas de tiempo milenarias. El paradigma actual contempla que estos cambios climáticos abruptos se produjeron por la reorganización de la circulación meridiana del océano Atlántico (AMOC, del inglés Atlantic meridional overturning circulation). Se cree que las condiciones climáticas frías en el Atlántico Norte estuvieron asociadas a un modo de circulación oceánica débil incapaz de transportar grandes cantidades de calor hacia el norte, mientras que las condiciones climáticas relativamente cálidas pudieron estar asociadas a la revitalización de este transporte meridiano de calor. Con frecuencia se ha considerado que los flujos de agua dulce procedentes del deshielo de los mantos polares pudieron haber sido los responsables de perturbar la estabilidad de la AMOC, provocando así las transiciones climáticas abruptas características del último período glacial. Sin embargo, todavía existe un alto grado de incertidumbre sobre el origen y la magnitud de dichos flujos, con lo que la implicación de este forzamiento en los cambios climáticos abruptos del último período glacial no está totalmente clara. Por lo tanto, aún se desconocen con exactitud los procesos que desencadenaron dichos cambios climáticos abruptos. Además, los impactos que provocaron sobre los mantos de hielo circundantes no se han investigado en profundidad. La ocurrencia de eventos climáticos abruptos parece estar ligada a las épocas en las que los mantos de hielo polares presentaron unas dimensiones intermedias. En términos de volumen de hielo, la variabilidad milenaria de los mantos polares conlleva la descarga de agua dulce hacia los mares nórdicos en

estas escalas de tiempo. Profundizar en estos aspectos es importante para cuantificar los aportes de agua dulce al Océano Atlántico Norte con el fin de mejorar nuestra comprensión de los mecanismos impulsores de los cambios climáticos abruptos del último periodo glacial.

## Objetivos y resultados principales

El objetivo de esta tesis es doble: por un lado, investigar el origen de los cambios climáticos abruptos del último periodo glacial; por otro, evaluar su impacto en los mantos de hielo del hemisferio norte. La primera parte de la tesis se centra en la primera pregunta. Aquí, se propone un nuevo mecanismo coherente con los registros paleoclimáticos a fin de explicar la variabilidad asociada a los eventos D/O y su huella climática global. Los registros indican que las variaciones de $CO_2$ acontecidas durante los cambios climáticos abruptos del último periodo glacial fueron precedidas por episodios de afloramiento intenso en el Océano Austral causados, a su vez, por la intensificación y/o el desplazamiento de los vientos superficiales sobre esa región. Las simulaciones llevadas a cabo con modelos numéricos en combinación con los registros paleoclimáticos revelan que los periodos de reducida formación de agua profunda del Atlántico Norte provocan el calentamiento del Océano Austral a través del llamado efecto del balancín bipolar, lo que conduciría a un desplazamiento hacia el sur de la zona de convergencia intertropical junto con una reorganización de los vientos del Océano Austral y, por lo tanto, a un aumento del afloramiento y de la concentración de $CO_2$ en la atmósfera. En este estudio se ha investigado, a través de la modelización numérica, el papel de estos cambios para evaluar si las variaciones de $CO_2$ y los vientos del Océano Austral podrían formar parte de una oscilación interna que eventualmente desencadenaría la aparición de los cambios climáticos abruptos mediante reorganizaciones de la AMOC. Nuestros resultados indican que las variaciones graduales de los niveles de $CO_2$ atmosférico y/o la cizalladura del viento en el Océano Austral son capaces de desencadenar fluctuaciones climáticas a escala milenaria en respuesta a los cambios en la intensidad de la AMOC. La evolución de la temperatura simulada sobre Groenlandia y la Antártida reproduce satisfactoriamente la señal climática de los eventos observados en los registros paleoclimáticos en estas regiones.

La segunda parte de la tesis se centra en la importancia de los mantos de hielo del hemisferio norte para modular la variabilidad climática del último periodo glacial a escala milenaria. Una forma eficaz de simular la evolución pasada de los mantos de hielo es forzar un modelo de mantos de hielo por medio de anomalías de los campos de temperatura y precipitación relativas al presente que se calculan combinando un campo simulado de anomalías climáticas glaciales-interglaciales, interpoladas a través de un índice derivado de los registros de testigos de hielo, con

las climatologías actuales. Sin embargo, un inconveniente importante de este enfoque es que, claramente, no representa adecuadamente la variabilidad climática a escalas de tiempo milenarias porque el campo de anomalías espaciales glaciales-interglaciales está asociado con variaciones climáticas orbitales, pero se incorpora siguiendo la evolución temporal característica del índice, que incluye tanto la variabilidad climática orbital como la de escala milenaria. Para solucionar esto se ha desarrollado un nuevo método de forzamiento para investigar la evolución pasada de los mantos de hielo del hemisferio norte en escalas de tiempo milenarias. Este enfoque proporciona una representación más realista de la variabilidad climática a escala orbital y milenaria y mejora el forzamiento transitorio de los mantos de hielo durante el último periodo glacial. Este método se aplica específicamente para investigar el impacto de las variaciones oceánicas en la evolución del manto de hielo euroasiático (EIS, del inglés, Eurasian ice sheet) a lo largo del último periodo glacial. Junto con Groenlandia, éste es el manto de hielo que probablemente sufrió los mayores impactos asociados a los cambios climáticos abruptos glaciales. Nuestros resultados muestran que la respuesta del EIS incluye la mejora de las descargas de iceberg que se producen en fase con los interestadiales de Groenlandia. La separación de los efectos atmosféricos y oceánicos confirma el importante papel que desempeña el océano en el control de la dinámica del EIS a escala milenaria. Junto con trabajos previos, nuestros resultados proporcionan una explicación consistente para el tiempo de las respuestas de todos los mantos de hielo del hemisferio norte a los cambios climáticos abruptos glaciales.

## Publicaciones

Los resultados principales de esta tesis han sido publicados en los siguientes artículos:

- Banderas, R., J. Alvarez-Solas, and M. Montoya, 2012: Role of $CO_2$ and Southern Ocean winds in glacial abrupt climate change, *Clim. Past*, 8, 1011–1021,http://doi:10.5194/cp-8-1011-2012.
- Banderas, R., J. Alvarez-Solas, A. Robinson, and M. Montoya, 2015: An interhemispheric mechanism for glacial abrupt climate change. *Clim. Dyn.*, 44, 2897–2908, https://doi:10.1007/s00382-014-2211-8.
- Banderas, R., J. Alvarez-Solas, A. Robinson, and M. Montoya, 2018: A new approach for simulating the paleo evolution of the Northern Hemisphere ice sheets. *Geosci. Model Dev.*, https://doi.org/10.5194/gmd-2017-158.
- Alvarez-Solas, J. R. Banderas, A. Robinson, and M. Montoya, 2018: Oceanic forcing of the Eurasian Ice Sheet on millennial time scales during the Last Glacial Period *Clim. Past*, submitted; online review: https://doi.org/10.5194/cp-2018-89.

# 1

# Introduction

This chapter introduces the background, motivation and scientific questions that are at the core of this thesis. The first part of the chapter reviews the history of glacial abrupt climate changes from their discovery in Greenland ice-core records to their implication in modulating the climate of the last glacial period. The imprints of glacial abrupt climate changes on the global climate, the paradigm to explain glacial abrupt climate changes, and the efforts in numerical modelling to improve our understanding on their underlying mechanisms are summarised. The second part of the chapter is structured following the four main scientific questions that motivate this thesis. Finally, a general overview of the publications included in this thesis is presented.

## 1.1 Background

### 1.1.1 Abrupt climate changes during the last glacial period: evidence from proxies

The climate of the last glacial period (LGP), ca. 110-10 kyr Before Present (BP), was characterised by the existence of remarkable abrupt changes that deeply contrast with the more stable climate observed during the Holocene (ca. 10-0 kyr BP). The analysis of oxygen isotopes from Greenland ice-core records has played a key role to reconstruct the signal of past climates. In particular, the Greenland Ice Core Project (GRIP) and the Greenland Ice Sheet Project 2 (GISP2) have revealed the existence of about 25 rapid fluctuations in the $\delta^{18}$O record during the past 120 kyr (Dansgaard et al., 1984; Grootes et al., 1993), referred to as Dansgaard-Oeschger (D/O) events (Figure 1.1). These are interpreted as abrupt temperature transitions which result in alternating phases of cold (stadial) and

relatively warm (interstadial) climatic conditions over Greenland during the LGP (Dansgaard et al., 1993). Subsequent high-resolution studies have indicated that the time evolution of a single D/O event is characterised by a rapid warming of up to 16°C (Lang et al., 1999; Huber et al., 2006; Kindler et al., 2014) from stadial to interstadial conditions which takes place within decades (Steffensen et al., 2008). Stadials and interstadials both vary in duration from centuries to a few millennia, with surface air temperatures gradually decreasing before an abrupt return to stadial conditions terminates the interstadial phase. The recurrence time of D/O events is, with decreasing probabilities, of about 1500, 3000 and 4500 years (Bond et al., 1997; Alley et al., 2001; Schulz, 2002). Similar research projects have confirmed that the asymmetric signal of D/O events can also be identified in other Greenland ice-core records (e.g. Johnsen et al., 2001; NGRIP members, 2004). In addition to D/O events, a second kind of glacial abrupt climate event is identified in marine sediment cores in the North Atlantic (Hemming, 2004). Six of the temperature minima in Greenland were coeval with unusual amounts of ice rafted debris (IRD) originating primarily from the areas around Hudson Bay (Bond et al., 1992), and interpreted as massive iceberg discharges (Bond and Lotti, 1995), or Heinrich events (HEs).

The climatic imprint of both types of glacial abrupt climate changes is widespreadly recorded throughout the whole globe during the LGP (Voelker and Workshop Participants, 2002). In the North Atlantic, a wealth of proxy records, including abundances in planktonic foraminifera, $\delta^{18}$O or alkenones, indicates rapid sea surface temperatures (SSTs) fluctuations as well as variations in sea-ice cover extent (Hoff et al., 2016) that closely resemble those registered in Greenland ice-core records (Bond et al., 1993; Dickson et al., 2008; Rasmussen et al., 2016).

Their impact can also be identified further south, at mid-latitudes. Marine records from the subtropical North Atlantic (Sachs and Lehman, 1999), from the Iberian margin (Shackleton et al., 2000; Salgueiro et al., 2010), and from the western sector of the Mediterranean sea (Cacho et al., 1999; Martrat et al., 2004, 2007) among others, feature SSTs fluctuations following the stadial-interstadial pattern but at lower intensities and rates of change than in the D/O events during MIS 3. Similar results are found in the North Eastern Pacific (Hendy and Kennett, 2000). Terrestrial records evidence rapid climate changes coinciding with the characteristic pattern of D/O events in western Europe (Genty et al., 2003). Furthermore, the evolution of $\delta^{18}$O values of Asian cave stalagmites, interpreted as a proxy for precipitation, reflects a strong similarity with the Greenland $\delta^{18}$O ice core record during the last glacial period (Wang et al., 2001). This suggests that East Asian Monsoon intensity varied in concert with Greenland surface air temperature (SAT) during this time.

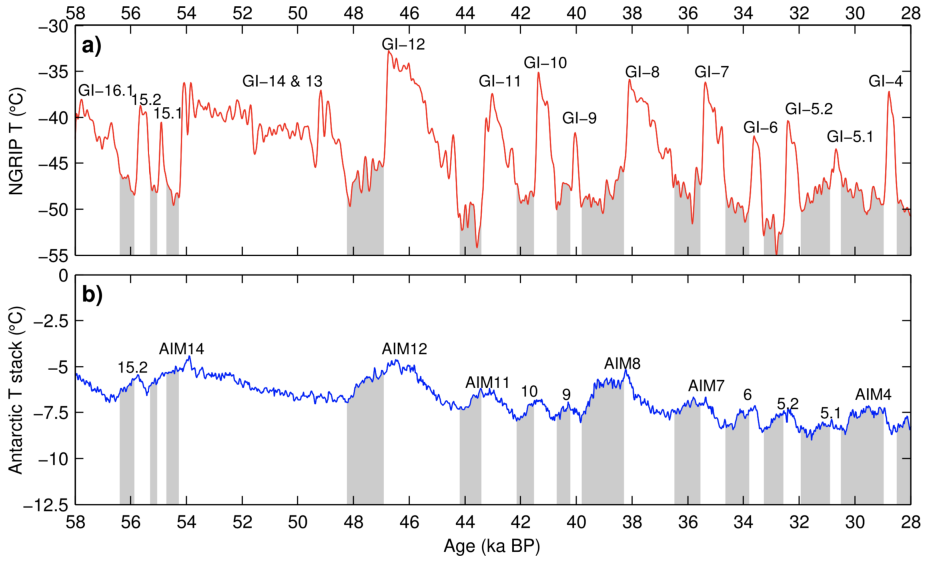


Fig. 1.1: Temperature reconstructions from Greenland and Antarctic ice cores spanning Marine Isotope Stage 3. a) North Greenland Ice Core Project (NGRIP) temperature reconstruction based on $\delta^1$5N and $\delta^1$8O records (NGRIP members, 2004; Kindler et al., 2014). b) Antarctic temperature stack based on stacked $\delta^1$8O and $\delta$D records from six Antarctic ice cores: EPICA Dome C, EPICA Dronning Maud Land (EDML), Vostok, Talos Dome, and Dome Fuji as published in Parrenin et al. (2013), to which data from the WAIS Divide Core have been added (Cuffey et al., 2016) (from: Pedro et al. 2018).

In the Tropics, Northern Hemisphere (NH) climate changes are also found to be in phase with Greenland temperature shifts, with increasing precipitation values coinciding with high latitude warming (Peterson et al., 2000; Peterson and Haug, 2006). On the contrary, Southern Hemisphere (SH) tropical precipitation variability evidences an anti-phase relationship with respect to the signal registered in Asian cave stalagmites, with relatively dry episodes in southern Brazil (Wang et al., 2007) and in western Amazonia (Mosblech et al., 2012) coinciding with Greenland interstadials. This interhemispheric asymmetry observed for tropical precipitation is consistent with a shift in the mean position of the intertropical convergence zone (ITCZ) toward the warmer hemisphere: during interstadials the ITCZ migrates northward leading to increased precipitation in the northern sector of the tropical belt and decreased precipitation in its southern sector; as a result, during interstadials relatively dry episodes prevail in its southern margin. D/O type climate variability has also been reported in other

low-latitude remote locations such as in the Arabian Sea (Schulz et al., 1998) and in the Western Equatorial Pacific (Stott et al., 2002).

In the high latitudes of the SH, $\delta^{18}O$ values of Antarctic ice-core records have revealed the existence of a more gradual and symmetric pattern of climate change over Antarctica than that registered in Greenland ice cores (Petit et al., 1999; Watanabe et al., 2003; EPICA-Project, 2004). In terms of temperature, this pattern consists of gradual variations of up to 3°C amplitude termed Antarctic Isotope Maxima (AIM) that recurred during the LGP on millennial time scales (EPICA-Project, 2006; Stenni et al., 2011; Parrenin et al., 2013; WAIS Divide Project Members, 2015). Synchronisation of Greenland and Antarctic ice cores using well-mixed gases as stratigraphic markers, including methane and the isotopic composition of trapped $O_2$ has confirmed the one to one correspondence that exists between D/O and AIM events consisting in a systematic relationship in which Antarctica gradually warms during Greenland stadials and gradually cools during Greenland interstadials (Barbante et al., 2006; Bender et al., 1994; Blunier and Brook, 2001; Brook et al., 2005; EPICA-Project, 2006; Pedro et al., 2011; WAIS Divide Project Members, 2015). High-resolution ice-core records show that, in general, the onset of the gradual Antarctic warming leads by several centuries the abrupt transition into the Greenland interstadial phase which, in turn, precedes the AIM cooling interval by 200 yr (WAIS Divide Project Members, 2015). A similar time lag is observed during the subsequent rapid transition into stadial conditions over Greenland which precedes the termination of the AIM event. Paleorecords have further shown that the characteristic signal of the Antarctic climate may have been globally pervasive during the last glacial period (Altabet et al., 2002; Lea et al., 2006; Barker and Knorr, 2007; Dubois et al., 2011). In particular, glacial atmospheric $CO_2$ concentration closely follows temperatures reconstructed from Antarctic ice-core records (Indermühle et al., 2000; Siegenthaler et al., 2005; Ahn and Brook, 2008; Bereiter et al., 2012; Ahn et al., 2012; Ahn and Brook, 2014) thus suggesting a potential connection between regional changes around Antarctica and global climate.

### 1.1.2 The prevailing paradigm to explain glacial abrupt climate changes

The widespread impact of glacial abrupt climate changes points to a global process involving a strong connection between the NH and the SH that can explain the characteristic timing and phasing of the responses in each hemisphere. Since the 80s attention has turned to the ocean and, in particular, to the Atlantic meridional overturning circulation (AMOC), in part because of its strong control of cross-equatorial heat transport.

The AMOC consists of warm waters flowing northward at surface of the Atlantic Ocean, sinking in the North Atlantic through deep water formation processes, and deep currents that flow southward, mixing with intermediate-depth waters before returning to the surface either through wind-driven isopycnal upwelling in the SO (Toggweiler and Samuels, 1995a; Munk and Wunsch, 1998; Marshall and Speer, 2012) or through diapycnal diffusion in the Indo-Pacific basins (Talley, 2013) (Figure 1.2). This circulation system is split into two overturning cells: a northern upper cell associated with North Atlantic Deep Water (NADW) formation and Northern Source Waters (NSW) and a deep southern cell associated with Antarctic Bottom Water (AABW) formation, hence Southern Source Waters (SSW). Its mean transport roughly ranges between 15-20 Sv around 25°N (Ganachaud and Wunsch, 2002; Lumpkin and Speer, 2007; McCarthy et al., 2015a). This warm northward surface flow, together with the deep southward return flow of the AMOC, result in a net northward heat transport at all latitudes in the Atlantic basin, with a maximum value at 24°N of ca. $1.2\times10^{15}$ W according both to direct observational and indirect estimates based on atmospheric reanalysis and top-of-atmosphere radiation data (Ganachaud and Wunsch, 2003; McCarthy et al., 2015a; Trenberth and Caron, 2001; Trenberth and Fasullo, 2018). The AMOC thus plays a pivotal role in modulating the Earth's climate due to the strong control that it exerts in the distribution of water masses and, in particular, in the transport of heat across the Atlantic Ocean (Kuhlbrodt et al., 2007; Buckley and Marshall, 2016, and references therein). Northward cross-equatorial Atlantic heat transport sets the mean position of the ITCZ (Marshall et al., 2014). Although its role for northwestern European climate is a matter of discussion (Seager et al., 2002; Seager and Battisti, 2006) ocean heat transport convergence is thought to control the sea-ice extension in the Arctic. At 25°N, the AMOC variability explains more than 90% of the estimated Atlantic northward heat transport variability (Johns et al., 2011). Variations in the AMOC strength at decadal and longer timescales are thought to imprint on the European climate (Palter, 2015; Yamamoto et al., 2015). The AMOC is believed to be the driver of the Atlantic Multidecadal Variability (AMV) by controlling the subpolar gyre heat content. This has been shown in a number of modelling studies (e.g. Delworth and Mann, 2000) and using indirect observations (Gulev et al., 2013; McCarthy et al., 2015b), since direct AMOC observations of sufficient length do not exist to rigorously prove the link (McCarthy et al., 2017).

The idea that reorganisations of the AMOC could be the mechanism underlying glacial abrupt climate changes was proposed already in the 80s by Broecker et al. (1985). The original idea was that glacial abrupt climate changes were understood as transitions between two states, one with a strong AMOC similar to that in the present-day, and one with a shut-down AMOC. This idea evolved

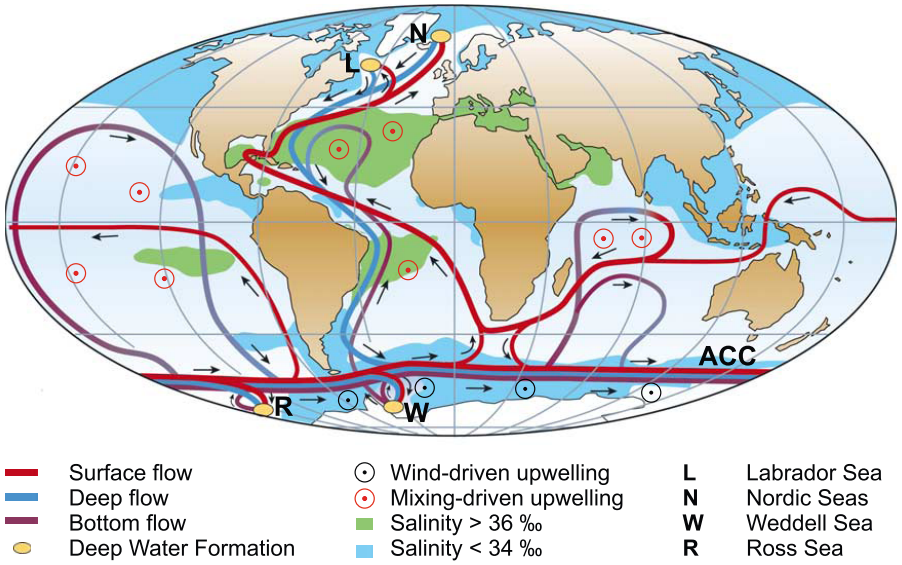


Fig. 1.2: Simplified sketch of the global overturning circulation system. In the Atlantic, warm and saline waters flow northward all the way from the Southern Ocean into the Labrador and Nordic Seas. By contrast, there is no deepwater formation in the North Pacific and its surface waters are fresher. Wind-driven upwelling takes place along the Antarctic Circumpolar Current (ACC) (from: Kuhlbrodt et al. 2007).

in time thanks to evidence both from proxy data and models (section 1.1.4). The prevailing paradigm is that stadials are associated with a weak mode of the AMOC, and therefore with a relatively weak northward transport of heat in the Atlantic Ocean; interstadials represent an invigoration of this northward heat transport; HEs in turn are associated with a practical collapse of NADW, or off model (see the reviews by Alley et al. (1999b); Clark et al. (2002); Alley (2007); Rahmstorf (2002); Lynch-Stieglitz (2017)). Perturbations of the AMOC and thus the cross-equatorial heat transport result in opposite temperature effects on both hemispheres (Crowley, 1992; Stocker, 1998). The slower Antarctic time response as compared to the fast Greenland temperature changes would be explained by damping and integration of the temperature anomalies by a large heat reservoir, commonly assumed to be the Southern Ocean (Stocker and Johnsen, 2003). This is referred to as the thermal ocean bipolar seesaw hypothesis.

### 1.1.3 Evidence for reorganisations of the Atlantic Ocean circulation associated to glacial abrupt climate changes

Evidence for variability of the glacial AMOC is based on changes in the properties of subsurface water masses (water-mass proxies) and in the strength (circulation proxies) of the deep flow. The evidence is most clear for HEs and for the deglaciation and less so, but increasingly gradually emerging, for D/O events (e.g. Lynch-Stieglitz, 2017). We start by reviewing the available proxies for changes in the AMOC and then the specific evidence from these proxies throughout the LGP, focusing mainly on their possible fluctuations in relation with glacial abrupt climate changes.

Several proxies in marine sediments reflect the origin of past oceanic water masses. Carbon isotopes of benthic foraminifera preserved in marine sediment cores have been shown to reflect the origin of past oceanic water masses (e.g. Ravelo and Hillaire-Marcel, 2007). In particular, the relative deviation of $^{13}$C to $^{12}$C values ($\delta^{13}$C) from a standard sample ratio can be used to constrain the relative contribution of NSW and SSW to the water-mass composition of the AMOC during glacial abrupt climate changes (e.g. Curry and Oppo, 1997; Shackleton et al., 2000). The presence of NSW in the South Atlantic is evidenced by anomalously high $\delta^{13}$C while SSW values are low as a result of a high sequestration in organic matter of respired $^{12}$C associated with high biological productivity (Lynch-Stieglitz et al., 2007). Similarly, Cd/Ca ratios can be used to reconstruct past changes in oceanic water masses (Marchitto and Broecker, 2006), with high ratios being generally related to SSW and low ratios to NSW (e.g. Lynch-Stieglitz, 2017). Because Cd is taken up by organisms at the ocean surface and released at depth during respiration, depleted Cd/Ca ratios are interpreted as shoaling of low-nutrient deep waters. Changes in the origin of water masses can also be traced using neodymium isotopes (e.g. Goldstein and Hemming, 2003). The dominant source of Neodymium (Nd) isotopes to the oceans is the continental weathering being the resulting $^{143}$Nd/$^{144}$Nd ratio ($\epsilon$Nd) of the eroded terrigenous material eventually recorded in marine sediments and foraminifera shells (Goldstein and Hemming, 2003). Because the signature of $\epsilon$Nd is heterogeneous across the continents, $\epsilon$Nd values are thought to reflect those of the source regions with a significantly less radiogenic (lower) $\epsilon$Nd signature of NSW as compared to that of SSW. Finally, to the extent that these are not affected by enhanced dilution by terrigenous sediments, the concentrations of carbonate ions in the deep Atlantic can also be interpreted as a measure of the relative proportion of NSW and SSW.

Circulation proxies include the terrigenous grain size as a measure of the energy in near-bottom flows, with large grains associated with energetic flow and smaller grains reflecting weak near-bottom currents (McCave and Hall, 2006). Also, because magnetic minerals mainly originate from one common source area,

the Nordic basaltic region, changes in the magnetic mineral content in sediment cores are interpreted as changes in the efficiency transport of magnetic particles by deep currents from the source to deposition site.

Finally, the $^{231}Pa/^{230}Th$ isotope ratio is generally interpreted as an indicator of the overall strength of the AMOC (Gherardi et al., 2009). $^{231}Pa$ and $^{230}Th$ are produced at a constant rate ratio of 0.093 from the radioactive decay of dissolved uranium in the ocean and scavenged by particles in the water column before being buried on the seafloor. However, $^{230}Th$ has a shorter residence time in the water column than $^{231}Pa$, which is thus more prone to be exported by the AMOC. Therefore, reduced $^{231}Pa$ export from the North Atlantic translates into higher sedimentary $^{231}Pa/^{230}Th$, a result which can be interpreted as an AMOC slowdown, with a total cessation coinciding with the $^{231}Pa/^{230}Th$ constant production ratio.

This wide range of proxies has evidenced substantial changes in the AMOC on millennial timescales during the LGP. Marine sediments from the Bermuda Rise have revealed benthic foraminiferal $\delta^{13}C$ decreases during Greenland stadials relative to interstadial values (Keigwin and Boyle, 1999). In the Iberian margin, prolonged Greenland stadials are also associated with a shift in benthic $\delta^{13}C$ towards SSW values, thus pointing to reduced ventilation of NADW during the cold phase of major D/O events (Shackleton et al., 2000; Skinner and Elderfield, 2007). However, similar excursions in $\delta^{13}C$ were initially not identified during the cold phase of minor D/O events. Subsequent studies have shown a more clear correspondence between low benthic $\delta^{13}C$ ratios and Greenland stadials. In particular, a highly resolved record located in the Bermuda Rise has featured alternating phases of low and high benthic $\delta^{13}C$ coinciding with relatively cold and mild conditions over Greenland, respectively, for all D/O events (Henry et al., 2016). Similar results have been found in the tropical Atlantic off Brazil (Burckel et al., 2015). Generally shifts in benthic $\delta^{13}C$ can be found during the earliest HEs within MIS-3, which can be interpreted as a transition from relatively strong AMOC background mode with NSWs to an off mode with the deep Atlantic Ocean filled by SSW (Böhm et al., 2015). However, this was not the case in the HEs of the late glacial period (stadials 2 and 3), consistent with the idea that the deep ocean at the time was anyway filled with SSWs. Nd isotopes at the Bermuda Rise suggest that SSWs persisted during the full glacial, with no indication of any additional changes in the deepwater source associated with the glacial-aged Heinrich stadials (stadials 1, 2, and 11) but rapid shifts accompanying D/O events (Böhm et al., 2015). In the South Atlantic, a highly resolved record also shows relatively low $\epsilon Nd$ values during major Greenland interstadials, thus indicating intensified export of NSW during interstadials (Piotrowski et al., 2008). Recently, Gottschalk et al. (2015b) obtained records from several related

proxies not affected directly by increased dilution by terrestrial material; good correspondence was found with many of the D/O events from the Greenland ice core, lending further support to the paradigm that links the origin of these abrupt warming events with reorganisations of the AMOC.

The combination of water-mass tracers and circulation proxies provides a general perspective of the oceanic circulation during the LGP. Concomitant with stadial to interstadial transitions, rapid shifts from relatively high to low $^{231}Pa/^{230}Th$ ratios are observed in sediment samples from the Bermuda Rise (Böhm et al., 2015; Henry et al., 2016), suggesting a reduced AMOC during Greenland stadials and a strengthening during interstadials. $^{231}Pa/^{230}Th$ ratios suggest that this pattern is also consistent with the global perspective of the AMOC during the deglaciation, with cold intervals being associated to episodes of reduced AMOC followed by rapid flow accelerations during abrupt temperature transitions over Greenland (McManus et al., 2004). The production ratio during Heinrich stadial 1 as well, as during MIS-3 Heinrich stadials, are all associated with a clear excursion to the production ratio, consistent with the conceptual model of an off circulation. However, a clear signal is not seen for Heinrich stadials during full glacial conditions (stadials 2 and 3). This does not support the conceptual model of an off circulation state during these HEs, although interpretations in terms of circulation strength could be not so straightforward interpretation (e.g. Burckel et al., 2015).

Finally, variations in the grain size and the concentration of magnetic mineral in several marine core-sediments in the North Atlantic have been interpreted as reflecting Greenland stadials being accompanied by reduced production rates of NADW and increased flow speed of NADW during interstadials (Kissel, 1999).

To summarise, the available paleoceanographic evidence for variations in the AMOC strength and in NADW formation is strongest throughout the deglaciation in many of the HEs, and gradually emerging for D/O events as well, although the lack of direct evidence for circulation changes over the shortest events, so that for these an alternative driving mechanism cannot be excluded (Lynch-Stieglitz, 2017).

### 1.1.4 Mechanisms: the insight from numerical models

Numerical modeling has largely contributed to improve our understanding of glacial abrupt climate changes. Destabilisation of the AMOC as a potential candidate to trigger glacial abrupt climate changes was first pointed out by Stommel (1961); Rooth (1982), whose simple density-driven conceptual models indicated that small variations in the balance of heat and/or salt could result in tipping of the oceanic circulation into an alternative stable regime. Following this hypothesis, Broecker et al. (1985) proposed that abrupt transitions in the glacial

climate could be the result of changes in the production rate of NADW formation. Proxy evidence together with theoretical studies support the existence of different modes of operation for the AMOC during the LGP.

A major milestone in paleoclimate modeling is the simulation of the Last Glacial Maximum (LGM; ca. 21 kyr BP) climate by means of the CLIMBER-2 coupled global model of intermediate complexity (Ganopolski et al., 1998). Previous attempts to simulate different aspects of the glacial climate involved coupled atmosphere-ocean General circulation models (GCMs) that included flux corrections to prevent the dramatic climate drift at the time. The use of such models to simulate a climate radically different from the present climate such as that of the LGM was hence not justified. CLIMBER-2 overcame this limitation through the coupling of its atmospheric and oceanic components without the inclusion of flux adjustments. In order to simulate the climate of the LGM, CLIMBER-2 was forced by insolation corresponding to 21 kyr BP, reduced atmospheric $CO_2$ concentration and prescribed continental ice sheets. In agreement with proxy evidence and theoretical studies, the resulting equilibrium climate was characterised by a substantial reduction in the oceanic heat transport into the high latitudes of the NH which leads to global cooling (ca. 6 °C) together with a southward shift of NADW formation and intrusion of AABW into the North Atlantic (Ganopolski et al., 1998). The stability of the glacial climate was subsequently investigated with the CLIMBER-2 model by imposing freshwater fluxes in the North Atlantic ocean and starting from a the LGM climate (Ganopolski and Rahmstorf, 2001). Results suggest that although the stable mode of the glacial oceanic circulation has reduced NADW formation and cold conditions over the North Atlantic, an abrupt climatic transition similar to those observed for D/O events can be triggered as a temporary flip of the conveyor mode with high rates of NADW formation in the Nordic seas in response to the freshwater forcing. In addition, the sequence of events in Antarctica shows a simulated gradual warming during Greenland stadials, a result that is consistent with the so-called thermal bipolar seesaw hypothesis (Stocker and Johnsen, 2003) as well as with paleorecords (Blunier and Brook, 2001; EPICA-Project, 2006; WAIS Divide Project Members, 2015) and other modelling experiments (Knutti et al., 2004; Lee et al., 2011; Kageyama et al., 2010).

The notion of a freshwater-driven throttling of oceanic convection has also been investigated using both EMICs and GCMs (e.g. Kageyama et al., 2010). In particular, Menviel et al. (2014) showed that anomalous North Atlantic freshwater fluxes lead to substantial changes in the AMOC which, in turn, generate a global climatic signal that is compatible with the continuum of millennial-scale climate variability observed in paleorecords. For the last deglaciation, Liu et al. (2009) showed that the abrupt warming during the Bølling-Allerød around 14.5

kyr BP, often considered as the youngest D/O event, could be simulated as a response to the shutdown of freshwater following HE1. Conversely, models have also shown that glacial abrupt climatic transitions can be promoted after imposing freshwater fluxes in the South Atlantic ocean (Weaver et al., 2003). In this experiment, freshwater input in the SO translates into a decline in AABW density at the expense of NADW which, in turn, undergo a density increase. This results in an intensification of NADW formation which eventually leads to a prominent warming in the North Atlantic consistent with that observed in paleorecords during the deglaciation.

An important limitation of hosing experiments is that the freshwater balance during the LGP is not sufficiently constrained in terms of its origin and magnitude, thus conditioning the realism of the forcing. While different studies point to NH ice-sheets as the main freshwater source to cause AMOC variations (Ganopolski and Rahmstorf, 2001; Vellinga and Wood, 2002), others claim that the freshwater imbalance stems from high latitudes of the the SH (Stocker, 2003; Weaver et al., 2003) or even from induced solar forcing (Braun et al., 2005). However, it is an open question whether simulating glacial abrupt climate changes of the LGP is possible using realistic freshwater fluxes (Alvarez-Solas et al., 2018b).

Alternatively, other different mechanisms have been proposed to explain glacial abrupt climate changes. Keeling and Whorf (2000) proposed that they were caused by periodic variations in the strength of the global oceanic tides caused by resonances in the periodic motions of the earth and moon. The role of sea ice in promoting abrupt transitions in climate has been addressed in atmospheric (Li et al., 2005) and conceptual models (Petersen et al., 2013). According to these studies, a reduction in the sea ice extent of the North Atlantic could explain the prominent warming observed during D/O events. The magnitude of the abrupt transitions could result from the amplification generated through the ice-albedo feedback and the initial sea-ice retreat could be caused by subtle shifts in wind stress near the ice edge (Fang and Wallace, 1994), small perturbations in the AMOC strength (Gildor and Tziperman, 2003; Kaspi et al., 2004) or changes in the stratification of the Nordic Seas (Dokken et al., 2013; Kleppin et al., 2015). In addition to sea-ice variations, a comprehensive fully coupled model has shown that gradual changes in the height of NH ice sheets can lead to rapid climate transitions that closely resemble those recorded in Greenland ice cores for D/O events (Zhang et al., 2014). This climatic transition is possible due to the coexistence of two glacial ocean circulation states at intermediate heights of NH ice sheets. Recently, D/O events have been explained as the result of a non-linear internal salt oscillator in the Atlantic (Peltier and Vettoretti, 2014; Vettoretti and Peltier, 2016, 2018) following Broecker et al. (1990)'s original idea without the need to invoke any external forcing.

Finally, model experiments have shown that slowly varying background climate conditions in the SO are capable of triggering a strong AMOC resumption leading to an abrupt warming in the North Atlantic (Knorr and Lohmann, 2003). The same result was found when applying gradual background climate changes from glacial to interglacial conditions on a global scale (Knorr and Lohmann, 2007). This led to the suggestion that fluctuations in atmospheric $CO_2$ concentration are not only a response of the SO state, but a potential candidate for generating gradual climate variations that eventually favor abrupt warming in the North Atlantic (Barker and Knorr, 2007). A myriad of mechanisms thus has been proposed to account for the occurrence of glacial abrupt climate changes.

### 1.1.5 Impact of glacial abrupt climate changes on Northern Hemisphere ice sheets

Regardless of their ultimate cause, an issue that has received little attention up to now is a detailed assessment of the impact of abrupt climate changes on the evolution of glacial ice sheets. Improving our understanding of this issue is important for a number of reasons (Alvarez-Solas et al., 2018a). Since meltwater discharge from the ice sheets surrounding the Nordic Seas is often implied as a cause of ocean instabilities, constraining freshwater inputs into the North Atlantic Ocean is crucial for a better understanding of the driving mechanisms of glacial abrupt climate changes (Rasmussen and Thomsen, 2013). Significant efforts have been invested in understanding the role of the LIS in glacial abrupt climate changes. However, the dynamics of the Eurasian Ice Sheet (EIS) during the LGP has received comparatively less attention from a modeling perspective. Yet, temperature anomalies associated with glacial abrupt climate changes were likely largest over Eurasia and thus the EIS, and therefore significant impacts on the EIS should be expected. Precursor events could have originated from the European and Icelandic ice sheets (Grousset et al., 2000; Scourse et al., 2000). Meltwater peaks in the Norwegian Sea during MIS-3 have been associated with HEs and millennial-scale climate variability (Lekens et al., 2006). From a broader perspective, the EIS, consisting of the Fennoscandian, the British Isles and the Barents-Kara ice sheets (FIS, BIIS and BKSIS, respectively) contained a large marine-based sector at its maximum extension (Hughes et al., 2016) that was exposed to oceanic variations, and the BKSIS is often considered as an analog for the current West Antarctic ice sheet (WAIS). At the LGM both had a similar size, but while the WAIS endured the deglaciation, the BKSIS completely disappeared (Andreassen and Winsborrow, 2009). Understanding the underlying mechanisms would provide important insights into the nature of the abrupt triggering processes but also on the future evolution of the WAIS (Gudlaugsson et al., 2013, 2017).

Some progress has been achieved in the past decade using ice-sheet models. Siegert and Dowdeswell (2004) used inverse modelling to simulate the EIS evolution during the second part of the LGP, optimising the fit with the geological evidence. Forsstrm and Greve (2004) used several versions of an ice-sheet model to simulate the EIS evolution throughout the LGP. Significant changes in the EIS ice volume in response to temperature and precipitation variations were simulated. Clason et al. (2014) additionally included a parameterisation of surface meltwater enhanced sliding. In both cases too much ice was simulated in the northeastern EIS. Gudlaugsson et al. (2017) used the same model but introducing a simple representation of the subglacial hydrological system, focusing on its role in the time evolution of the EIS. More recently, Patton et al. (2016) used an ice-sheet model constrained by data to simulate the EIS evolution throughout part of LGP. By targeting the most probable EIS distribution at different time slices, the model reproduced substantial ice-volume variations. However, all these models suffer from important limitations, notably the lack of an explicit treatment of the oceanic forcing. Marshall and Koutnik (2006) investigated the iceberg production from all the North American ice sheets with a parameterized calving model. They found different behaviors on millennial time-scales depending on the local glaciological and climatic characteristic, with increased iceberg production both during stadials (e.g. from Iceland) or during interstadials (e.g. from Barents Sea). Nonetheless, submarine melting at the grounding line has not been explicitly considered until now and its impacts on millennial-scale variability has not been investigated up to now from a modelling perspective.

## 1.2 Motivation

Ice core records have shown that atmospheric $CO_2$ levels and Antarctic temperatures varied in concert during the LGP, with the warming phase of AIM events coinciding with $CO_2$ rises (Ahn and Brook, 2008; Bereiter et al., 2012) and episodes of SO upwelling (Anderson et al., 2009; Gottschalk et al., 2015a). Poleward migration of SH westerlies at the onset of stadials is supported by ice-core deuterium excess data from the WAIS Divide core (WAIS Divide Project Members, 2015). Further evidence for the adjustment of the structure and intensity of SH westerly winds during glacial abrupt climatic transitions can be found in Chilean-margin marine cores (Lamy et al., 2007), New Zealand mountain glacier reconstructions (Putnam et al., 2010) and Patagonian lake records (Moreno et al., 2012). Precise dating of the sequence of glacial climatic events furthermore indicates that Antarctic gradual warmings precede abrupt temperature transitions over Greenland by several centuries (WAIS Divide Project Members, 2015). These findings have led to the suggestion that the SO could be the origin

of glacial abrupt climate changes. Several studies have proposed that the increase of both SO upwelling and $CO_2$ levels were the consequence of a southward shift of the Intertropical Convergence Zone (ITCZ) and a strengthening and/or southward shift of SO winds in response to an AMOC slowdown through the bipolar seesaw effect (Anderson et al., 2009; Lee et al., 2011).

The aim of this thesis is to investigate the origin of glacial abrupt climate changes and to assess their impact on NH ice sheets. The first goal focuses on the description of a new mechanism consistent with proxy records which allows to explain glacial D/O variability and its global climatic imprint. The main motivation behind this study was to find a mechanism that does not invoke the use of prescribed freshwater forcing. This entails coupled climate model simulations performed under glacial boundary conditions and a forcing scenario based on gradual changes in the concentration of atmospheric $CO_2$ and SO winds. To allow simulations over long timescales an EMIC is used. The second goal was pursued forcing an ice-sheet model offline. A new off-line forcing method is developed to investigate the paleo-evolution of the NH ice sheets on millennial time scales. This approach provides a more realistic representation of orbital and millennial-scale climate variability and improves the transient forcing of ice sheets during the LGP, and is applied specifically to investigate the impact of oceanic variations in the evolution of the EIS throughout the LGP. This thesis is structured around the following scientific questions:

**Could gradual changes related to the slowly-varying conditions in the Southern Ocean promote abrupt climatic transitions during the last glacial period?**

The SO has been proposed as an alternative origin to the North Atlantic glacial abrupt climate changes. Ice core records have revealed that the evolution of atmospheric $CO_2$ concentration and Antarctic temperatures follow a similar pattern during the last glacial period, with $CO_2$ rises coinciding with the warming phase of AIM events and Greenland stadials. Several studies have proposed that the increase of both SO upwelling and $CO_2$ levels were the consequence of a shift in atmospheric circulation patterns including a southward shift of the Intertropical Convergence Zone (ITCZ) and a strengthening and/or southward shift of SO winds in response to a reduction of the AMOC through the bipolar seesaw effect. Here, we investigate whether an increase of $CO_2$ and SO winds can promote an abrupt transition from a state with weak to a state with strong AMOC. To this end a coupled model of intermediate complexity (including a OGCM) is used in an experimental setup designed such that the climate system resides close to a threshold found in previous studies. This question is addressed in Chapter 2 (Banderas et al., 2012).

**What is the origin of Dansgaard-Oeschger variability? Does the SO play a role in glacial abrupt climate change?**

The previous study showed that increasing atmospheric $CO_2$ and SO winds is able to to trigger abrupt transitions from stadial to interstadial conditions via AMOC intensification (Banderas et al., 2012). In response, the ITCZ would be expected to shift northward again leading to a weakening of the SO winds, decreased upwelling and reduced atmospheric $CO_2$ levels in response to the AMOC strengthening, providing a negative feedback. A return of the climate system to the stadial state would imply that glacial abrupt climate changes are part of an internal oscillation involving the AMOC, $CO_2$ and SO wind variations. This hypothesis was investigated by performing a transient simulation of the glacial climate using a coupled climate model forced by prescribed atmospheric $CO_2$ and SO wind-stress variations in an idealized experimental design inspired by the characteristic climatic imprint of the SO during the last glacial period. This question is addressed in Chapter 3 (Banderas et al., 2015).

**How can we investigate the response of NH ice sheets on millennial time scales?**

The occurrence of D/O events appears to be related to glacial climatic conditions with global ice volumes varying at intermediate levels. This indicates that NH ice sheets could have modulated the phasing and timing of millennial-scale climate variability during the last glacial period. Investigating the variability of NH ice sheets during D/O events can contribute to improve our understanding of glacial abrupt climate change. ESMs including fully coupled ice-sheet components are the most appropriate tool to simulate the past as well as the present and future evolution of ice sheets. However, because of their high computational cost, the long-term simulation with coupled ice sheets is currently unaffordable. Previous studies have used an alternative and more efficient approach which consist in forcing ice sheet models off-line by a synthetic time-varying climatology but its skill to reproduce millennial-scale climate variability needs to be improved. This question is discussed in Chapter 4 (Banderas et al., 2018).

**How did the Eurasian ice sheet respond to millennial scale climate variability?**

While an important effort has been made to investigate the dynamics and evolution of the LIS during the LGP, the EIS has not received much attention, in particular from a modeling perspective. However, meltwater discharge from this and other ice sheets surrounding the Nordic Seas is often implied as a potential

cause of ocean instabilities that lead to glacial abrupt climate changes. Thus, a better understanding of its variations during the LGP is important to understand its role in glacial abrupt climate changes. Here we investigate the response of the EIS to millennial-scale climate variability during the LGP using the methods developed in the previous chapter. This issue is discussed in Chapter 5 (Alvarez-Solas et al., 2018a).

## 1.3 Overview

The former questions have led to four published (or in review) scientific articles. Each paper provides its specific motivation and background. The implications of this work and its relevance to paleoclimate modelling has been discussed in a broader context in a final section following the articles. Here the articles and authors are listed:

**Article 1: Role of $CO_2$ and Southern Ocean winds in glacial abrupt climate change**. *Rubén Banderas, Jorge Álvarez Solas, Marisa Montoya.*

In this study, the role of $CO_2$ and SO winds in glacial abrupt climate change is investigated using a coupled climate model of intermediate complexity. The experimental setup includes glacial background climatic conditions and a linear forcing rate of atmospheric $CO_2$ levels consistent with proxy records. An abrupt temperature transition over Greenland comparable to that observed in ice core records is simulated in response to the rise of atmospheric $CO_2$. This transition is accompanied by an AMOC strengthening and a northward shift of NADW formation sites. Similar results are obtained when imposing a linear increase in wind-stress over the SO thus suggesting the importance of the SH in modulating and potentially triggering glacial abrupt climate changes.

**Article 2: An interhemispheric mechanism for glacial abrupt climate change**. *Rubén Banderas, Jorge Álvarez Solas, Alexander Robinson, Marisa Montoya.*

This study emerges as an extension of the preceding article and focuses on the potential of the SH to generate D/O variability in a glacial climate. In a similar experimental setup to that of the previous study, the design of the forcing follows the style of Antarctic climate variability. The simulated AMOC exhibits an oscillatory behaviour in response to gradual changes in $CO_2$ and

SO wind-stress which results from variations in the meridional density gradient of the Atlantic ocean. The evolution of the simulated climatic patterns matches the amplitude and timing of the largest events that occurred during the last glacial period and their widespread climatic impacts thus suggesting that glacial abrupt climate change could be part of an internal oscillation mediated by changes originated in the SH.

**Article 3: A new approach for simulating the paleo-evolution of the Northern Hemisphere ice sheets**. *Rubén Banderas, Jorge Álvarez Solas, Alexander Robinson, Marisa Montoya.*

In this article we illustrate the problems derived from usual approaches used to force ice-sheet models offline throughout the LGP and propose a new offline climate forcing method that attempts to better represent the characteristic pattern of millennial-scale climate variability by including an additional spatial anomaly field associated with this timescale. Our new method provides, on one hand, a more realistic representation of orbital and millennial-scale climate variability and improves the transient forcing of ice sheets during the LGP. On the other hand, it suggests that weighting the spatial variability over time through a single index, as often done in previous studies, can lead to an overestimation of the response of some of the NH ice sheets during abrupt changes.

**Article 4: Oceanic forcing of the Eurasian Ice Sheet on millennial time scales during the Last Glacial Period**. *Jorge Álvarez Solas, Rubén Banderas, Alexander Robinson, Marisa Montoya.*

In this article we applied the former method to investigate the response of the EIS to millennial-scale climate variability during the LGP. We use a hybrid, three-dimensional, thermomechanical ice-sheet model that includes ice shelves and ice streams. The model is forced offline through a novel perturbative approach that includes the effect of both atmospheric and oceanic variations and provides a more realistic treatment of millennial-scale climatic variability than conventional methods. Our results show that the EIS responds with enhanced iceberg discharges in phase with interstadial warming in the North Atlantic. Separating the atmospheric and oceanic effects demonstrates the major role of the ocean in controlling the dynamics of the EIS on millennial time scales. Together with previous work, our results provide a consistent explanation for the timing of the responses of the LIS and the EIS to glacial abrupt climate changes.

# 2

# The role of $CO_2$ and Southern Ocean winds in glacial abrupt climate change[1]

## 2.1 Introduction

The last glacial period (ca. 110-10  kyr BP) was characterised by remarkable climatic instability on millennial timescales, mainly associated with so-called Dansgaard-Oeschger (D/O) events (Alley et al., 1999b). These are considered to be the most abrupt, i.e., large and rapid, climate changes of the past 110 kyr, repeatedly manifested as warming in Greenland by more than 10 K on decadal timescales (e.g., Lang et al., 1999) with widespread global climatic effects (Voelker and Workshop Participants, 2002).

Both modeling and reconstruction efforts have contributed to increase our understanding of these glacial abrupt climate changes. The current paradigm is that these were caused by reorganisations of North Atlantic deep water (NADW) formation (Alley et al., 1999b; Ganopolski and Rahmstorf, 2001). This is supported by the close agreement between results of climate simulations involving variations in NADW formation and the Atlantic meridional overturning circulation (AMOC), and the evidence from paleoclimate reconstructions. Models are in this way able to reproduce the so-called bipolar seesaw behaviour between Greenland and Antarctica (Blunier and Brook, 2001; EPICA-Project, 2006). The idea is that an intensification of the AMOC translates into an increase in northward heat transport at the expense of the southernmost latitudes; conversely, a weakening of the AMOC reduces northward heat transport, thereby warming the south (Crowley, 1992; Stocker, 1998). The different timescale between northern and southern latitudes can be explained by the fact that the Southern Ocean acts

[1] The main contents of this chapter are published in: Banderas, R., J. Alvarez-Solas, and M. Montoya, 2012: Role of $CO_2$ and Southern Ocean winds in glacial abrupt climate change, *Clim. Past*, 8, 1011–1021,http://doi:10.5194/cp-8-1011-2012.

as a heat reservoir, that dampens and integrates in time the more rapid North Atlantic signal (Stocker and Johnsen, 2003).

However, the causes of NADW formation reorganisations remain yet unknown. Model studies generally employ freshwater forcing in the North Atlantic to mimic D/O-like fluctuations (e.g., Ganopolski and Rahmstorf, 2001) but the ultimate source of such a forcing has not been identified. Alternatively, a Southern Ocean origin of abrupt climate changes has also been proposed. Enhanced surface freshwater fluxes (Weaver et al., 2003) and slowly varying background climate conditions in the Southern Ocean (Knorr and Lohmann, 2003) have been shown to be able to trigger an AMOC intensification leading to an abrupt warming in the North Atlantic. The same result was found when applying gradual background climate changes from glacial to interglacial climate conditions on a global scale, including temperature and wind-stress (Knorr and Lohmann, 2007). As suggested by the latter study, fluctuations in atmospheric $CO_2$ concentration are a potential candidate to generate such gradual climate variations. Ice core data and marine sediment proxies furthermore suggest atmospheric $CO_2$ levels rose during the last glacial period coinciding with periods of halted NADW formation and reduced stratification in the Southern Ocean (Ahn and Brook, 2008). Such $CO_2$ variations are strongly correlated with Antarctic temperature, and predate abrupt warmings in Greenland associated with the largest D/O events. Taken together, these results led Knorr and Lohmann (2007) to suggest $CO_2$ increases could have contributed to rapid AMOC intensification after Heinrich events, corresponding with the largest DO events.

The close correspondence between atmospheric $CO_2$ variations and Antarctic temperature variability on millennial timescales suggests an important role of the Southern Ocean in controlling the carbon cycle during the last glacial period. Recently, biogenic opal reconstructions have suggested that during deglaciation, as well as throughout the last glacial period, $CO_2$ rises were preceded by an increase in deep upwelling in the Southern Ocean (Anderson et al., 2009). Denton et al. (2010) and Toggweiler and Lea (2010) have proposed that the increase of both Southern Ocean upwelling and $CO_2$ levels was the consequence of a shift in atmospheric circulation patterns in response to a reduction of the AMOC through the bipolar seesaw effect. Southern Ocean winds indeed appear to have strengthened and shifted southward at the end of the last glacial period as well as during extreme cold periods in the Northern Hemisphere (Toggweiler, 2009). Recent model studies suggest that a southward shift of the intertropical convergence zone (ITCZ) and Southern Ocean winds intensification can also take place via atmospheric teleconnections, that is, without involving the bipolar seesaw, in response to a cooling in the North Atlantic, and leading to a rise in atmospheric $CO_2$ by 20-60 ppmv, consistent with proxy records (Lee et al., 2011).

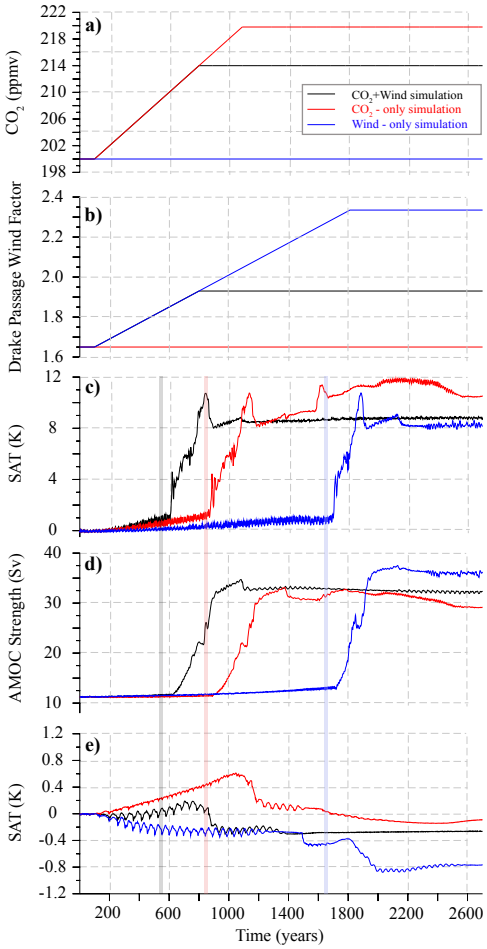


Fig. 2.1: Timeseries of forcings and relevant climatic variables: **a)** $CO_2$ forcing in ppmv; **b)** wind amplification factor over the Drake Passage (no units); **c)** anomalies of North Atlantic SAT (67.5°N 11°W, in the Nordic Seas) with respect to the stadial state in K; **d)** AMOC strength in Sv; **e)** anomalies of Antarctic SAT (86.2°S 11°E) with respect to the stadial state in K. Black, red and blue lines show the simulation combining $CO_2$ and wind forcings, the $CO_2$-only experiment, and the wind-only forced run, respectively. Black, red and blue shaded bars indicate the transition stages for the simulation combining $CO_2$ and wind forcings, the $CO_2$-only experiment and the wind-only forced run, respectively.

These results indicate several mechanisms by which a decrease in the AMOC strength leading to northern cooling would have translated into a southward shift and/or intensification of Southern Ocean westerlies, which through enhanced deep upwelling would have contributed to increase the atmospheric $CO_2$ concentration.

Southern Ocean winds are one of the main driving factors of the AMOC (Kuhlbrodt et al., 2007). Thus, increased Southern Ocean westerlies could have contributed to an AMOC strengthening through the so-called Drake Passage effect (Toggweiler and Samuels, 1995a). On the other hand, the concomitant effect of increasing atmospheric $CO_2$ levels on the glacial AMOC has not yet been assessed. Here, the evidence from all the former studies is taken together to investigate the effect of $CO_2$ and Southern Ocean winds variations on the glacial AMOC.

## 2.2 Model and experimental design

The model used in this study is CLIMBER-3$\alpha$ (Montoya et al., 2005). Its atmospheric component is a 2.5-dimensional statistical-dynamical model based on the assumption of a universal vertical structure of temperature and humidity in the atmosphere with a horizontal resolution of $7.5° \times 22.5°$ (Petoukhov et al., 2000). Its oceanic component contains the state-of-the-art Geophysical Fluid Dynamics Laboratory (GFDL) MOM-3 ocean general circulation model, with a horizontal resolution of 3.75° and 24 variably spaced vertical levels, and the ISIS thermodynamic-dynamic snow and sea-ice model (Fichefet and Maqueda, 1997). CLIMBER-3$\alpha$ satisfactorily describes the large-scale characteristics of the atmosphere, ocean and sea-ice on seasonal and longer timescales.

The present study builds upon a previous climate simulation of the Last Glacial Maximum (LGM, ca. 21 kyr BP; Montoya and Levermann, 2008). Boundary conditions followed the specifications of the Paleoclimate Modeling Intercomparison Project Phase II (PMIP2), namely: changes in insolation, a reduced equivalent atmospheric $CO_2$ concentration of 167 ppmv to account for the lowered $CH_4$, $N_2O$ and $CO_2$ concentrations, the ICE-5G ice-sheet reconstruction (Peltier, 2004), and land-sea mask changes plus a global increase of salinity by 1 PSU to account for the $\sim$120 m sea-level lowering. Montoya and Levermann (2008) investigated the sensitivity of the glacial AMOC to wind-stress strength by integrating the CLIMBER-3$\alpha$ model to equilibrium with the Trenberth et al. (1989) surface wind-stress climatology multiplied globally by varying factors $\alpha \in [0.5, 2]$. At $\alpha = 1.7$ a threshold, associated with a drastic AMOC increase of more than 10 Sv and a northward shift of NADW formation north of the Greenland-Iceland Scotland (GIS) ridge, was found. We hypothesise herein that the glacial AMOC

is close to this threshold. However, because D/O events take place within Marine Isotopic Stage (MIS) 3 (ca. 60-27 kyr BP) rather than at the LGM, an equivalent atmospheric $CO_2$ level of 200 ppmv resulting from the higher $CH_4$, $N_2O$ and atmospheric $CO_2$ concentrations registered during the former period (Schilt et al., 2010) has been imposed to mimic MIS3 climatic conditions. Consequently, the starting point for the experiments shown herein is the final equilibrium state of a control climate simulation with $\alpha = 1.65$ and an equivalent atmospheric $CO_2$ level of 200 ppmv, hereafter our stadial state.

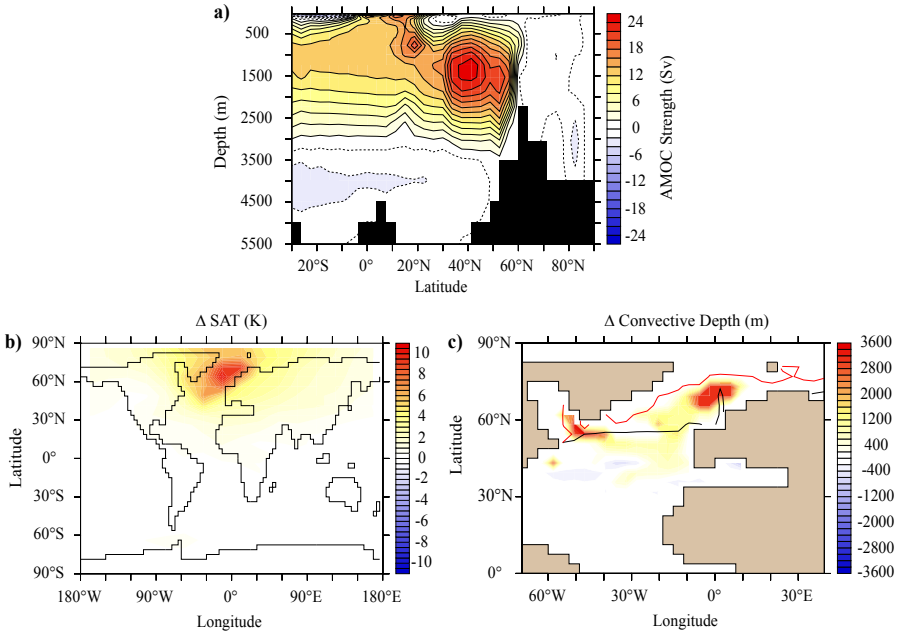


Fig. 2.2: Climatic patterns describing the interstadial state: **a)** AMOC stream-function in Sv; **b)** SAT anomalies with respect to the stadial state in K; **c)** interstadial minus stadial maximum convective depth differences in m. Black and red lines show the locations of the 90% northern summer (June-August) average sea-ice concentration for the stadial and the interstadial regime, respectively.

Three transient experiments have been performed to test the AMOC sensitivity to $CO_2$ and wind forcings: a simulation combining both factors, a scenario considering $CO_2$ forcing only and, finally, a wind-only forced experiment (Figs. 2.1a and 2.1b). $CO_2$ forcing consists of a linear increase in $CO_2$ levels by 20 ppmv in 1000 yr, thus at the highest end of the $CO_2$ increase rates suggested

by Ahn and Brook (2008) and recent climate carbon-cycle simulations (Bouttes et al., 2011). Wind forcing implies wind-stress over the latitudinal band of Drake Passage is linearly increased with a wind-amplification rate of 0.4 in 1000 yr. This increase is roughly consistent with results of a recent atmospheric model study in which cold conditions in the North Atlantic were shown to lead to an intensification of Southern Ocean winds by ∼25% (Lee et al., 2011).

## 2.3 Stadial to interstadial transition

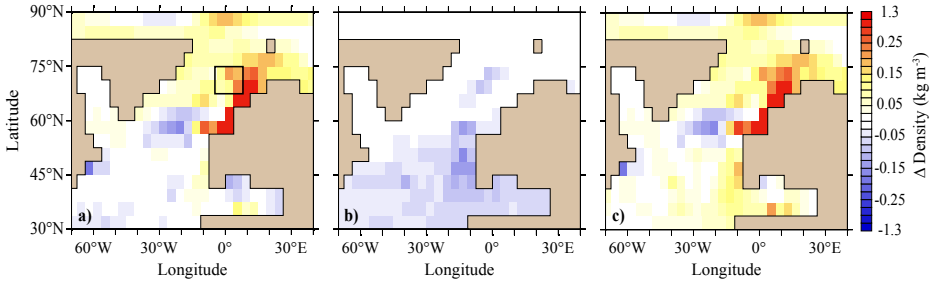


Fig. 2.3: **a)** Surface density anomalies at the transition stage relative to the stadial regime for the $CO_2$-only experiment and contribution to the latter by **b)** temperature and **c)** salinity in kg $m^{-3}$ assuming a linear equation of state. The black box in panel a) indicates the region where the surface freshwater flux balance was calculated.

Increasing $CO_2$ levels and wind strength lead to a gradual warming in the Nordic Seas area (Fig. 2.1c, black). After about 700 yrs the system is found to cross a critical point leading to an abrupt temperature increase in the North Atlantic sector which is accompanied by a strong AMOC strengthening by more than 20 Sv (Fig. 2.1d). The simulated interstadial state is thus characterised by a more vigorous AMOC, deeper convective areas together with reduced sea-ice in the Nordic Seas, and a temperature increase of up to 10 K in the North Atlantic relative to the stadial state (Fig. 2.2).

In order to elucidate the mechanism behind this abrupt climate shift, we assess the precursors of the interstadial state. To this end, we analyse the climate system 30 years before the jump into the interstadial (450, 750, and 1550 years after switching on the forcing for the $CO_2$-plus-wind, $CO_2$-only, and wind-only experiments, respectively), hereafter the transition stage (see Figs. 2.1c and 2.1d).

We furthermore assess separately those simulations in which only $CO_2$ and only Southern Ocean winds were changed, respectively.

Under $CO_2$-only forcing conditions, an abrupt surface air temperature (SAT) increase of up to 4 K in less than a decade occurs in the Nordic Seas once $CO_2$ reaches a level of ca. 215 ppmv (Fig. 2.1c). At this point the AMOC remains almost unchanged (Fig. 2.1d). This first abrupt warming is related to widespread loss of sea ice in the Nordic Seas and the resumption of NADW formation.

Density variations in the Nordic Seas are thus analysed as a precursor for triggering the AMOC recovery. Surface density anomalies at the transition stage reveal significant changes over the North Atlantic with respect to the stadial state, notably over the Nordic Seas and Fennoscandian coast (Fig. 2.3a). Temperature and salinity contributions to density variations indicate the major density anomalies are related to changes in salinity (Fig. 2.3). The surface density evolution, which results in a gradual erosion of vertical stratification previous to the jump into the interstadial state, indeed strongly correlates with surface salinity contribution to density changes (Fig. 2.4).

Table 2.1: Surface freshwater fluxes balance in m $yr^{-1}$ over the Nordic Seas (67.5°N - 75°N, 4°W - 7.5°E) for the stadial and the transition state, and for the difference between them (transition minus stadial) during summer months (June-August) for the $CO_2$ only and wind-only experiments (left and right, respectively). SFF: total vertical freshwater flux, decomposed in precipitation (P), evaporation (E) and sea-ice melting or formation (SI): SFF = P-E+SI; positive values indicate freshwater flux into the ocean.

| | $CO_2$-only | | | Wind-only | |
|---|---|---|---|---|---|
| | Stadial | Transition | Transition minus stadial | Transition | Transition minus stadial |
| SFF | 2.35 | 1.76 | -0.59 | 1.82 | -0.53 |
| P | 0.22 | 0.23 | 0.01 | 0.23 | 0.01 |
| E | 0.11 | 0.18 | 0.07 | 0.18 | 0.07 |
| P-E | 0.11 | 0.05 | -0.06 | 0.05 | -0.06 |
| SI | 2.24 | 1.71 | -0.53 | 1.77 | -0.47 |

To understand the causes behind these salinity changes, surface freshwater fluxes over the Nordic Seas region have been analysed. Northern summer freshwater flux anomalies closely correlate with surface salinity anomalies at the transition stage (Figs. 2.5a and 2.5b). The latter persist throughout the year, explaining the less clear relationship in winter and in the annual mean (Figs. 2.5c-2.5f).

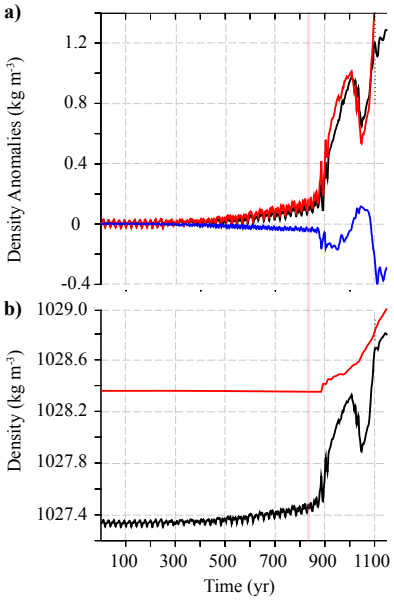


Fig. 2.4: **a)** Surface anomalies with respect to the stadial state of density (black), together with salinity (red) and temperature (blue) contributions to density changes in kg $m^{-3}$ over the Nordic Seas area (67.5°N - 75°N, 4°W - 7.5°E; black box in Figure 3a) assuming a linear equation of state for density for the $CO_2$-only experiment; **b)** density evolution in kg $m^{-3}$ over the same region at the surface (0-87.5 m; black line) and depth (2800 m; red line). The red shaded bar indicates the transition stage for the $CO_2$-only experiment.

The ultimate causes of the northern summer surface freshwater flux change have been unravelled through a detailed analysis of its balance (precipitation, evaporation and sea-ice changes) over the Nordic Seas region (Fig. 2.3a, black box) at the transition and stadial states (Table 2.1). The net northern summer surface freshwater flux in the area is found to be reduced by 0.59 m $yr^{-1}$ (25%) relative to the stadial state. This is partly due to a reduction in precipitation minus evaporation by 0.06 m $yr^{-1}$, but mostly due to a reduction in sea ice melting by 0.53 m $yr^{-1}$. Although rising temperatures due to increased $CO_2$ levels result in local widespread freshening, a northward shift of the northern summer polar front takes place north of the Fennoscandian coast (Fig. 2.5a). As a consequence, summer sea-ice import into the region, most notably in the northeastern North Atlantic and north of the Fennoscandian coast, and thus melting there, is strongly

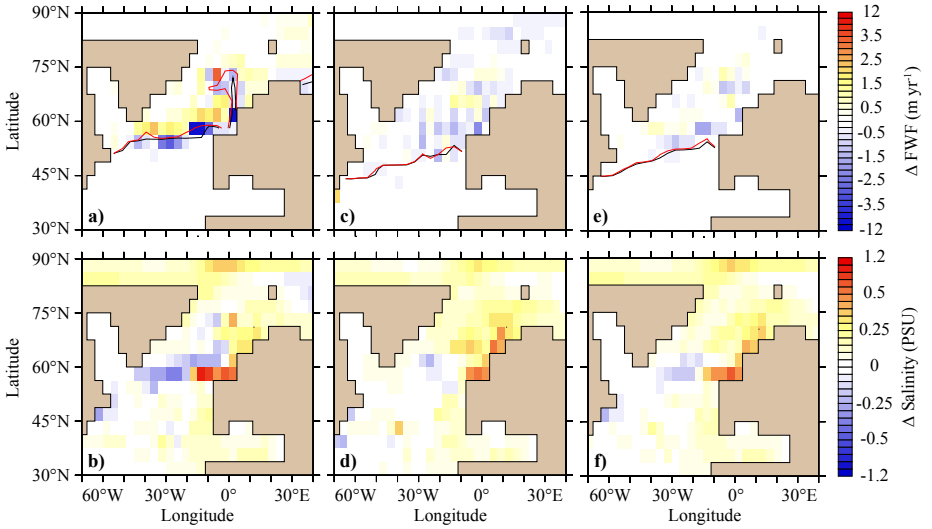


Fig. 2.5: Anomalies at the transition stage relative to the stadial regime under $CO_2$-only forcing conditions of **a)** surface freshwater fluxes in m $yr^{-1}$ and **b)** surface salinity during summer months (June-August) in PSU; **c-d)**, **e-f)** same fields during winter (January-February) and for the annual mean, respectively. Black and red lines show the locations of the 90% northern average sea-ice concentration for the stadial and the transition stage, respectively.

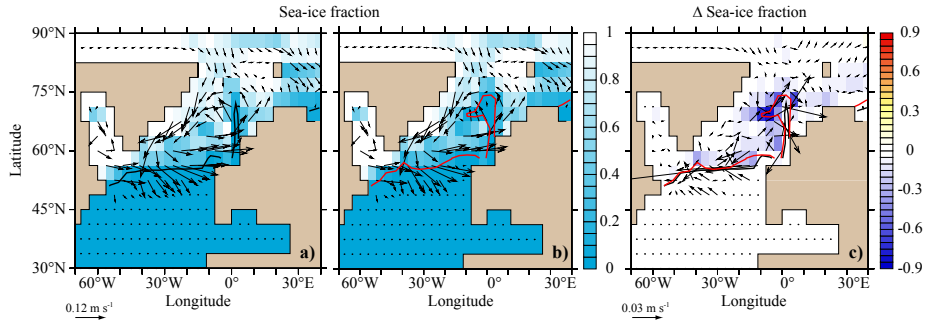


Fig. 2.6: Sea-ice fraction (shaded) and sea-ice velocities (vectors) in m $s^{-1}$ during summer (June-August) for the $CO_2$-only scenario in **a)** the stadial state; **b)** the transition state; **c)** transition minus stadial state. Black and red lines show the locations of the 90% northern summer (June-August) average sea-ice concentration for the stadial and the transition stage, respectively.

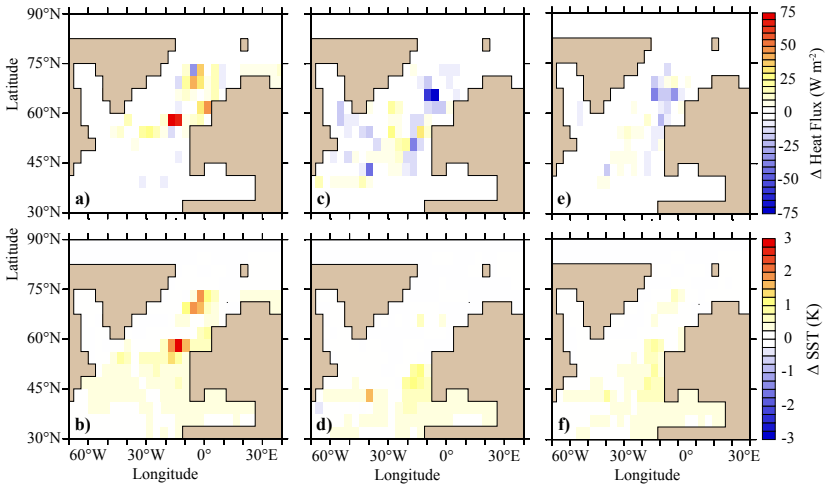


Fig. 2.7: Anomalies at the transition stage relative to the stadial regime under $CO_2$-only forcing conditions of **a)** surface heat flux in W $m^{-2}$ (negative values indicate heat loss by the ocean to the atmosphere) and **b)** sea surface temperature during summer months (June-August) in K; **c-d)**, **e-f)** same fields during winter (January-February) and for the annual mean, respectively.

reduced (Fig. 2.6). This counteracts the effect of sea-ice melting, and eventually results in local net negative freshwater flux anomalies.

To summarise, increased $CO_2$ levels translate into a modest radiative forcing of about 0.35 W $m^{-2}$ which leads to warming in the Nordic Seas by about 1 K (Fig. 2.1c) and, thereby, impacts the sea-ice distribution in this region, especially its southernmost margins, by leading to a northward retreat of the summer polar front. This allows for increased heat loss in this region that contributes to foster convection (Fig.2.7) and leads to enhanced surface salinity and thereby denser surface waters in the vicinity of the Fennoscandian coast. This results in a resumption of NADW formation in open-water areas which were previously capped by sea-ice during the stadial state. The onset of convection in the Nordic Seas contributes to increase the density of NADW, while South Atlantic densities barely change. This translates into a substantial increase in the meridional density gradient which eventually leads to a strong AMOC strengthening (Fig. 2.8).

Note the SAT evolution over Antarctica exhibits a behaviour which resembles the bipolar seesaw (Fig. 2.1e). The simulated gradual warming over Antarctica precedes the abrupt temperature increase in the North Atlantic. Nordic and Antarctic SATs reach peak warming roughly at the same time. The system subsequently switches into the interstadial state in centennial timescales at the expense

of a more gradual cooling of the Southern Ocean. Note that the initial warming in Antarctica here is exclusively caused by the increase in atmospheric $CO_2$ rather than by a previous AMOC weakening. Yet, the final state is characterised by high AMOC and northern SAT values, and cold southern SATs, as expected according to the bipolar seesaw. In the latter case the Antarctic cooling is indeed the response to the redistribution of heat by the reactivation of the AMOC.

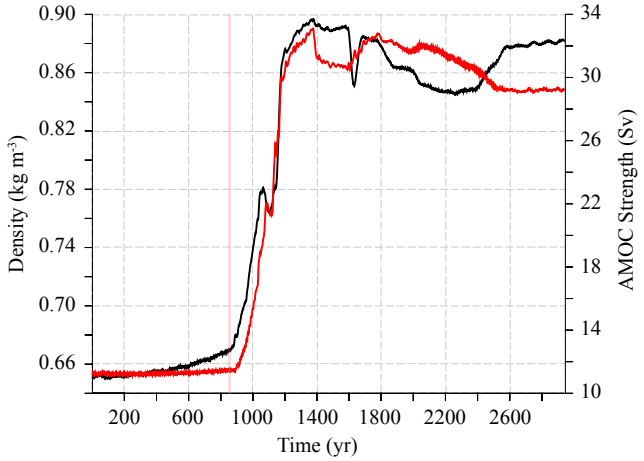


Fig. 2.8: Temporal evolution of the meridional north-south density contrast in kg $m^{-3}$, estimated as the density difference between the North Atlantic (35°N - 80°N, 60°W - 10°E) and the South Atlantic (40°S, 60°W - 10°E) at 750 m depth (black line) and AMOC strength in Sv (red line), for the $CO_2$-only experiment. The red shaded bar indicates the $CO_2$-only transition stage.

Within the wind-only forcing scenario, an abrupt SAT increase by 4 K in less than a decade is also found in the North Atlantic about 1650 years after switching on the forcing. In this case, however, the increased temperatures at the transition stage over the area result from a significant AMOC intensification (Figs. 2.1c and 2.1d). Enhanced winds over the Southern Ocean lead to an increase in deep upwelling over the latitudinal band of Drake Passage. This results in stronger outcropping of isopycnals in the Southern Ocean, and thereby a reduction of the density of Antarctic Intermediate Water (AAIW, not shown) which translates into an increase of the Atlantic outflow (Schewe and Levermann, 2010) by nearly 2 Sv (Fig. 2.9a). As a result, northward heat transport by the Atlantic Ocean is intensified at almost all latitudes (Fig. 2.9b). This suggests the AMOC is initially reactivated from southern latitudes in contrast with the $CO_2$-only run, in

which virtually no changes in the AMOC and heat transport are found prior to the onset of the interstadial state (Fig. 2.9). As a result, North Atlantic waters become warmer in response to a slightly more vigorous AMOC. Increased North Atlantic SATs related to enhanced northward heat transport driven by the AMOC result in melting of the Nordic sea-ice cover. The summer sea-ice polar front retreats to the north, which translates into enhanced heat loss and reduced freshwater fluxes and thereby increased surface salinity in critical convective areas in the North Atlantic. Again, sea-ice changes related to surface salinity increase dominate the freshwater flux balance over this area (Table 2.1). In this case the reduction in freshwater flux over the Fennoscandian coast is of 0.53 m $yr^{-1}$, of which 0.47 m $yr^{-1}$ ($\sim$90%) are due to the sea-ice reduction and, again, only 0.06 m $yr^{-1}$ to a reduction in precipitation minus evaporation. The resulting salinity anomalies and the enhanced density gradient between both hemispheres are considered to be the precursors of NADW formation recovery and the AMOC reactivation, respectively, leading to the interstadial state. Note in this case, in the transient stage, the bipolar seesaw effect is less evident than in the $CO_2$-only forcing scenario. However, the final state clearly evidences the cold Antarctica state associated with the strong AMOC and high northern temperatures.

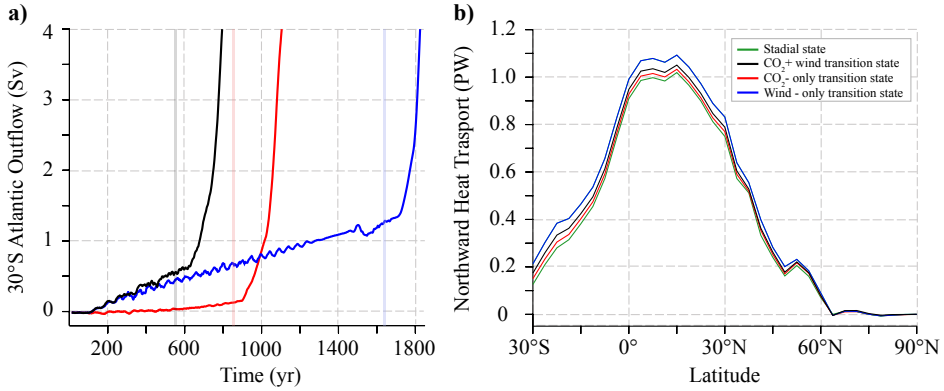


Fig. 2.9: **a)** Evolution of AMOC outflow at 30°S in Sv for the $CO_2$-plus-wind simulation (black), $CO_2$-only (red) and wind-only (blue) forced experiments; **b)** northward oceanic heat transport (0 -1000 m depth) in PW for the stadial state (green) and transition stages for the $CO_2$-plus-wind (black), $CO_2$-only (red) and wind-only (blue) forced experiments. Black, red and blue shaded bars indicate the transition stage for the simulation combining $CO_2$ and wind forcings, the $CO_2$-only run and the wind-only experiment, respectively.

Finally, combining $CO_2$ and wind forcings translates into a prompter climate response, suggesting both forcings work in the same sense to trigger an abrupt climate shift (Fig. 2.1).

## 2.4 Conclusions and discussion

We have investigated the climatic response to increasing atmospheric $CO_2$ levels and Southern Ocean winds when the glacial climate state is close to a threshold. Both are found to lead to an initial abrupt SAT increase on decadal timescales over the Nordic Seas followed by further warming on centennial timescales, resembling the large and rapid warmings associated with D/O events occurred during the last glacial period. The initial simulated abrupt warming is caused by reduced seasonal sea-ice cover in the North Atlantic within all forcing scenarios.

Despite the similarities in the Nordic Seas temperature response between these three scenarios, the mechanism behind the transition to the interstadial in the $CO_2$-only run is quite different from the experiment considering exclusively the wind amplification factor. In the $CO_2$-only simulation, the sea-ice retreat is mainly due to the increased temperatures following the enhanced $CO_2$. In contrast, in the wind-only run it is caused by higher temperatures due to a more vigorous heat transport from Southern latitudes in response to enhanced Southern Ocean winds.

Our results are consistent with previous studies suggesting an important role of sea-ice in abrupt warming (Gildor and Tziperman, 2003; Li et al., 2005). Yet, in our simulations sea-ice retreat causes the initial abrupt SAT increase in response to the onset of convection in the Nordic Seas, but it is the AMOC intensification which helps to sustain the system in the warm state. Note despite the abruptness of the initial SAT increase, the AMOC response is more gradual, lasting several decades until the interstadial state is reached. Thus the fact that an abrupt response of the AMOC is not found does not preclude the latter playing an important role in abrupt climate change.

Our results support those of Knorr and Lohmann (2003, 2007), who found that, starting from glacial conditions, slowly varying background climate conditions in the Southern Ocean, as well as globally, are able to trigger rapid climate change. Note that in our case global warming was achieved by incorporating increasing atmospheric $CO_2$ levels rather than prescribing gradually warmer conditions as in Knorr and Lohmann (2007). This result might seem contradictory with future projections, which suggest an increase in atmospheric $CO_2$ levels leads to North Atlantic warming and freshening, both of which weaken NADW formation. The question as to how abrupt climate change can be promoted in a context of global warming was investigated by Knorr and Lohmann (2007), who specifically

assessed this issue in the context of deglaciation, which involves surface warming and freshening associated to melting ice sheets. In that case the mechanism responsible for the transition was found to be the preconditioning by an increase in ventilation of the warm subsurface water in the northern North Atlantic which resulted in an increase in the meridional transport of salt to the northern high latitudes leading to a resumption of convection and a rapid intensification of the AMOC. In our case an increase in atmospheric heat loss together with a reduction in freshwater fluxes is found in response to enhanced $CO_2$ mainly through sea-ice changes at its margins. Because the $CO_2$ change is small, the response of atmospheric freshwater fluxes is minor. However, the reduction in sea-ice allows for a non-linear response of the system. Thus, in our view, the background climate, and particularly the North Atlantic sea-ice configuration, plays an important role in setting the climate sensitivity and its stability properties. This view is supported by Weaver et al. (2007) who found that the North Atlantic sea-ice distribution of the initial mean climate determines the amplitude of the thermal response as well as the sign of the freshwater flux forcing associated with increasing greenhouse gases. For cold climates, freshwater flux forcing acted to reduce the transient AMOC decrease whereas for warmer climates it reinforced the transient AMOC decrease.

The freshwater flux mechanism found herein is different from the salinity advection mechanism in the North Atlantic leading to a rapid AMOC switch-on described by Montoya and Levermann (2008). Note that in the latter study the model was integrated to the equilibrium by changing globally the oceanic wind-stress in different simulations. Within this context, enhanced surface wind-stress in the North Atlantic was found to increase the horizontal gyre circulation both in the subtropics and the subpolar regions, leading to enhanced salinity transport from the Tropics to the North Atlantic in the upper ocean layers. This mechanism is initially absent here, where only the Southern Ocean wind-stress and/or the $CO_2$ concentration are varied. Note that the precursors are analysed at the transition state, thus prior to the interstadial. By contrast, once a relatively large change in the AMOC is accomplished (i.e. once the interstadial state is fully reached), the northward salinity transport does increase considerably as found by Montoya and Levermann (2008).

Although the abrupt warming simulated in the North Atlantic resembles those reported for D/O events, the comparison against the paleorecord is not fully satisfactory. The simulated rapid warming in the Nordic Seas in our case takes place in two steps: a sudden increase by 4 K in less than a decade, followed by more gradual warming greater than 10 K on centennial timescales, rather than warming by more than 10 K in only a few years found in proxy records (Steffensen et al., 2008). The difficulty to simulate climate changes as abrupt as those registered in

the paleorecord is a common feature to many models, and the possible reasons are yet unclear. Recent studies point out the necessity to improve the ability of state-of-the-art models to simulate abrupt climate changes within the context of threshold values. This highlights the necessity to explore new research lines of past forcing factors which may help to understand the ensuing climate response (Valdes, 2011; Stocker and Marchal, 2000). Yet, up to now glacial abrupt climate change has almost exclusively been investigated from a modelling perspective using intermediate or simpler complexity models. Interestingly, it would be desirable to reassess our results with more comprehensive models in the future when this is computationally affordable. In this line, the current model setup has been chosen so that the system resides close to a threshold associated with drastic changes in the oceanic circulation. The existence and location of such thresholds are model dependent. In addition, it is conceivable that small perturbations of a different origin could cause such a transition, assuming such perturbations are able to significantly affect density in the Nordic Seas area. Here, we have identified a mechanism which is consistent with proxy records by which abrupt climate change can be promoted through the idealised experiments exhibited. Up to now climate simulations focusing on abrupt climate changes have mainly been based on imposing freshwater fluctuations in the North Atlantic as reviewed by Kageyama et al. (2010). However, the sources of these freshwater fluxes have not yet been identified. Here, we propose such freshwater flux variations could be connected with rearrangements in the Nordic Seas sea-ice extent in response to $CO_2$ and Southern Ocean wind intensifications.

Our results confirm a recent study by Oka et al. (2012) suggesting that if the glacial climate were close to a threshold, small perturbations leading to a reduction in the sea-ice cover could have pushed the system across the latter. Through the sea-ice cover control of deep water formation, this provides an explanation for the different stability of the glacial AMOC compared to the present one, and thereby the different variability of glacial and interglacial periods (Marotzke, 2012).

Reconstructions suggest that during deglaciation, as well as throughout the last glacial period, $CO_2$ rises were primarily caused by the increase in deep upwelling in the Southern Ocean (Anderson et al., 2009). Models furthermore indicate that wind and $CO_2$ increases could themselves be the response to a previous North Atlantic cooling leading to a southward shift of the ITCZ and/or strengthening of the westerlies over the Southern Ocean (Chiang and Bitz, 2005; Lee et al., 2011; Timmermann et al., 2007). The oceanic explanation is that during stadial conditions, northward oceanic heat transport is strongly diminished in response to a weak overturning. As a consequence, the Southern Hemisphere warms at expense of the Northern Hemisphere through the bipolar seesaw effect. The tem-

perature asymmetry is thereby reduced and the ITCZ and the westerlies shift to the south and/or possibly strengthen. In this situation Southern Ocean westerlies are better aligned with the Antarctic Circumpolar Current (ACC). Within these conditions, atmospheric $CO_2$ levels increase in response to an oceanic upwelling intensification (Denton et al., 2010; Toggweiler and Lea, 2010). Alternatively, atmospheric models also indicate cooling in the North Atlantic (as would follow from a decrease in NADW formation and AMOC strength) leads to a southward shift of the ITCZ and Southern Ocean winds intensification, with a marginal southward shift, via atmospheric teleconnections leading to a rise in atmospheric $CO_2$ by 20-60 ppmv, consistent with proxy records (Lee et al., 2011). The upper limit is obtained when taking into account exclusively the physical process of increased outgassing of $CO_2$ due to enhanced upwelling; the lower limit includes as well the biological response to the increased upwelling. This results in an increase in surface nutrients which fuels biological productivity, thereby damping the atmospheric $CO_2$ rise and accounting for the smaller increase found previously by Menviel et al. (2008) and Tschumi et al. (2008).

According to our results, higher atmospheric $CO_2$ concentration and enhanced westerlies act to promote NADW formation over the Nordic Seas region through vital sea-ice variations which eventually enhance the meridional density gradient. Thus, the AMOC is intensified and thereby its associated northward oceanic heat transport. At this point, in the light of the above studies, the ITCZ would shift northward again and Southern westerlies progressively weaken, decreasing upwelling and atmospheric $CO_2$. This constitutes a negative feedback that favours the return into stadial conditions through an AMOC weakening, which would lead to enhanced westerlies and higher atmospheric $CO_2$ concentration. As a conclusion this suggests that D/O events could be part of an internal oscillation which involves changes in $CO_2$, surface winds and AMOC on millennial timescales.

# 3

# An interhemispheric mechanism for glacial abrupt climate change[2]

## 3.1 Introduction

Ice core records and marine sediments have revealed the existence of two types of abrupt climate changes operating throughout the last glacial period (ca. 110-10 kyr BP). Dansgaard-Oeschger (D/O) events show up as abrupt transitions from cold stadial to warm interstadial conditions, with warming in Greenland of up to 16 K (Lang et al., 1999; Landais et al., 2004; Huber et al., 2006) within a few decades followed by a gradual cooling phase lasting from several centuries to a few millennia which ends with a rapid return to stadial conditions (Dansgaard et al., 1993). Heinrich (H) events are identified as unusually high concentrations of ice-rafted debris in deep ocean sediment cores interpreted as iceberg discharges from the Laurentide ice-sheet into the North Atlantic coinciding with prolonged stadials (H stadials) and preceding the largest D/O events (Bond et al., 1992). The strong coupling between D/O and Antarctic warm (A) events indicates the existence of a climatic link operating between both hemispheres (Blunier and Brook, 2001). Models suggest this link is provided by changes in ocean heat transport through the bipolar seesaw effect (Stocker, 1998; Crowley, 1992) in response to reorganizations of the Atlantic meridional overturning circulation (AMOC) (Alley et al., 1999a). However, the ultimate causes of these oceanic reorganizations remain unclear.

Previous attempts to simulate D/O events have generally involved freshwater flux perturbations over the North Atlantic (Ganopolski and Rahmstorf, 2001)

[2] The main contents of this chapter are published in: Banderas, R., J. Alvarez-Solas, A. Robinson, and M. Montoya, 2015: An interhemispheric mechanism for glacial abrupt climate change. *Clim. Dyn.*, 44, 2897–2908, https://doi:10.1007/s00382-014-2211-8.

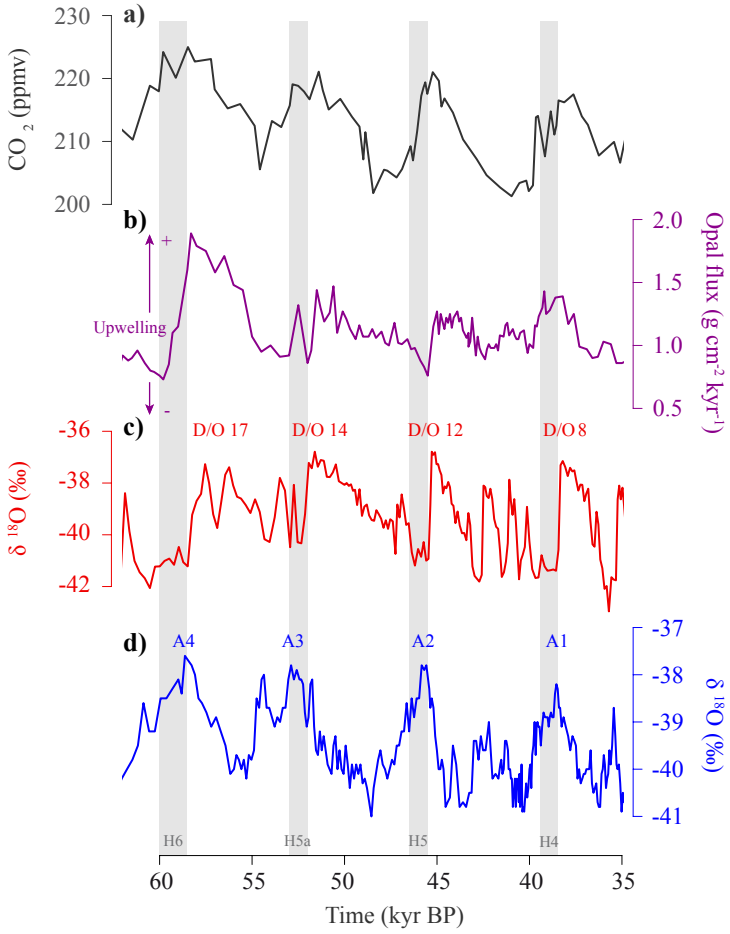


Fig. 3.1: Proxy records showing a global perspective of MIS 3 climate on the GISP2 time scale: **a)** atmospheric $CO_2$ concentration inferred from Byrd ice cores (Ahn and Brook, 2008); **b)** Opal flux proxy for upwelling in core TN057-14PC (51°59.059' S, 4°30.976' E, 3648 m) (Anderson et al., 2009); **c)** $\delta^{18}O_{ice}$ from the Greenland Ice Core Project 2 as a proxy of Greenland surface temperature (Blunier and Brook, 2001). The largest D/O events are labeled in red; **d)** $\delta^{18}O_{ice}$ from Byrd station, Antarctica (Blunier and Brook, 2001). Antarctic warm (A) events are denoted in blue. Vertical gray bars show the approximate timing of Heinrich events (H4-H6) (Rashid et al., 2003).

but the source of such a forcing has not been identified. Alternatively, episodes of abrupt warming in the North Atlantic could have been triggered from southern latitudes (Stocker, 2003). Model studies have shown that slowly varying background climate conditions in the Southern Ocean (SO) are capable of triggering a strong AMOC resumption leading to an abrupt warming in the North Atlantic (Knorr and Lohmann, 2003). The same result was found when applying gradual background climate changes from glacial to interglacial conditions on a global scale (Knorr and Lohmann, 2007). This led to the suggestion that fluctuations in atmospheric $CO_2$ concentration are a potential candidate for generating gradual climate variations that eventually favor abrupt warming in the North Atlantic (Barker and Knorr, 2007).

Ice core data indicate a close correspondence between atmospheric $CO_2$ variations and Antarctic temperature, with increases in both coinciding with H stadials and predating the largest D/O events (Ahn and Brook, 2008). Reconstructions show that during the last deglaciation, as well as throughout the last glacial period, $CO_2$ increases were concurrent with episodes of enhanced ventilation in the SO as inferred from opal flux records (Fig. 3.1). This has led to the interpretation that intervals of elevated $CO_2$ concentration would have resulted from increased wind-driven upwelling in the SO (Anderson et al., 2009). A wide variety of models indicate meridional migrations of the intertropical convergence zone (ITCZ) and the Southern Hemisphere (SH) mid-latitude jet in response to imposed high-latitude temperature changes in the North Atlantic (Chiang and Bitz, 2005; Ceppi et al., 2013), as would follow from variations in the AMOC strength. Thus, $CO_2$ increases during stadials could be the response to the preceding North Atlantic cooling. During stadial conditions, northward oceanic heat transport is expected to strongly decrease in response to a weak overturning. In this case, the SH warms at the expense of the Northern Hemisphere (NH) via the bipolar seesaw effect. The interhemispheric temperature asymmetry thereby decreases and the ITCZ and the SH westerlies shift to the south, improving their alignment with the Antarctic Circumpolar Current (ACC) (Toggweiler et al., 2006), and possibly strengthen. Both responses lead to increased upwelling via enhanced Ekman divergence (Toggweiler et al., 2006; Toggweiler and Samuels, 1995a) and thereby to higher atmospheric $CO_2$ levels (Lee et al., 2011; Toggweiler, 2009). This mechanism has been proposed to be relevant for ice age terminations and suggested to operate during stadial-interstadial transitions as well (Denton et al., 2010; Toggweiler and Lea, 2010).

Increasing atmospheric $CO_2$ and SO winds have recently been shown to trigger abrupt transitions from stadial to interstadial conditions via AMOC intensification (Banderas et al., 2012). In light of the above studies, the ITCZ would shift northward again leading to a weakening of the SO winds, decreased upwelling

and reduced atmospheric $CO_2$ levels in response to the AMOC strengthening. The return of the climate system to the stadial state would imply that glacial abrupt climate changes are part of an internal oscillation involving the AMOC, $CO_2$ and SO wind variations.

We herein investigate this hypothesis by performing a transient simulation of the glacial climate using a coupled climate model forced by prescribed atmospheric $CO_2$ and SO wind-stress variations in an idealized experimental design inspired by the characteristic climatic imprint of the SO during the last glacial period.

The paper is organized as follows: the model and experimental design are described in section 3.2. The mechanism by which the AMOC reacts to $CO_2$ and SO wind-stress variations and its climatic implications are presented in section 3.3. Two additional sensitivity experiments have been carried out in order to investigate the isolated effect of $CO_2$ and SO wind-stress variations. A freshwater flux experiment is also presented and compared to the main simulation. Finally, discussion and conclusions are given in section 3.4.

## 3.2 Model and experimental design

The model used in this study is the CLIMBER3-$\alpha$ climate model of intermediate complexity (Montoya et al., 2005). Its atmospheric component is a 2.5-dimensional statistical-dynamical model based on the assumption of a universal vertical structure of temperature and humidity in the atmosphere with a horizontal resolution of $7.5^\circ \times 22.5^\circ$. Its oceanic component contains the Geophysical Fluid Dynamics Laboratory (GFDL) MOM-3 ocean general circulation model, with a horizontal resolution of $3.75^\circ$ and 24 variably spaced vertical levels, and the ISIS thermodynamic-dynamic snow and sea-ice model. CLIMBER-3$\alpha$ satisfactorily describes the large-scale characteristics of the atmosphere, ocean and sea-ice on seasonal and longer time scales. Vegetation and other land-surface characteristics as well as river-runoff routing were unchanged with respect to the present-day control run (Montoya et al., 2005).

The simulations presented here stem from a previous climate simulation of the Last Glacial Maximum (Montoya and Levermann, 2008) (LGM, ca. 21 kyr BP), with boundary conditions following the specifications of the Paleoclimate Modeling Intercomparison Project Phase II (PMIP2), namely: changes in insolation, a reduced equivalent atmospheric $CO_2$ concentration of 167 ppmv to account for the lowered $CH_4$, $N_2O$ and $CO_2$ concentrations, the ICE-5G ice-sheet reconstruction (Peltier, 2004), and land-sea mask changes plus a global increase of salinity by 1 PSU to account for the $\sim$120 m sea-level lowering. Owing to the coarse resolution of its atmospheric component and to the simplified atmospheric dynamics,

the wind-field simulated by the model is not adequate to force the ocean. Thus, the surface wind-stress was prescribed to the Trenberth et al. (1989) climatology (Montoya et al., 2005). The sensitivity of the glacial AMOC to wind-stress strength was investigated by integrating the CLIMBER-3$\alpha$ model to equilibrium (Montoya and Levermann, 2008) with the surface wind-stress climatology multiplied globally by varying factors $\alpha \in [0.5, 2]$. At $\alpha = 1.7$ a threshold, associated with a drastic AMOC increase of more than 10 Sv and a northward shift of NADW formation north of the Greenland-Iceland Scotland (GIS) ridge, was found. We hypothesize herein that the glacial AMOC is close to this threshold. However, an equivalent atmospheric $CO_2$ level of 200 ppmv resulting from the higher $CH_4$, $N_2O$ and atmospheric $CO_2$ concentrations registered during MIS 3, when D/O events take place, has been imposed. The starting point for the experiment shown herein is thus the final equilibrium state of a glacial control climate simulation with $\alpha = 1.65$ and an equivalent atmospheric $CO_2$ level of 200 ppmv (Banderas et al., 2012).

The model was then forced by periodic variations of atmospheric $CO_2$ concentration and SO wind-stress. $CO_2$ forcing consists of linearly varying atmospheric $CO_2$ levels qualitatively resembling the characteristic saw-tooth shape of glacial $CO_2$ reconstructions. The SO wind-stress forcing is prescribed following an identical signal under the hypothesis that atmospheric $CO_2$ variations are the response to enhanced/reduced SO ventilation as a result of stronger/weaker winds (Figs. 3.1 and 3.2). To force the model we implicitly assume that a weak AMOC results in a linear increase both in atmospheric $CO_2$ concentration and SO wind-stress. The forcing is thus maintained until NADW formation resumes. The $CO_2$ and SO wind-stress forcing trends are then reversed in order to account for the hypothesized reduction in SO ventilation and $CO_2$ outgassing as a result of the AMOC reactivation. As explained below, this pushes the system into a new stadial state, leading to the onset of a new cycle. The model has been integrated in this way over 20 kyr. This procedure results in a forcing signal with the characteristic imprint of the SO climate during MIS 3 (Fig. 3.2).

## 3.3 Results

### 3.3.1 AMOC response to $CO_2$ and SO wind-stress variations

The AMOC is found to alternate between weak and strong circulation regimes in response to the imposed forcing cycle (Fig. 3.2). The meridional density gradient is known to extert a strong control of the AMOC strength. Therefore, the impact of $CO_2$ and SO wind-stress variations on the Atlantic densities is investigated in order to elucidate the causes of glacial abrupt climatic transitions.

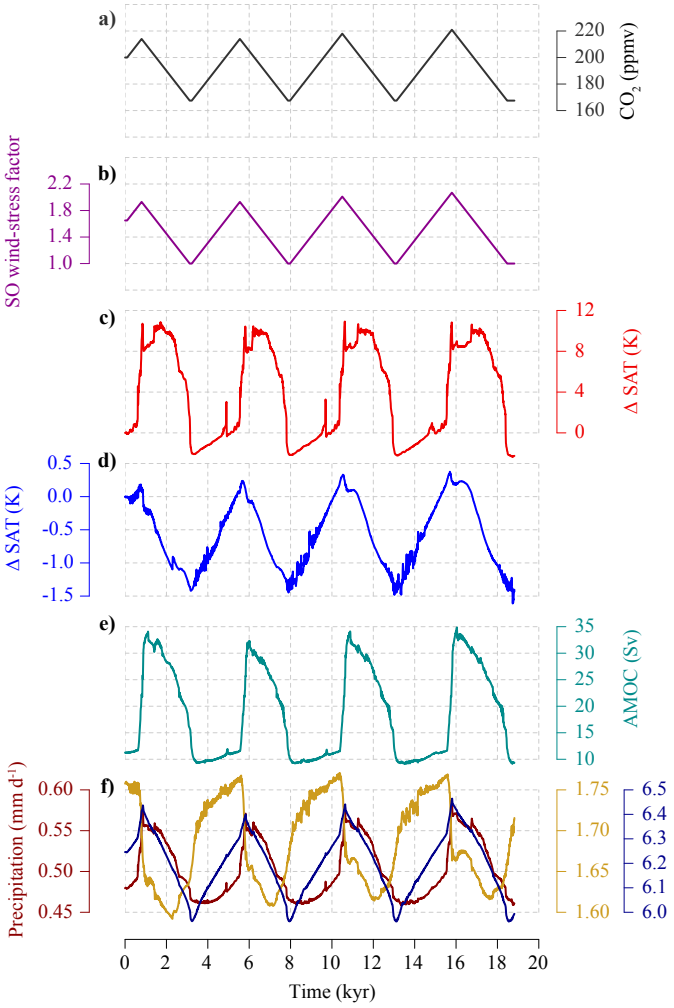


Fig. 3.2: Simulated MIS 3 climate. Time series of forcings and relevant climatic variables: **a)** $CO_2$ forcing in ppmv; **b)** Southern Ocean wind amplification factor (no units); **c)** anomalies of North Atlantic SAT (67.5°N 11°W, in the Nordic Seas) with respect to the initial state in K; **d)** anomalies of Antarctic SAT (86.2°S 11°E) with respect to the initial state in K; **e)** AMOC strength in Sv; **f)** precipitation in east Asia (34°N 101°E, close to the Hulu Cave, in dark red), southern Brazil (26°S 56°W, close to Caverna Botuverá, in gold) and in the West Equatorial Pacific (4°N 124°E, in dark blue) in mm day$^{-1}$.

Increasing atmospheric $CO_2$ levels cause gradual and moderate warming in the North Atlantic (i.e. nearly 2 K in two millennia) but also around Antarctica, where the bipolar seesaw effect during the stadial state contributes to increase Antarctic temperatures further. Enhancing wind-stress leads to an increase in deep upwelling in the SO that results in stronger outcropping and deepening of isopycnals, and thereby a decrease of Antarctic Intermediate Water (AAIW) density (Schewe and Levermann, 2010). These processes translate into a progressive decrease of density in the Atlantic basin that is more pronounced in the South Atlantic (Figs. 3.3 and 3.4). As a result, the meridional density gradient shows a gradual increase that leads to a slight AMOC intensification. Together with freshwater flux readjustments in the North Atlantic related to a northward migration of the sea ice front (Banderas et al., 2012), this favors an eventual resumption of NADW formation and facilitates a strong AMOC recovery by more than 25 Sv, leading the system to interstadial conditions (Figs. 3.3 and 3.4).

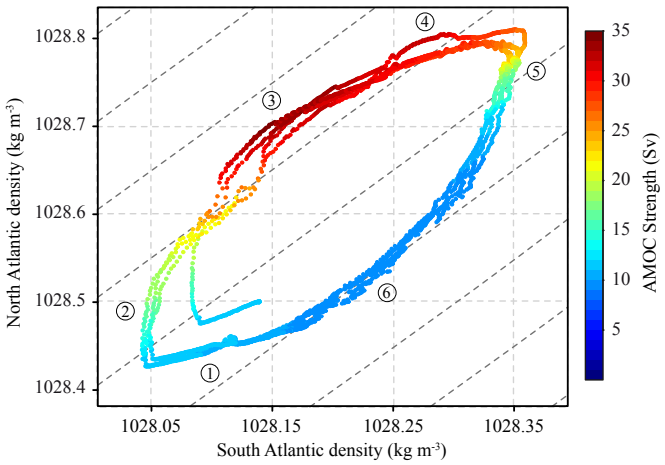


Fig. 3.3: AMOC trajectories and density changes of the Atlantic Ocean. AMOC strength (colors) as a function of density variations in the North Atlantic (35°N - 80°N, 60°W - 10°E, 750 - 1500 m depth; y-axis) and in the South Atlantic (30°S, 60°W - 10°E, 750 - 1500 m depth; x-axis). Dark gray dashed lines show isolines of the meridional density gradient between the North and the South Atlantic. Numbers refer to different states of the climate system: **(1)** Gradual increase of the meridional density gradient related to significant density decrease in the South Atlantic. Slight AMOC strengthening; **(2)** Abrupt transition from stadial to interstadial conditions essentially due to density increase in the North Atlantic. AMOC recovery; **(3)** Stable meridional density gradient. Strong AMOC; **(4)** Gradual decrease of the meridional density gradient related to significant density increase in the South Atlantic. Progressive AMOC slowdown; **(5)** Drastic reduction of NADW formation and AMOC strength. Abrupt transition to stadial conditions essentially due to density decrease in the North Atlantic; **(6)** Stable meridional density gradient. Weak AMOC.

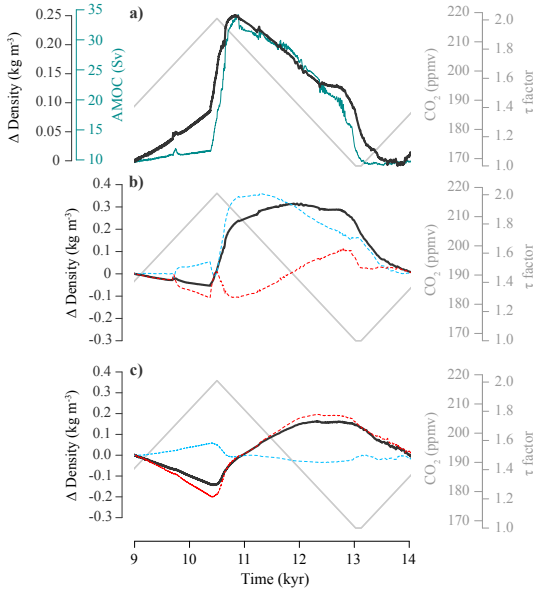


Fig. 3.4: North-south density variations. **a)** Temporal evolution of the meridional north-south density contrast (black) in kg $m^{-3}$, estimated as the density difference between the North Atlantic (35°N - 80°N, 60°W - 10°E, 750 - 1500 m depth) and the South Atlantic (30°S, 60°W - 10°E, 750 - 1500 m depth) relative to yr 9000 and AMOC strength (cyan) in Sv; **b)** anomalies of density (black) relative to the onset of the third cycle (yr 9000) and contributions to the latter by temperature (red) and salinity (blue) in the North Atlantic in kg $m^{-3}$; **c)** same fields as in b) in the South Atlantic. Gray curves show the representation of both $CO_2$ and SO wind-stress ($\tau$ factor) forcing trends.

A strong AMOC results in loss of heat in the SO and enhanced transport of salt into the Nordic Seas, that translate into a density increase both in the North and South Atlantic (Figs. 3.3 and 3.4). At this point, both forcing trends are reversed under the assumption that the reactivation of the AMOC would lead to reduced wind-driven upwelling in the SO, thus resulting in decreasing atmospheric $CO_2$ levels. Lower atmospheric $CO_2$ levels lead to global cooling. In the North Atlantic, this is partially counteracted by enhanced oceanic heat transport resulting from a vigorous AMOC. In the South Atlantic, however, the $CO_2$-induced decrease in temperature adds to the progressive cooling related to the bipolar seesaw effect. Additionally, decreasing wind-stress over the SO leads to reduced upwelling there. All in all, these processes result in a gradual density increase in the Atlantic which is more pronounced in the SH. The resulting meridional density gradient shows a progressive reduction which translates into a gradual AMOC slowdown (Figs. 3.3 and 3.4) that favors sea-ice regrowth in the

Nordic Seas and the southward migration of the polar front, leading to fresher surface waters in the area. This causes a drastic reduction of NADW formation and returns the AMOC to its stadial values. The wind and $CO_2$ forcing is then linearly increased again, leading the climate system to the onset of a new cycle (Figs. 3.2 and 3.3).

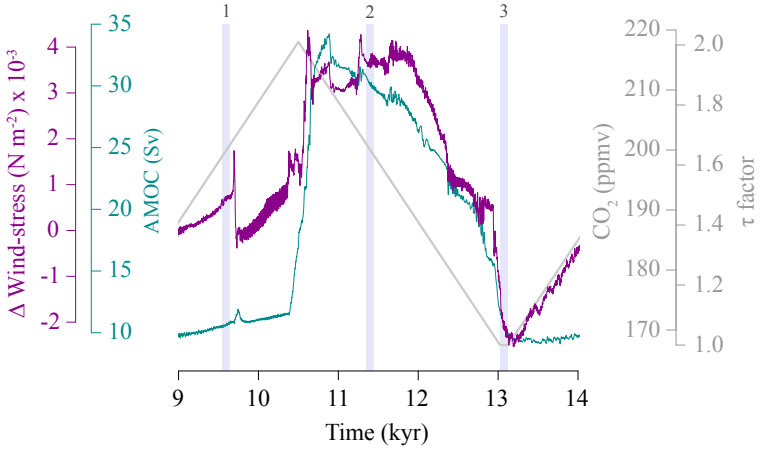


Fig. 3.5: Hysteresis. Anomalies of effective oceanic wind-stress (magenta) in the North Atlantic (35°N - 80°N, 60°W - 10°E) relative to yr 9000 in N $m^{-2}$ and AMOC strength (cyan) in Sv. Gray curve shows the representation of both $CO_2$ and SO wind-stress ($\tau$ factor) forcing trends. Vertical bars and numbers refer to different states of the climate system: **(1)** the state with the same forcing values as in the initial state (stadial conditions); **(2)** the same as (1) within interstadial conditions; **(3)** the state at which the climate system reaches stadial conditions again.

Note that the climate system does not return to stadial conditions when the forcings are decreased to their initial stadial values (Fig. 3.2). This reflects the existence of hysteresis of the AMOC with respect to the forcings as a result of the positive salinity advection feedback (Rahmstorf, 1996). In addition, the effective oceanic wind-stress is controlled by the sea-ice cover. Therefore, under interstadial conditions, both a strong AMOC and enhanced surface wind-driven currents as a result of the decreased sea-ice cover contribute to a positive feedback favoring the transport of salt to NADW formation sites (Fig. 3.5). The existence of hysteresis plays an important role in modulating the amplitude of the oscillation over the SO, as warming and cooling phases over Antarctica are regulated by the duration of stadials and interstadials through the bipolar seesaw. In other words, the existence of hysteresis provides inertia to the system, so that it does not simply

react to the forcing cycle in a linear way and determines, together with the bipolar seesaw effect, the antiphase climatic relationship between the North and the South Atlantic. Therefore, transitions between stadial and interstadial regimes can be explained as a result of crossing the identified threshold of the AMOC through changes in the meridional density gradient in response to the forcing cycle.

### 3.3.2 Climatic implications

The alternation between stadial and interstadial oceanic circulation regimes results in an interhemispheric climatic connection that reproduces several major features of glacial millennial-scale climate variability registered by proxies. The evolution of the Nordic Seas surface air temperature (SAT) shows four abrupt oscillations that are accompanied by gradual temperature variations in Antarctica. The shape and timing of both patterns closely resemble the four largest D/O and A events that took place during the last glacial period (Figs. 3.1 and 3.2).

Stadial conditions are characterized by a minimum in NH temperatures, gradual warming in the SH and reduced AMOC (Fig. 3.2). The subsequent AMOC recovery translates into an abrupt temperature increase in the Nordic Seas by more than 10 K, while Antarctica initially cools down in response to the bipolar seesaw (Fig. 3.2). Interstadial conditions consist of relatively mild temperatures in the NH, gradual cooling in the SH and a vigorous AMOC. The nearly stable warm phase in the Nordic Seas SAT lasting several centuries can be explained by the counteracting effects of lower atmospheric $CO_2$ levels leading to global cooling and the enhanced oceanic heat transport resulting from a vigorous AMOC. The transition into a new stadial phase is characterized by a progressive AMOC reduction which eventually leads to an abrupt temperature decline back to stadial conditions in the Nordic Seas, while Antarctic SAT shows a gradual warming in response to the weakening of the AMOC.

The signal of millennial-scale climatic events can also be identified far from high latitudes (Fig. 3.2). The simulated east Asian precipitation closely follows the Nordic Seas SAT while precipitation in southern Brazil shows an antiphase behavior with respect to that simulated in eastern Asia as a result of meridional shifts of the ITCZ during stadial-interstadial transitions. The time evolution of the simulated precipitation in the vicinity of the western equatorial Pacific (WEP) region clearly reflects the Antarctic-style temperature variability. Thus, the global imprint of the Antarctic climate can also be found in our simulation.

### 3.3.3 Sensitivity experiments: the isolated effect of $CO_2$ and SO wind variations

Two sensitivity experiments have been carried out in order to explore the role of the isolated contributions of $CO_2$ ($CO_2$-only) and SO wind-stress (wind-only) variations (Fig. 3.6). Both have been designed following a similar experimental setup as in the main run ($CO_2$+wind).

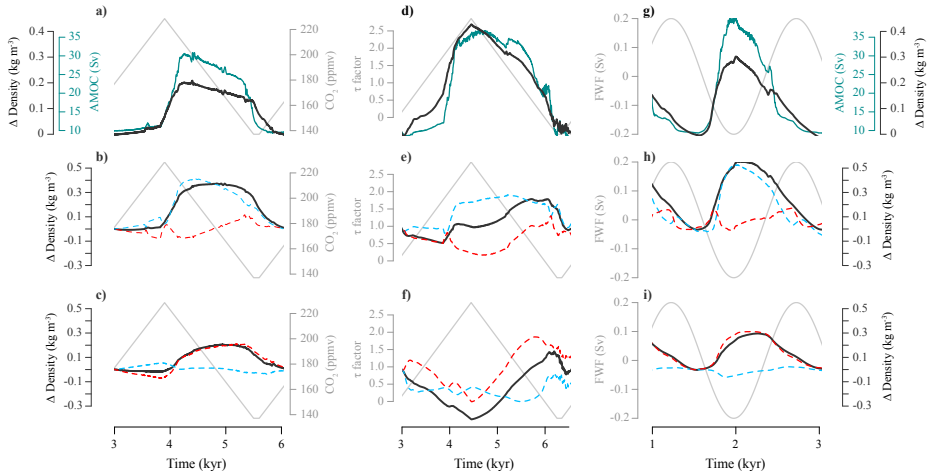


Fig. 3.6: North-south density variations for the isolated contributions of $CO_2$, SO wind-stress and FWF. **a)** Temporal evolution of the meridional north-south density contrast (black) in kg $m^{-3}$, estimated as the density difference between the North Atlantic (35°N - 80°N, 60°W - 10°E, 750 - 1500 m depth) and the South Atlantic (30°S, 60°W - 10°E, 750 - 1500 m depth) and AMOC strength (cyan) in Sv for the $CO_2$-only experiment; **b)** anomalies of density (black) and contributions to the latter by temperature (red) and salinity (blue) in the North Atlantic in kg $m^{-3}$; **c)** same fields as in b) in the South Atlantic. **d-f)** and **g-i)** Same information for the wind-only and hosing experiments, respectively. Gray curves show the representation of the forcing trends.

In the $CO_2$-only experiment, increasing atmospheric $CO_2$ levels contributes to warmer and more saline water both in the North and the South Atlantic. In the North Atlantic, the increase in salinity dominates over warming. This results in a density increase which favors convection in the Nordic Seas (Banderas et al., 2012). Density is found to decrease slightly in the South Atlantic. As a result, the meridional density gradient gradually increases leading to a slight AMOC strengthening (Figs. 3.6 and 3.7).

Under the wind-only scenario, enhancing SO wind-stress leads to an increase in deep upwelling that results in stronger outcropping and deepening of isopycnals

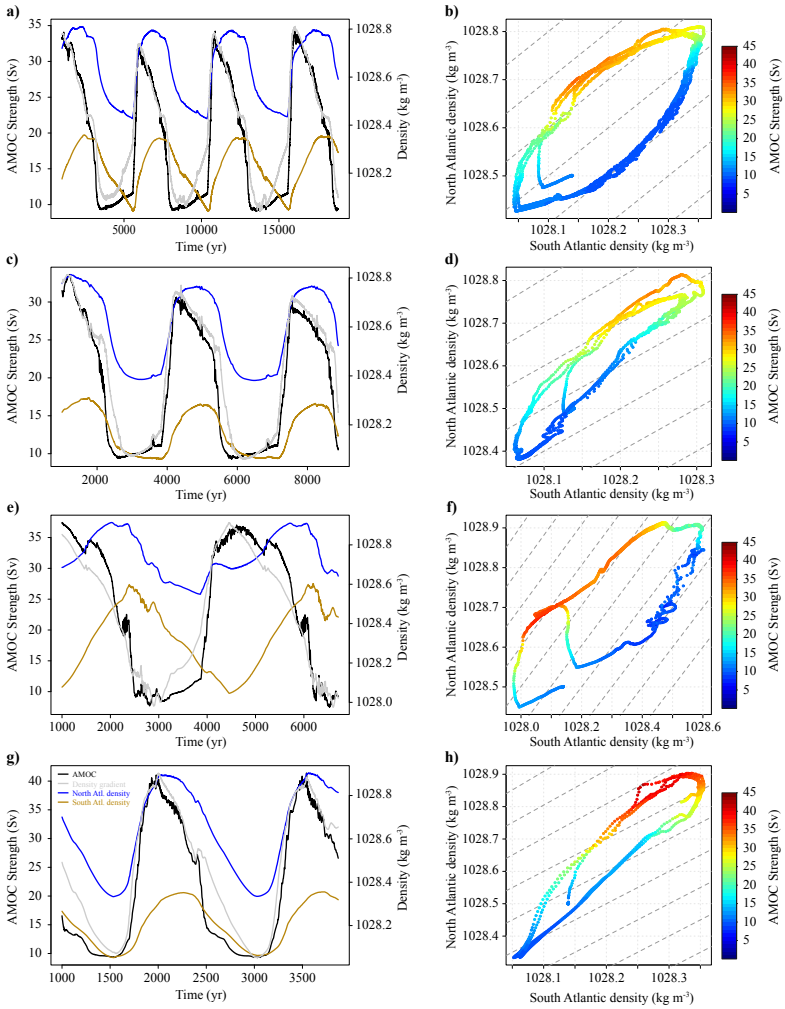


Fig. 3.7: AMOC trajectories and density changes of the Atlantic Ocean. **a)** Temporal evolution of the meridional north-south density contrast (gray) in kg $m^{-3}$ for the main experiment, estimated as the density difference between the North Atlantic (35°N - 80°N, 60°W - 10°E, 750 - 1500 m depth) and the South Atlantic (30°S, 60°W - 10°E, 750 - 1500 m depth), AMOC strength (black) in Sv and evolution of density in the North Atlantic (dark blue) and in the South Atlantic (gold) in kg $m^{-3}$; **b)** AMOC strength (colors) as a function of density variations in the North Atlantic (x-axis) and in the South Atlantic (y-axis). Dark gray dahsed lines show equal values of the meridional density gradient; **c-d)**, **e-f)** and **g-h)** same information for the $CO_2$-only, wind-only and FWF experiment, respectively.

(Schewe and Levermann, 2010). This adds to the Antarctic warming caused by the bipolar seesaw effect during the stadial phase, resulting in a gradual density decrease in the South Atlantic that causes an increase in the meridional density gradient and thus an initial slight AMOC strengthening (Figs. 3.6 and 3.7).

In both cases, a drastic increase of the meridional density gradient results in a strong AMOC recovery once convection is triggered (Figs. 3.6 and 3.7). At this moment the forcing trends are reversed and the AMOC is found to weaken. The first phase of the AMOC weakening is associated with a decrease in the meridional density gradient that mainly results from the density increase in the South Atlantic related to cooling through the bipolar seesaw effect. In the North Atlantic, the density increase is attenuated by the opposing effects of temperature and salinity (Figs. 3.6 and 3.7). In the $CO_2$-only experiment, density in the South Atlantic further increases due to cooling induced by the reduced $CO_2$ levels (Fig. 3.6) that is transmitted into the subsurface, leading to a continuous decrease of the meridional density gradient and thus to a significant AMOC slowdown (Figs. 3.6 and 3.7). Under the wind-only scenario, reduced wind-stress over the SO leads to decreased deep upwelling that results in an increase of Antarctic Intermediate Water (AAIW) density. As a result, the meridional density gradient gradually decreases leading to a slowdown of the AMOC (Figs. 3.6 and 3.7). In both experiments North Atlantic cooling translates into a southward migration of the summer sea-ice polar front which contributes to freshen convective sites in the Nordic Seas via sea-ice melting. This eventually results in a large reduction of NADW formation.

The threshold identified in the climate system by which the strength of the AMOC changes as a result of reorganizations of the meridional density gradient is also reachable under the two new sensitivity scenarios. Note, however, that in both cases, the forcing rates and amplitudes at which the transition is found are higher than in the main experiment. This indicates that both contribute in the same sense in order to push the climate system into a different regime.

### 3.3.4 AMOC response to freshwater flux in the Nordic Seas

A freshwater flux (FWF) scenario has also been included to study the classical bipolar seesaw without accounting for the effects of $CO_2$ and SO wind-stress variations in the climate system. A periodic FWF anomaly has been imposed in the Nordic Seas (70°N - 80°N, 15°W - 15°E) with amplitude of 0.2 Sv and period of 1500 yr (Fig. 3.6). Negative freshwater flux input into the Nordic Seas causes salinity to increase in the North Atlantic leading to a rapid start of vigorous convection. Denser waters related to salinity increase support the formation of NADW and favors the AMOC to strengthen. South Atlantic density increases as well in response to cooling associated to the bipolar seesaw effect. The increase

of salinity in the North Atlantic dominates the interhemispheric density balance leading to a rapid intensification of the meridional desity gradient which results in a strong AMOC resumption (Figs. 3.6 and 3.7). Enhanced northward salinity transport from the tropics and the subtropical South Atlantic as a result of the AMOC stengthening provides an additional source of salt to the North Atlantic which keeps the system into interstadial conditions through the positive salt-advection feedback. The meridional density gradient starts to decrease when the forcing cycle is reversed causing a progressive AMOC weakening (Figs. 3.6 and 3.7). While North Atlantic density is reduced in response to the positive freshwater flux input into the Nordic Seas, density in the South Atlantic decreases as a result of warming associated to the bipolar seesaw effect. The transition into stadial conditions takes place when the decrease in North Atlantic density is sufficient to inhibit NADW formation in the Nordic Seas, causing a strong AMOC reduction.

The pivotal role of the North Atlantic in controlling abrupt transitions in the FWF scneario can be identified in the trajectory diagram (Fig. 3.7), where significant changes in the AMOC strength follow nearly-vertical displacements in the meridional density gradient space. This translates into a narrower width of the loop in the meridional density gradient space with respect to both experiments including SO wind-stress variations. This indicates that although the implication of the SO does not represent a necessary condition for triggering glacial abrupt climate change, its role contributes to facilitate stadial to interstadial transitions and vice-versa without the need to invoke freshwater fluxes.

## 3.4 Conclusions and discussion

We have shown that the characteristic instability of the last glacial climate can be simulated as a result of AMOC reorganizations originating from changes in the meridional density gradient in response to prescribed variations in atmospheric $CO_2$ concentration and SO wind-stress. The scaling relationship between the meridional density gradient and the AMOC strength was postulated long ago in conceptual models (Stommel, 1961; Rooth, 1982; Gnanadesikan, 1999) and subsequently confirmed in comprehensive ocean general circulation models (OGCMs) (e.g. Rahmstorf, 1996). Our experiments provide a plausible explanation for the driver of such changes.

Although our mechanism gathers processes of very different characteristic times (e.g. atmospheric teleconnections, sea ice migrations and large-scale oceanic circulation), its time scale is ultimately determined by the time needed by the meridional density gradient for triggering major AMOC reorganizations. Density changes in the South Atlantic are more gradual than in the North Atlantic

where they are found to be more abrupt during transitions. The character of millennial-scale climate variability registered in proxies worldwide can therefore be interpreted as the result of an integral signal that accounts for gradual changes in the SH plus the abrupt imprint provided by changes in the NH.

Several studies suggest that the East Asian Monsoon region was tightly connected to the North Atlantic climate during the last deglaciation and the last glacial period (Wang et al., 2001). The oxygen isotope record of stalagmites from the Hulu Cave (32°30'N 119°10'E, east Asia), interpreted as a proxy of precipitation, shows a close resemblance to $\delta^{18}$O values from Greenland ice cores, indicating that interstadial and stadial intervals in the North Atlantic nearly coincided with wet and dry episodes in East China, respectively (Wang et al., 2001). On the contrary, the same record at Caverna Botuverá (27°13'S 49°09'W, southern Brazil) evidences an antiphase relationship (Wang et al., 2007). This is consistent with a more recent study from the Santiago Cave (3°1'S 78°9'W, western Amazonia in Ecuador) showing a tight correspondence between nearly all the D/O warming events in the North Atlantic and dry episodes in the Amazon basin (Mosblech et al., 2012). Proxy records from the equatorial Pacific furthermore show a similar behavior to Antarctic temperature variability on millennial time scales, suggesting that the Antarctic climate signal was globally pervasive during the last glacial period (Barker and Knorr, 2007). Our results are consistent with all of these records. This good agreement arises, in part, from the suitable representation of the simulated bipolar seesaw of the AMOC. However, the novelty of this work is that such a characteristic bipolar seesaw pattern shown in previous studies can be triggered by $CO_2$ and SO wind-stress changes without using freshwater forcings (e.g. Liu et al., 2009; Menviel et al., 2014) of doubtful origin.

Although our experimental setup consists of an externally-forced oscillation involving $CO_2$ and SO wind-stress variations, the underlying idea of this study is that $CO_2$, SO winds and the AMOC are coupled in such a way that the proposed interhemispheric oscillation could be an internal solution of the real climate system that promotes abrupt climatic transitions. During prolonged stadials, a weak AMOC translates into warming of the SH at the expense of the NH. The southward shift in the atmospheric circulation patterns favors upwelling and thereby outgassing of $CO_2$. This results in gradual global warming and, eventually, in an abrupt transition from stadial to interstadial conditions associated with the resumption of NADW formation. The AMOC recovery maintains the NH in a warm phase while the SH gradually cools down following the bipolar seesaw mechanism. In this situation the atmospheric circulation patterns migrate northward reducing atmospheric $CO_2$ levels and SO winds and helping to revert the climate system back to the stadial state, thus starting the cycle again (Fig. 3.8). The assessment of the internal nature of the mechanism presented here would require

the use of a climate model accounting for an interactive carbon cycle module and a more comprehensive atmospheric component.

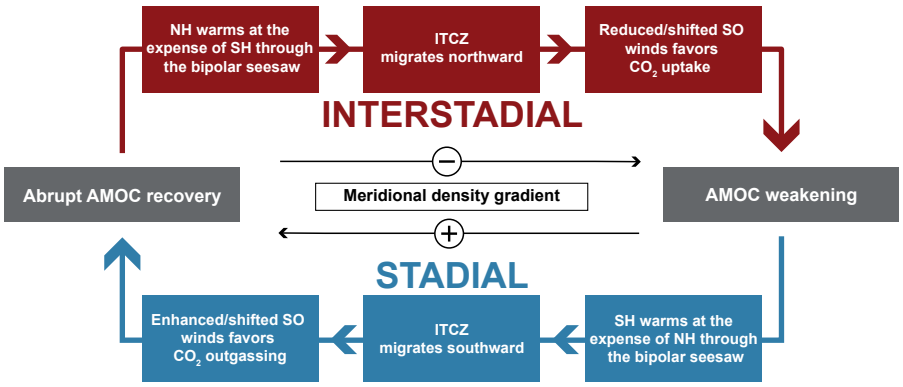


Fig. 3.8: Schematic of the glacial oscillatory mechanism.

An important caveat of this study is that our setup is based on the assumption that $CO_2$ variations were caused by enhanced wind-driven upwelling in the SO (Anderson et al., 2009). Recent findings indicate that disruptions in the glacial biological pump could also operate in concert with wind-driven upwelling to produce millennial-scale $CO_2$ oscillations (Martínez-García et al., 2014). As suggested by Anderson et al. (2009), increased buoyancy forcing (Watson and Naveira Garabato, 2006) might actually be necessary together with the enhanced wind-stress in order to account for the upwelling intensification. An increase in the northward Ekman transport leading to a steepening of the isopycnals would result in an increase in the baroclinicity of the ACC leading to an intensification of the southward eddy transport that could partially offset the increased northward Ekman transport (e.g. Hallberg and Gnanadesikan (2006)). Recent studies with eddy-permitting and eddy-resolving models indicate this *eddy compensation* could depend strongly on how surface buoyancy fluxes are affected, with increased surface buoyancy flux in response to increased wind-stress leading to a larger sensitivity than previously thought (Abernathey et al., 2011). This is a fundamental matter currently subject of active research but still unaffordable for millennial-scale simulations. A shift or increase of the SO winds could also affect wind-driven mixing there. The deep SO is responsible for a large fraction

of global diapycnal mixing (Watson and Naveira Garabato, 2006, and references therein) that is generated almost entirely over restricted regions of rough bottom topography below the ACC through the interaction of its deep-reaching flow and its associated eddies with the sea floor (Watson et al., 2013). If the westerly winds shifted south or strengthened, the mixing of heat and freshwater into the deep ocean would most probably increase.

Our mechanism does not preclude the existence of others that could help to trigger glacial abrupt climate changes. These include advection of salinity anomalies from the tropics induced by tropical teleconnections (Krebs and Timmermann, 2007), SO warming (Knorr and Lohmann, 2003), gradual global warming (Knorr and Lohmann, 2007) and sea-ice reorganizations in the North Atlantic (Li et al., 2010; Dokken et al., 2013; Petersen et al., 2013). In addition, changes in the location and strength of the SO westerlies could also contribute indirectly. For example, Antarctic sea ice has been proposed to act as a physical barrier to freshwater input to the deep SO at glacial periods by advecting freshwater northward until it melts north of the polar front, thus in a region disconnected from the deep ocean (Keeling and Stephens, 2001). In this way brine rejection during sea-ice formation and sea-ice export would both act to densify the deep ocean at glacial times. A south-shifted westerly wind belt would shift sea-ice formation and export southward and thereby de-densify the deep SO, which would contribute to the resumption of the AMOC via an increase in the meridional density gradient (Liu et al., 2009).

To conclude, we have identified a new mechanism for triggering glacial abrupt climate changes that brings together the bipolar seesaw effect, its impact on atmospheric reorganizations and their feedback on the oceanic circulation, which is consistent with widespread climatic proxies, and provides an explanation of the enigmatic pervasive Antarctic influence.

Our results represent an attractive challenge for the paleoclimate community. The study of proxy records could confirm that interhemispheric changes in density underlie glacial abrupt climate change. Furthermore, in the light of the diagrams shown in Fig. 3.7, the existence of high-resolution sea-water density proxies for both the North and the South Atlantic would allow to discern the ultimate mechanism for D/O events.

# 4

# A new approach for simulating the paleo evolution of the Northern Hemisphere ice sheets[3]

## 4.1 Introduction

The climate history of the late Quaternary is marked by alternating episodes of growth and decay of Northern Hemisphere (NH) ice sheets on orbital time scales as evidenced by different proxy data (e.g. Hays et al., 1976; Imbrie et al., 1992). Geological and geomorphological data show that during the Last Glacial Period (LGP, ca. 110-10 ka BP) large fractions of North America and Eurasia were covered by ice sheets that reached their maximum extent and volume at the Last Glacial Maximum (LGM, ca. 21 ka BP; e.g. Clark and Mix, 2002; Dyke et al., 2002; Svendsen et al., 2004). Sea level reconstructions derived from coral dating (Bard et al., 1996) as well as from the isotopic signal recorded in marine sediments (Bond et al., 1993; Waelbroeck et al., 2002; Rohling et al., 2009; Grant et al., 2012) show substantial variations as a result of the waxing and waning of ice sheets, with differences relative to the present roughly ranging between +6 m at the maximum of the Last Interglacial (ca. 125 ka BP) and -130 m at the LGM (note the present is meant here and after to indicate preindustrial conditions).

In addition to proxy data, glacial isostatic adjustment (GIA) models have been used to reconstruct the past temporal evolution of ice sheets (Peltier and Andrews, 1976). By inverting relative sea-level records and accounting for the isostatic deformation of the solid Earth in response to ice-mass changes and re-distributions, these models have facilitated estimation of the global ice volume at the LGM (Yokoyama et al., 2000; Milne et al., 2002) and reconstruction of

[3] The main contents of this chapter are published in: Banderas, R., J. Alvarez-Solas, A. Robinson, and M. Montoya, 2018: A new approach for simulating the paleo evolution of the Northern Hemisphere ice sheets. *Geosci. Model Dev.*, https://doi.org/10.5194/gmd-2017-158.

the sea-level equivalent (SLE) ice volume throughout different intervals around this period (Lambeck et al., 2000; Lambeck and Chappell, 2001; Lambeck et al., 2002, 2014). Recently they have been refined by applying additional constraints based on the available global positioning system (GPS) measurements of vertical motion of the Earth's crust. This technique has been used to simulate the spatial configuration of ice sheets during the last deglaciation (Peltier et al., 2015). However, GIA models fail to provide a unique solution for the temporal history of ice thickness.

Forward ice-sheet modelling can help overcome the intrinsic limitations of the GIA technique by directly simulating the paleo evolution of ice sheets. Ideally, Earth System Models (ESMs) including fully coupled ice-sheet components are the appropriate tools to simulate the past, as well as the present and future evolution of ice sheets. However, because of their high computational cost, the long-term simulation of ice sheets generally relies on simpler tools such as intermediate complexity climate models coupled to ice-sheet models (e.g. Deblonde and Peltier, 1991; Marsiat, 1994; Peltier and Marshall, 1995; Bonelli et al., 2009; Langebroek et al., 2009; Ganopolski and Calov, 2011; Goelzer et al., 2016).

An alternative and even simpler method is to use ice-sheet models forced offline by a time-varying climatology. These exercises are carried out on a regular basis, as they are needed to calibrate ice-sheet models, to assess model sensitivity to different parameters, and to compare the sensitivities of different models. To obtain adequate initial conditions for the ice sheet, a relatively long spin-up is required, involving one or more glacial cycles depending on the ice sheets involved. Because of the lack of continuous, spatially well distributed proxy data, a synthetic time-varying climatology is often built based on a combination of climate-model and proxy data and used to force the ice-sheet model. Often an index approach is followed in which temperature anomalies relative to present are calculated by combining a simulated glacial-interglacial climatic anomaly field, interpolated through an index derived from the Greenland ice-core temperature reconstruction, with present-day climatologies. A similar procedure is applied to precipitation but considering ratios rather than anomalies (e.g. Marshall et al., 2000, 2002; Charbit et al., 2002, 2007; Zweck and Huybrechts, 2005).

Zweck and Huybrechts (2005) suggested that until fully coupled, comprehensive ice-sheet and climate models are available, this index approach is probably the best method to simulate the long-term evolution of ice sheets. However, an important drawback of this approach is that it clearly misrepresents climate variability at millennial timescales. The reason for this is that the spatial glacial-interglacial anomaly field used is associated with orbital climatic variations, while it is scaled following the characteristic time evolution of the index, which includes orbital and millennial-scale climate variability. The spatial patterns of orbital and

millennial variability are clearly not the same, as indicated by a wealth of models and data (see Section 4.3). As a result, this method can be expected to lead to a misrepresentation of climate variability and thus of the past evolution of NH ice sheets.

Here we illustrate the problems derived from this approach, and propose a new offline climate forcing method that attempts to better represent the characteristic pattern of millennial-scale climate variability. Ice core records (e.g. Dansgaard et al., 1993; NGRIP members, 2004) as well as a wide range of coupled climate models (Ganopolski and Rahmstorf, 2001; Menviel et al., 2014; Peltier and Vettoretti, 2014; Banderas et al., 2015; Zhang et al., 2014, 2017) suggest that millennial scale variability during the LGP was associated with the transition between two different climatic regimes: a stadial and an interstadial state that differ in the location and/or strength of North Atlantic Deep Water (NADW) formation. Here we assume the stadial state represents the background glacial climate at the LGM, with NADW formation south of Iceland, and include the interstadial state as an additional independent snapshot that represents a millennial-scale excitation away from the background state as a result of a northward shift and intensification of NADW formation. A synthetic time-varying temperature climatology is built by combining present-day observations, the simulated LGM anomalies relative to present, scaled by an orbital-timescale index, and the simulated stadial-interstadial anomalies, scaled by a millennial-timescale index. An important, model-dependent issue is the extent to which the orbital and millennial-scale anomaly fields are well captured, in particular their amplitudes. To account for this, a refinement of the method is proposed consisting in a scaling of both temperature anomalies, orbital and millennial. We then compare the effect of the synthetic climatologies built through the three methods on the simulated evolution of NH ice sheets throughout the last glacial cycle.

The paper is organized as follows: in Section 4.2 the ice-sheet model and the three climate forcing methods used are described. In Section 4.3 the results of applying these methods to force the ice-sheet model are shown, and their capability to simulate the evolution of the NH ice-sheets during the last glacial cycle is compared. Finally, the main conclusions are summarised in Section 4.4.

## 4.2 Methodology

### 4.2.1 The ice-sheet model description

The model used in this study is the GRISLI ice-sheet model, developed by Ritz et al. (2001). GRISLI has been used in a number of studies in different domains including Antarctica (Ritz et al., 2001; Philippon et al., 2006; Alvarez-Solas et al.,

2011a), Greenland (Quiquet et al., 2012, 2013), and glacial NH ice sheets (Peyaud et al., 2007; Alvarez-Solas et al., 2011b, 2013). For this reason and because the focus of our study is the climate forcing used to drive the model, only a brief description is given here; further details about the model can be found in these previous studies.

GRISLI is a hybrid three-dimensional thermomechanical ice-sheet model combining the Shallow Ice Approximation (SIA, Hutter, 1983) for grounded ice and the Shallow Shelf Approximation (SSA, MacAyeal, 1989) for ice shelves and ice streams. In this model configuration, inland ice that is frozen to the bed is treated using SIA dynamics. When the base of the ice sheet becomes temperate (ie, there is water at the base), or when the ice is floating, then SSA dynamics apply. The basal friction ($\boldsymbol{\tau}_b$) is calculated as a linear function of the basal velocity ($\mathbf{u}_b$) that is proportional to effective pressure ($N_{\text{eff}}$): $\boldsymbol{\tau}_b = C N_{\text{eff}} \cdot \mathbf{u}_b$ (see Table 5.1 to check the exact value of basal dragging coefficient $C$). GRISLI uses finite differences on a staggered Cartesian grid at a 40 km resolution, corresponding to 224×208 grid points for the NH domain, with 21 vertical levels. Initial topographic conditions are provided by present surface and bedrock elevations built from the ETOPO1 dataset (Amante and Eakins, 2009) and ice thickness (Bamber et al., 2001). Boundary conditions include the surface mass balance (SMB) and basal melting. The SMB is given by the sum of accumulation and ablation, both of which are calculated from monthly surface air temperatures (SATs) and monthly total precipitation. As these variables are strongly influenced by topographic effects, GRISLI accounts for changes in elevation at each time step considering a linear atmospheric vertical profile for temperature with different lapse rates in summer and in the annual mean to account for the smaller summer atmospheric vertical stability (Table 4.1) (Ohmura and Reeh, 1991), and an exponential dependency of precipitation on temperature. Accumulation is calculated by assuming that the fraction of solid precipitation is proportional to the fraction of the year with mean daily temperature below 2°C. The daily temperature is computed from monthly SATs assuming that the annual temperature cycle follows a cosine function. Ablation is calculated using the positive-degree-day (PDD) method (Reeh, 1989). All PDD parameters are kept constant in all simulations over the entire domain (see Table 4.1 for the exact parameter values).

Note that as indicated by Bauer and Ganopolski (2017), using fix PDD factors it is not possible to realistically simulate the glacial evolution of the NH ice sheets in coupled climate - ice-sheet models. The reason being that the increase of $CO_2$ and insolation after the LGM is not efficient enough to satisfactorily simulate the deglaciation when using a PDD approach. Here, and for all the index methods, the deglaciation is explicitly driven by an imposed increase in temperatures, thus the mentioned problem does not appear. Nevertheless, our goal is not to provide the

Table 4.1: Key ice sheet model and climate forcing parameters.

| Parameter | Value [units] |
|---|---|
| Basal dragging coefficient | C = 20 [$10^{-5}$ yr $m^{-1}$] |
| Calving threshold | $H_{calv}$ = 200 [m] |
| Conversion factor PDDs to melt for snow | $f_{PDD_{snow}}$ = 0.003 [mwe/PDD] |
| Conversion factor PDDs to melt for ice | $f_{PDD_{ice}}$ = 0.008 [mwe/PDD] |
| Standard deviation of near-surface temperature | $\sigma$ = 5 [K] |
| Annual lapse rate | $\Gamma_{tann}$ = 0.0080 [K $m^{-1}$] |
| Summer lapse rate | $\Gamma_{tsum}$ = 0.0065 [K $m^{-1}$] |

most realistic simulation, which should include coupling with the climate system, higher resolution, and a better representation of surface mass balance processes, but rather to highlight and overcome an important deficiency of current offline methods. Basal melting inland is determined through a recent reconstruction of the present-day geothermal heat flux (Shapiro and Ritzwoller, 2004), while in the ocean it is set to a fixed value of 2 m $a^{-1}$ in regions where depth is larger than 450 m and fixed to 0 m $a^{-1}$ in shallower areas to favour the growth of ice sheets during cold periods. Increasing background basal melting values modulates the response of NH ice sheets to millennial-scale forcing. A more detailed analysis of the effect of oceanic changes on NH ice sheets will be addressed in future work.

### 4.2.2 The forcing methods

Synthetic time-varying climatologies are built using three different methods. All three use a perturbative approach as explained above (Section 1) by combining the present-day (PD) climatology obtained from observational data with simulated climate snapshots of the last glacial cycle and a time dependent index derived from proxy records. In all cases the indices used were built based on two recent complementary temperature reconstructions over Greenland (Figure 4.1): one from the NGRIP ice-core record for the LGP (Kindler et al., 2014), and another one from several ice-core records for the Holocene (Vinther et al., 2009). Their combination (hereafter, the KV reconstruction) results in a continuous temperature reconstruction over Greenland for the past 120 kyr (Figure 4.1a).

The present-day climatology (Figure 4.2a-c) is taken from the ERA-INTERIM reanalysis (Dee et al., 2011). The climatic snapshots (Figure 4.2d-i) are obtained from climate simulations performed with the CLIMBER-3$\alpha$ model (Montoya and Levermann, 2008; Banderas et al., 2015, see Sections 4.2.2-4.2.2). Due to the relatively low resolution of the atmospheric model (7.5° × 22.5°; latitude × longitude), we perform a two-step interpolation procedure to obtain the forcing

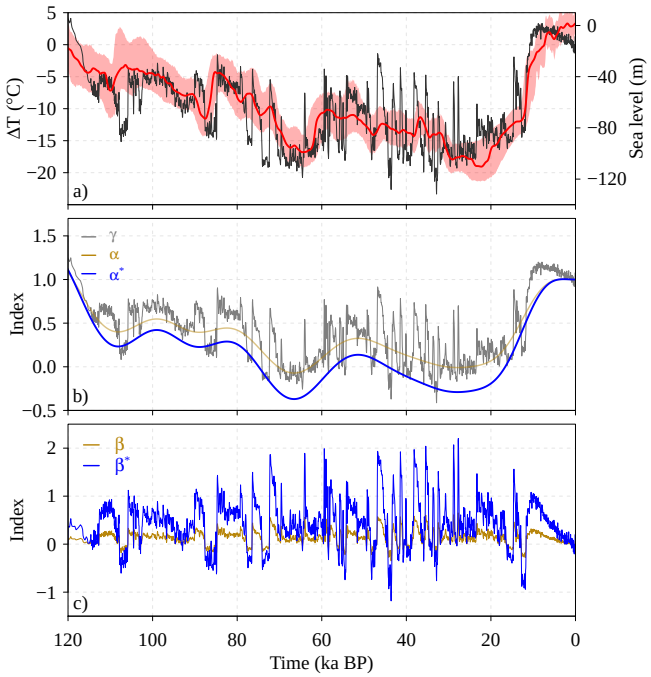


Fig. 4.1: Temporal components of the three forcing methods: **a)** Sea level forcing (m) as estimated by Grant et al. (2012). The light red shaded area represents the 95% confidence level interval of the prescribed sea level reconstruction. The black curve shows the evolution of temperature anomalies (°C) relative to present over Greenland from which the index is derived (Vinther et al., 2009; Kindler et al., 2014); **b)** Index used in M1 ($\gamma$; gray) together with the orbital components of the indices used in M2 ($\alpha$; gold) and M3 ($\alpha^\star$; blue), respectively; **c)** Millennial components of the index used in M2 ($\beta$; gold) and M3 ($\beta^\star$; blue), respectively.

fields at the resolution of the ice-sheet model. First, the fields were interpolated conservatively to the ice-sheet model grid. Then, to eliminate artefacts related to model resolution, Gaussian smoothing (also conservative) was applied with a standard deviation of 250 km. Several smoothing windows were tested, with the final choice representing the minimum amount of smoothing necessary to ensure that sharp boundaries between the atmospheric grid cells could not be distinguished on the ice sheet model grid. The resulting anomalies with respect to present have been corrected by elevation using the ICE-5G topography (Peltier, 2004). Oceanic temperatures are fixed in all experiments to present-day values to ensure that any ice sheet changes are exclusively due to the atmospheric forcing. Finally, sea-level variations are prescribed according to the reconstruction by

Grant et al. (2012, Figure 4.1a). The specific details of each method are described below.

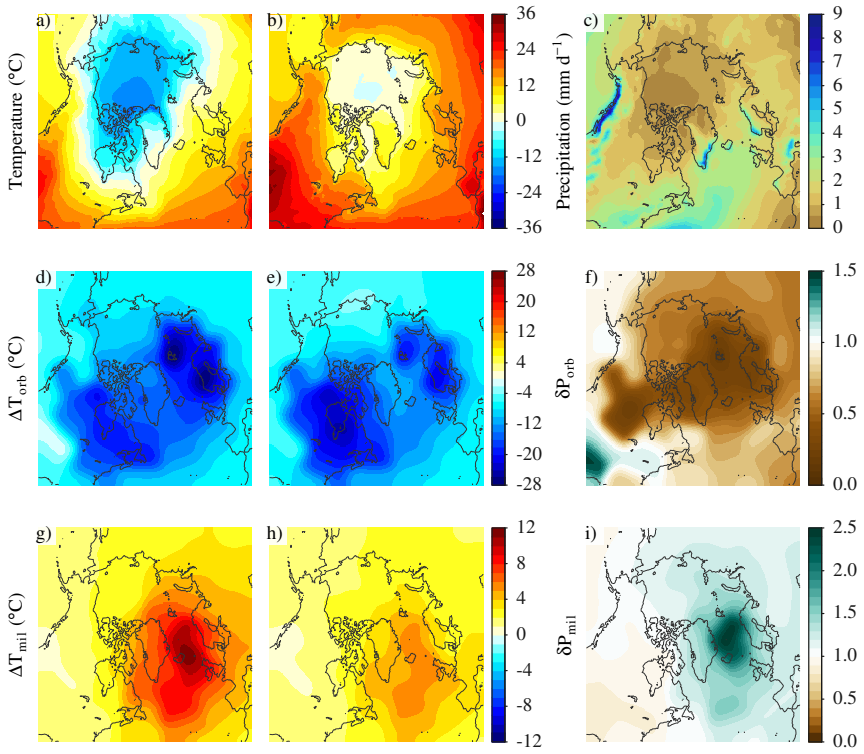


Fig. 4.2: Spatial components of the different methods. The reference climate is based on the ERA-INTERIM (1981-2010) reanalysis (Dee et al., 2011) and consists of: **a)** annual SAT (°C); **b)** summer (JJA) SAT (°C) and **c)** annual precipitation (mm d$^{-1}$). The orbital component of the spatial forcing comprises the anomalies between the LGM and the present-day climates obtained from the CLIMBER-3$\alpha$ model (Montoya and Levermann, 2008): **d)** annual SAT (°C), **e)** summer (JJA) SAT (°C) and **f)** annual precipitation ratio ($\delta P_{\mathrm{orb}} = P_{\mathrm{lgm}}/P_{\mathrm{pd}}$). Panels **g)**, **h)** and **i)** show the same fields as in **d)**, **e)** and **f)** for the millennial component of the spatial forcing generated from the combination of the Is and the St climatic states simulated by CLIMBER-3$\alpha$ (Banderas et al., 2012, 2015). All variables have been corrected by elevation assuming a linear vertical atmospheric profile (see Section 4.2.1).

### Method 1

The first method (hereafter M1) follows the usual index approach used in many previous studies (Marshall et al., 2000, 2002; Charbit et al., 2002, 2007; Zweck and Huybrechts, 2005). The time-varying temperature and precipitation are given by

$$\boldsymbol{T}(t) = \boldsymbol{T}_0 + (1 - \gamma(t)) \cdot \boldsymbol{\Delta T}_{\text{orb}} \tag{4.1}$$

$$\boldsymbol{P}(t) = \boldsymbol{P}_0 \cdot [\gamma(t) + (1 - \gamma(t)) \cdot \delta \boldsymbol{P}_{\text{orb}}] \tag{4.2}$$

where $\boldsymbol{T}_0$ and $\boldsymbol{P}_0$ are the ERA-INTERIM present-day temperature and precipitation climatologies (Figure 4.2a-c), and $\boldsymbol{\Delta T}_{\text{orb}} = \boldsymbol{T}_{\text{lgm}} - \boldsymbol{T}_{\text{pd}}$ and $\delta \boldsymbol{P}_{\text{orb}} = \boldsymbol{P}_{\text{lgm}} / \boldsymbol{P}_{\text{pd}}$ are the orbital temperature anomaly and precipitation ratio relative to the present day, respectively, obtained from equilibrium simulations for the preindustrial and LGM climates performed with the CLIMBER-3$\alpha$ model (Figure 4.2d-f, Montoya and Levermann, 2008). Bold symbols indicate two-dimensional spatial fields. $\gamma$ is the time index, based on the KV reconstruction, normalized between 0 and 1 for the LGM and the present-day, respectively (Figure 4.1a). Thus, the index dictates the timing of both orbital and millennial-scale variability. Note that the $\gamma$ index can be defined as here (Charbit et al., 2007) or instead as a glacial index (1-$\gamma$) that is 0 for the present and 1 for the LGM (e.g. Marshall et al., 2000, 2002; Zweck and Huybrechts, 2005).

### Method 2

The second method (M2) is similar to M1 but the temperature and precipitation variability are split into two spectral components, corresponding to orbital and millennial timescales, respectively. The time-varying climatology is now given by

$$\boldsymbol{T}(t) = \boldsymbol{T}_0 + (1 - \alpha(t)) \cdot \boldsymbol{\Delta T}_{\text{orb}} + \beta(t) \cdot \boldsymbol{\Delta T}_{\text{mil}} \tag{4.3}$$

$$\boldsymbol{P}(t) = \boldsymbol{P}_0 \cdot \{\alpha(t) + (1 - \alpha(t)) \cdot \delta \boldsymbol{P}_{\text{orb}} \cdot [(1 - \beta(t)) + \beta(t) \cdot \delta \boldsymbol{P}_{\text{mil}}]\} \tag{4.4}$$

Here $\boldsymbol{\Delta T}_{\text{orb}}$ and $\delta \boldsymbol{P}_{\text{orb}}$ are as in M1, and $\boldsymbol{\Delta T}_{\text{mil}} = \boldsymbol{T}_{\text{is}} - \boldsymbol{T}_{\text{st}}$ and $\delta \boldsymbol{P}_{\text{mil}} = \boldsymbol{P}_{\text{is}} / \boldsymbol{P}_{\text{st}}$ are the millennial temperature anomaly and precipitation ratio, respectively, for the interstadial relative to the stadial state. The stadial mode in our study is represented by the aforementioned LGM climate simulation with CLIMBER-3$\alpha$ (Montoya and Levermann, 2008), while the interstadial mode (Figure 4.2g-i) is taken from a transient simulation performed with the same model under glacial climatic conditions, but with intensified NADW formation (Banderas et al., 2015). Finally, $\alpha$ and $\beta$ are two indices that separately modulate the contribution of the orbital and millennial anomalies (Figure 4.1). $\alpha$ is obtained

after applying a low-pass frequency filter ($f_c = 1/18$ kyr$^{-1}$) based on a spectral decomposition to the original KV reconstruction and normalising the resulting signal to be consistent with the forcing equations (Eqs. 4.3 and 4.4); $\beta$ is obtained following a similar procedure but retaining the high frequency signal of the KV reconstruction. Thus $\gamma = \alpha + \beta$. Inspection of equations 4.1 and 4.3 shows that the difference between M1 and M2 is just

$$\beta(t) \cdot \boldsymbol{\Delta T}_{\mathrm{mil}} + \beta(t) \cdot \boldsymbol{\Delta} T_{\mathrm{orb}} = \beta(t) \cdot (\boldsymbol{T}_{\mathrm{is}} - \boldsymbol{T}_{\mathrm{pd}}) \tag{4.5}$$

that is, the difference between the interstadial and the present-day simulated fields, scaled by the millennial-scale $\beta$ index.

### Method 3

M2 significantly underestimates the amplitudes of millennial-scale fluctuations at the NGRIP ice-core location, as compared to the KV reconstruction (see Figure 4.3 and section 4.3.1). This is a consequence of the attenuated magnitude of the orbital (LGM minus present-day) and, particularly, the millennial (interstadial minus stadial) temperature anomalies simulated by the CLIMBER-3$\alpha$ model.

To correct for this, method 3 (M3) introduces a refinement with respect to M2 that consists of an adjustment to the time-varying climatology in such a way that the resulting synthetic temperature time series at the NGRIP site exactly matches the KV reconstruction (Figure 4.3a). To this end, two additional amplification factors ($f_{\mathrm{orb}}$, $f_{\mathrm{mil}}$) are included in the equation that governs the temperature forcing (Eq. 4.6). Each factor is given by the ratio of the corresponding temperature anomaly component of the KV reconstruction (either orbital, $\Delta T^{KV}_{\mathrm{orb}}$, or millennial $\Delta T^{KV}_{\mathrm{mil}}$) to the corresponding temperature anomaly component simulated by the climate model at the NGRIP location ($\Delta T_{\mathrm{orb}}$(NGRIP), $\Delta T_{\mathrm{mil}}$(NGRIP)), respectively. We thus have:

$$\boldsymbol{T}(t) = \boldsymbol{T}_0 + (1 - \alpha(t)) \cdot \boldsymbol{\Delta T}_{\mathrm{orb}} \cdot f_{\mathrm{orb}} + \beta(t) \cdot \boldsymbol{\Delta T}_{\mathrm{mil}} \cdot f_{\mathrm{mil}} \tag{4.6}$$

where

$$f_{\mathrm{orb}} = \frac{\Delta T^{KV}_{\mathrm{orb}}}{\Delta T_{\mathrm{orb}}(\mathrm{NGRIP})} \tag{4.7}$$

and

$$f_{\mathrm{mil}} = \frac{\Delta T^{KV}_{\mathrm{mil}}}{\Delta T_{\mathrm{mil}}(\mathrm{NGRIP})} \tag{4.8}$$

Here, $\Delta T^{KV}_{\mathrm{orb}}$ represents the temperature difference between the PD and the LGM in the orbital component of the KV reconstruction whereas $\Delta T^{KV}_{\mathrm{mil}}$ is the

maximum temperature amplitude of the millennial-scale component of the KV reconstruction.

$$\Delta T_{\mathrm{orb}}(\mathrm{NGRIP}) = T_{\mathrm{lgm}}(\mathrm{NGRIP}) - \mathrm{T}_{\mathrm{pd}}(\mathrm{NGRIP}) \tag{4.9}$$

$$\Delta T_{\mathrm{mil}}(\mathrm{NGRIP}) = T_{\mathrm{is}}(\mathrm{NGRIP}) - \mathrm{T}_{\mathrm{st}}(\mathrm{NGRIP}) \tag{4.10}$$

are, as in M2, the simulated orbital and millennial-scale temperature anomaly fields of Montoya and Levermann (2008) and Banderas et al. (2015), respectively, evaluated at the NGRIP ice-core location. This tuning to the NGRIP KV reconstruction (Figure 4.3) also introduces a scaling of the synthetic temperature amplitudes elsewhere.

Finally, in order to keep the same structure as in the previous methods, the amplification factors are both included within the so-called optimized indices ($\alpha^\star$, $\beta^\star$). Thus

$$\boldsymbol{T}(t) = \boldsymbol{T}_0 + (1 - \alpha^\star(t)) \cdot \boldsymbol{\Delta T}_{\mathrm{orb}} + \beta^\star(t) \cdot \boldsymbol{\Delta T}_{\mathrm{mil}} \tag{4.11}$$

$$\boldsymbol{P}(t) = \boldsymbol{P}_0 \cdot \{\alpha^\star(t) + (1 - \alpha^\star(t)) \cdot \delta \boldsymbol{P}_{\mathrm{orb}} \cdot [(1 - \beta^\star(t)) + \beta^\star(t) \cdot \delta \boldsymbol{P}_{\mathrm{mil}}]\} \tag{4.12}$$

with

$$\alpha^\star(t) = 1 - (1 - \alpha(t)) \cdot \frac{\Delta T^{KV}_{\mathrm{orb}}}{\Delta T_{\mathrm{orb}}(\mathrm{NGRIP})} \tag{4.13}$$

$$\beta^\star(t) = \beta(t) \cdot \frac{\Delta T^{KV}_{\mathrm{mil}}}{\Delta T_{\mathrm{mil}}(\mathrm{NGRIP})} \tag{4.14}$$

The amplification factors reflect the skill of the climate model to reproduce the characteristic spectral amplitudes of the KV reconstruction at the NGRIP site. Since the model tends to underestimate the KV reconstruction, $\alpha^\star$ and $\beta^\star$ are both found to increase the amplitudes of the orbital and millennial-scale fluctuations, respectively, relative to the original $\alpha$ and $\beta$ indices (Figure 4.1b, c).

## 4.3 Results

### 4.3.1 Reconstruction of the NH climate

To evaluate the capability of the different methods to provide a realistic forcing for the ice-sheet model, the resulting synthetic climatologies should be compared against reconstructions. However, continuous, high resolution NH temperature reconstructions spanning the entire last glacial cycle are scarce. We now compare the performance of each method in regions where proxies are available (see

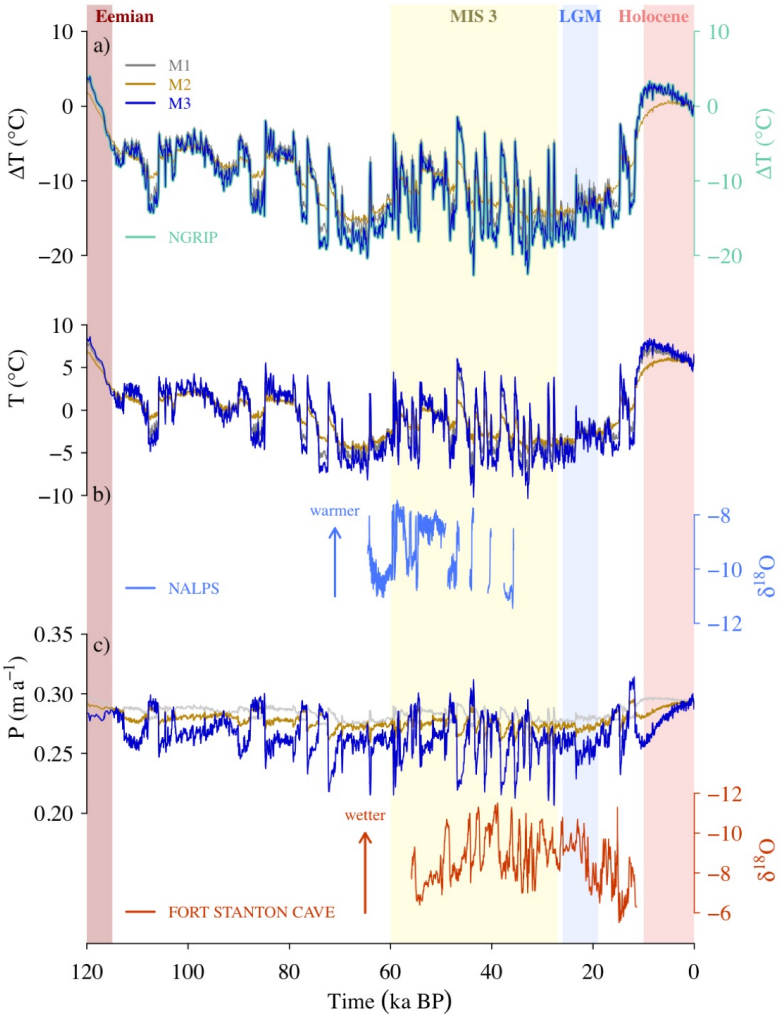


Fig. 4.3: **a)** Temporal evolution of SAT anomalies (°C) at the NGRIP site (75.1°N, 42.32°W) relative to present day obtained in M1 (gray), M2 (gold) and M3 (blue) as compared to the KV (light green) temperature reconstruction (Vinther et al., 2009; Kindler et al., 2014). **b)** Temporal evolution of SAT (°C) in central Europe from the three methods together with $\delta^{18}$O (‰ SMOW) variations inferred from stalagmites of northern European Alps (47.38°N, 10.15°E) as a proxy for air temperature (Moseley et al., 2014). **c)** Temporal evolution of precipitation (m $a^{-1}$) in southwestern North America from the three methods together with $\delta^{18}$O (‰ VPDB) variations registered in Fort Stanton Cave (33.3°N, 105.3°W) as a proxy for precipitation (Asmerom et al., 2010). Note the reversed axis in $\delta^{18}$O to facilitate the interpretation of this panel. Vertical colored bars indicate key periods of the past 120 kyr BP.

locations in Figure 4.4a). Then we discuss the specific features of each method in continental regions that are relevant for ice-sheet growth even though reconstructions are not available.

We first compare the synthetic temperature curves generated in the location of the NGRIP ice-core using each method to the KV reconstruction (Figure 4.3a). M1 shows an almost perfect agreement with the KV reconstruction. This is due to the fact that the temperature evolution is dictated by $\gamma$ alone, which comes from the NGRIP record, and that the absolute amplitude, given by the LGM minus present temperature anomaly simulated by the CLIMBER-3$\alpha$ model, at the NGRIP location turns out to be very similar to the glacial-interglacial temperature amplitude ($\sim$ 15 K) of the KV reconstruction (Eq. 4.1 and Figures 4.1 and 4.2). In contrast, M2 strongly underestimates the amplitude of the KV reconstruction, particularly at millennial time scales. The reason for this is that the amplitude of stadial-interstadial temperature changes simulated by the CLIMBER-3$\alpha$ model at the NGRIP location ($\sim$ 7 K) is smaller than those indicated by the KV reconstruction (up to 16.5 K). In the model actually the maximum temperature anomaly is placed over the Nordic seas, as opposed to off the southeast coast of Greenland, the location where glacial abrupt climate changes are thought to reach their maximum amplitude in terms of temperature (Voelker and Workshop Participants, 2002). Meanwhile, the exact agreement in the temperature evolution between M3 and the KV reconstruction is predetermined by construction (Section 4.2.2).

We further evaluate the three methods through comparison with available temperature and precipitation reconstructions derived from speleothems in Central Europe (the Alps) and North America. Time series of SAT in central Europe show an overall qualitative agreement among all three methods (Figure 5.3b), which reproduce the phasing and timing of millennial-scale climate variability registered in terrestrial records from the northern European Alps (Moseley et al., 2014). Nevertheless, there are important quantitative differences among the three methods, with M3 showing the SAT changes with the largest amplitudes, followed by M1, and M2 the smallest ones. Furthermore, the simulated temporal evolution of precipitation in southwestern North America reveals important differences among the methods. In particular, M1 follows the Greenland ice-core temperature evolution with a relatively small amplitude. However M2, and most notably M3 with a much larger amplitude, show an antiphase relationship with respect to simulated precipitation in M1 (and temperature) on millennial time scales (Figure 5.3c). The reason for this lies in the differences that exist within the spatial patterns of orbital and millennial scale climate variability in this particular region. While the millennial-scale pattern shows slightly wetter conditions during the stadial (i.e. colder climate) as compared to the interstadial

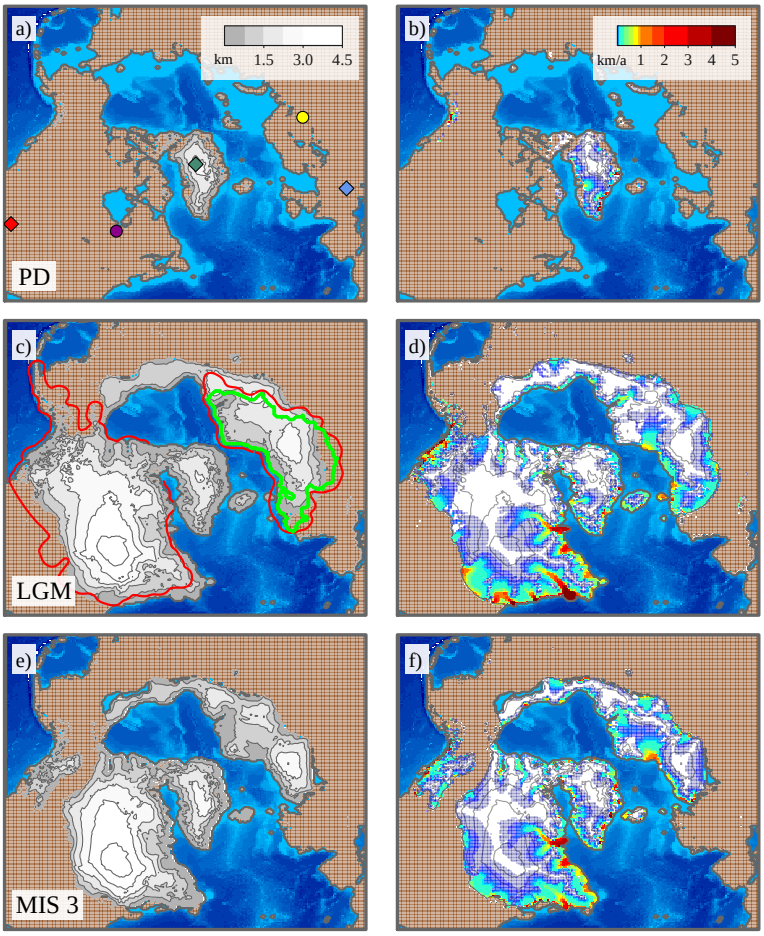


Fig. 4.4: NH ice-sheet configurations at different stages of the last glacial-interglacial period as simulated under M3: **a)** present-day ice thickness (km) and **b)** present-day ice velocities (km $a^{-1}$). Panels **c)-d)** and **e)-f)** show the same information as **a)-b)** for the LGM and MIS3 stages, respectively. Red and green contours in panel **c)** represent the ICE-5G (Peltier, 2004) and DATED-1 (Hughes et al., 2016) extent of NH ice sheets at the LGM (Peltier, 2004), respectively. Colored diamonds (proxy-based information) in panel **a)** show the approximate locations of the NGRIP site (light green), Fort Stanton Cave (red) and NALPS stalagmites (light blue), respectively. Colored dots (proxy-based reconstructions unavailable) show the locations of the two central sites considered at the LIS (purple) and the FIS (yellow).

($\delta P_{\mathrm{mil}} < 1$) in southwestern North America, the orbital spatial pattern exhibits slightly drier conditions at the LGM (i.e. colder climate) as compared to PD conditions ($\delta P_{\mathrm{orb}} < 1$). Available proxy information indicates that increased precipitation in this area is associated with NH cooling (Asmerom et al., 2010) as opposed to the pervasive NH signal inferred to a wealth of records (Wang et al. 2001; NGRIP members, 2004) which evidences that wetter conditions generally occur during interstadials. Thus, M3 successfully reproduces precipitation variability as interpreted by proxies in this particular region, a result that cannot be achieved by means of the usual index approach.

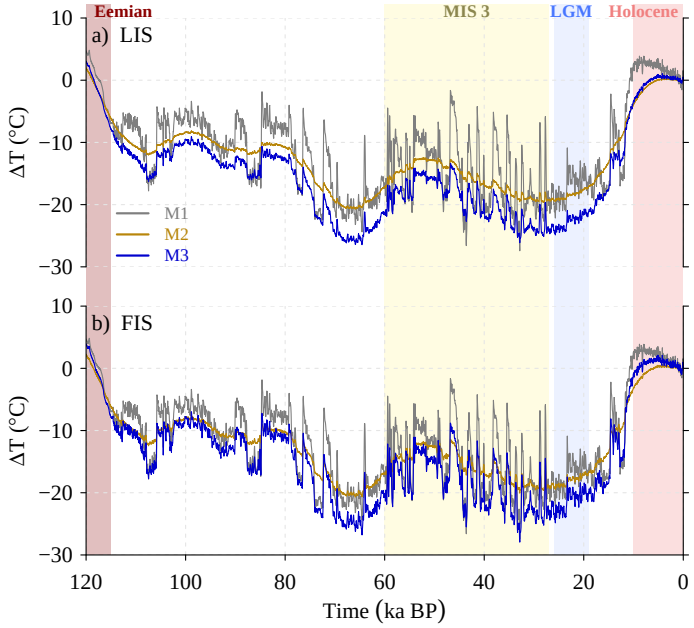


Fig. 4.5: Temporal evolution of SAT anomalies (°C) relative to present day reconstructed under M1 (gray), M2 (gold) and M3 (blue) scenarios at two central locations of the LIS and the FIS in: **a)** North America and **b)** Eurasia. Vertical colored bars indicate key periods of the past 120 kyr BP.

The lack of continuous reconstructions in NH continental areas hampers the evaluation of the temperature signal derived from the three methods. Nonetheless, the synthetic temperature timeseries obtained in two sites, in North America and Fennoscandia, respectively, are assessed (Figure 4.5). These sites correspond to areas covered by the Laurentide (LIS) and the Fennoscandian (FIS) ice sheets during the LGP, respectively (see locations in Figure 4.4a). Several aspects stand

out that can be traced back to the structural differences among the methods. First, at orbital time scales, the temperature variations obtained by all methods in both sites show warmer climate conditions at the Eemian (ca. 125 ka BP) with respect to the Holocene (10 ka BP to present day) and colder temperatures throughout the LGP. By construction, M1 and M2 are identical at these time scales, while in M3 the orbital amplitude is larger, resulting in temperatures 2-5 K colder throughout most of the LGP. Second, at millennial time scales, the amplitudes of the temperature variations obtained with the three methods are very different in both locations. M1 and M2 show the largest and smallest amplitudes, respectively, with differences above 10 K in the most prominent transitions. As previously discussed, M1 and M2 differ only at the millennial scale, by an amount given by Eq. 4.5. Thus the difference between these two methods resides in the difference between the orbital and the millennial scale temperature anomaly fields used in M1 and M2, respectively, scaled by the $\beta$ index. This boils down to the difference between the present-day and the interstadial temperature fields used in M1 and M2, respectively. These generally result in much larger positive deviations in M1 that, as will be shown below, affect the ice growth. M3 shows variations with intermediate temperature amplitudes between M1 and M2, reflecting the fact that, even with the refined scaling, the amplitude of the millennial temperature anomaly at these sites is much lower than the orbital one (Figure 4.2d, g).

Finally, in M1 the amplitude of millennial scale fluctuations is very similar in both sites as a consequence of the nearly-symmetric temperature pattern around Greenland, with two centers of negative values of similar amplitude coinciding with the selected sites (Figure 4.2d). In contrast, in M2, and most notably in M3, the differences between the two sites are larger, with larger amplitudes in the FIS than in the LIS site. This is a consequence of the more asymmetric millennial scale temperature anomaly, characterized by a single centre of positive values in the Nordic seas (Figure 4.2g).

### 4.3.2 Reconstruction of NH ice-sheets

The temporal evolutions of the simulated NH ice sheets that result from imposing the different forcings to the GRISLI model all show the characteristic modulation by orbital climate variability over the last glacial cycle (Figure 4.6). Ice volume increases from 120 ka BP throughout the LGP until around 20 ka BP, where it reaches its maximum value, subsequently decreasing throughout the Holocene until the present day.

Important differences are found among the three methods. For all ice sheets, M1 and M3 show the smallest and largest volumes throughout the LGP, respectively; M2 shows intermediate values between the two. As a consequence, of all

three methods only M3 agrees with the available LGM minus present SLE reconstructions within their ranges of uncertainties, both for the LIS and the FIS. As mentioned before, by construction, the climates of M1 and M2 are identical at orbital timescales, only differ at millennial timescales. The lower ice volume in M1 relative to M2 is due to the larger amplitude of its millennial-scale fluctuations, resulting from the large amplitude of its orbital spatial component. Indeed, the orbital anomalies used by stardard index methods to represent millennial changes are larger than the millennial-scale anomalies. Thus the forcing and the response are overestimated. Although these sometimes lead to smaller temperatures with respect to the orbital background curve, in general they result in large positive anomalies that, through enhanced ablation, induce a disruption of the growth of large ice sheets in the NH. In contrast, at millennial timescales M2 shows a muted response of ice-volume variations in all ice sheets as a result of the small amplitude of its millennial-scale component. Finally, the higher volumes in M3 compared to M2 are a result of tuning to the lower NGRIP temperature, that results in colder temperatures throughout most of the LGP in the NH (Figure 4.5), despite its larger millennial-scale temperature fluctuations. The temperature fluctuations in M3 incorporate both the larger orbital and the smaller millennial amplitude fluctuations compared to M1.

Throughout the LGP, differences in global SLE between the most extreme ice-volume cases, M1 and M3, are generally larger for the LIS, than for the FIS. Regarding the evolution of the LIS, M2 resembles M1 more than M3, but for the evolution of the FIS, M2 resembles more M3 than M1. Around 48 ka BP M1 shows a large ice-volume drop in the FIS that has no counterpart in the LIS (Figure 4.6c). M2, in contrast, shows a more gradual evolution. Since the difference between M1 and M2 is exclusively their millennial scale variability, this would suggest a more important role of their differential millennial scale variability in the FIS than in the LIS site. However, a simple explanation in terms of local temperature is not possible: at millennial timescales, the temperature difference between M1 and M2 (or M3) is actually smaller for the FIS than for the LIS (Figure 4.5). From 60-40 ka, the FIS ice volume shows a similar evolution in M1 and M3, with large sub-orbital ice-volume variability and decreasing trend compared to M2 that can be related to the strong millennial scale variability after D/O event number 14, around 60 ka. The large drop in the FIS ice volume in M1 at 48 ka BP appears to be linked to D/O event number 12, possibly that with the highest amplitude in the whole LGP. However this D/O event appears both in M1 and M3, and in the latter case it barely has an impact. Thus, a nonlinear response must be invoked to explain the larger impact of millennial-scale variability in M1 in the FIS. Since the magnitudes of the warmings at the LIS and the FIS sites in M1 associated to this D/O are very similar, one possibility is that the lower ice

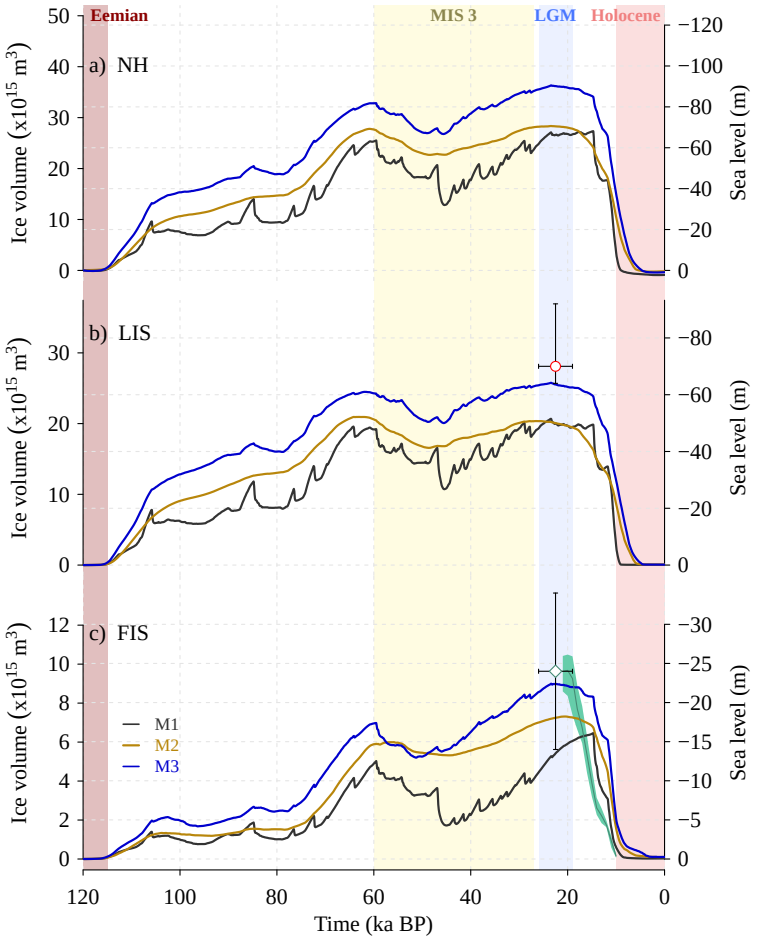


Fig. 4.6: Temporal evolution of ice volume ($m^3$) relative to initial conditions simulated in M1 (gray), M2 (gold) and M3 (blue) for: **a)** the NH domain; **b)** the LIS and **c)** the FIS. Ice volume variations have also been expressed in sea level equivalent units (m). Estimates of the SLE change at the LGM relative to present for the LIS (red dot; Tarasov et al. 2012) and for the FIS (light green diamond; Hughes et al. 2016) are indicated for comparison in panels **b)** and **c)**, respectively. Vertical error bars represent the range of SLE estimates at the LGM for the LIS and the FIS (Denton and Hughes, 1981; Clark and Mix, 2002; Clark and Tarasov, 2014). Horizontal error bars represent the approximate timing of the LGM (ca. 26.5-19 ka BP; Clark et al. 2009). The temporal evolution of ice volume ($m^3$) for the Eurasian ice sheet from the most-credible DATED-1 reconstruction (light green solid line; Hughes et al. 2016) together with its minimum and maximum lines (shaded area) have also been included in panel **c)**. Vertical colored bars indicate key periods of the past 120 kyr BP.

volume of the FIS in M1 around 40 ka leads to a larger reduction in response to the warming of this D/O event through the positive feedbacks between surface elevation and temperature as well as precipitation.

In terms of the extent of NH ice sheets at the LGM, M3 appears to be the best of the three methods, showing the most satisfactory agreement with reconstructions: ICE-5G (Peltier, 2004) for the LIS and DATED-1 (Hughes et al., 2016) for the FIS (Figure 4c). Major deficiencies are found in the southeastern margin of the Scandinavian Ice Sheet (SIS), the southwestern border of the LIS and the northern part of the Cordilleran Ice Sheet (CIS), where the ice extent is underestimated as compared to reconstructions and northwestern Siberia, where it is overestimated. In M1 and M2, these discrepancies with reconstructions are more evident. Furthermore, in the corridor that separates the CIS and the LIS a significant ice retreat is observed that is absent in M3.

Finally, the deglaciation shows a different behaviour in the three methods. M1 shows a much more abrupt transition into the Holocene, with ice already vanishing by the beginning of this period. This is a consequence of the abrupt temperature evolution in NGRIP that, by construction, in M1 is extrapolated to the rest of the globe, leading to peak temperatures already reached at the beginning of the Holocene and subsequently decreasing. In contrast, M2 and M3 show a smoother temperature evolution at the NH ice-sheet sites (Figure 4.5) that also leads to a smoother deglaciation. In all three methods the deglaciation of the FIS is more abrupt than than the one suggested by DATED-1 (Figure 5.6c). In M3, however, the beginning of the deglaciation (ca. 22 ka BP) is satisfactorily captured. In contrast, the onset of the deglaciation is remarkably lagged in M1, with SLE starting to increase only around 15 ka BP.

We now focus specifically on M3, which provides the best time-varying climatology. The time slices of ice thickness and velocities simulated under M3 provide a consistent picture of the spatial structure of NH ice sheets throughout the LGP (Figure 4.4). In particular, the present-day configuration is satisfactorily reconstructed, showing a unique ice sheet over Greenland with regions of intense ice flow predominantly distributed along its southeastern and the northwestern margins (Figure 4.4b). Full glacial climatic conditions lead to the growth of two additional vast masses of ice over North America and Eurasia (Figures 4.4c and d). On the one hand, the simulated North American ice sheet (NAIS) comprises a merged dome that aggregates the LIS, the Innuitian (IIS) and the Cordilleran (CIS) ice sheets in the western, northern and eastern parts of the continent, respectively. The spatial extent of the NAIS shows a good agreement with respect to that estimated in previous studies (e.g. Peltier et al., 2015). The complexity of the NAIS spatial configuration is also reflected in the map of simulated velocities that present two active ice streams in the vicinity of the Hudson Bay and in the

area of the Gulf of St. Lawrence in accordance with recent reconstructions (Margold et al., 2015). Meanwhile, the FIS covers the entire Scandinavian region as well as the British isles and a large fraction of the Barents and the Kara seas as suggested by geological and geomorphological constraints (Hughes et al., 2016; Svendsen et al., 2004). During MIS3, the extension of the NAIS is reduced as compared to the LGM, with an ice-free corridor separating the LIS from the CIS (Figures 4.4e and f). The FIS exhibits a decline in terms of volume and extension, particularly in the southwestern sector of the FIS where the British isles and its surroundings alternate between glaciated and ice-free periods on millennial time scales as a result of glacial abrupt climate variability.

## 4.4 Discussion and conclusions

In this study, a new method to force ice-sheet models offline is presented and compared with the more traditional approach. Three different time-varying climatologies are developed for the past 120 kyr following a perturbative approach and applied to an ice-sheet model to evaluate their consequences for the paleo evolution of ice sheets. In the first case, following the usual approach, temperature anomalies relative to present are calculated by combining the present-day climatologies, a simulated glacial-interglacial climatic anomaly field, and an index derived from ice-core data that includes orbital as well as millennial scale variability. In the second case, anomalies relative to present day are decomposed into an orbital and a millennial-scale component. Depending on the frequency either the glacial-interglacial climate anomaly field (orbital variability) or the stadial-interstadial field (millennial) is varied. The third case is a refinement of the second case in which the amplitudes of both orbital and millennial-scale variations are tuned to fit the NGRIP ice-core record. We herein focus essentially on the differences between the traditional and the novel, refined method.

The time series derived from these methods are compared at several locations with the available proxy data: the Greenland ice-core record and reconstructions of temperature and precipitation based on $\delta^{18}$O variations from speleothems located in central Europe and southwestern North America, respectively. By construction, the new method provides a perfect agreement with the ice-core record, improving the performance of previous methods. For temperature, the three methods follow a similar evolution, as dictated by the Greenland ice-core record, but the new method shows a larger amplitude. For precipitation, the new method yields a very different time evolution as a result of the spatial millennial-scale anomaly pattern which successfully reproduces the phasing and timing of $\delta^{18}$O variability in southwestern North America on millennial time scales, a result that cannot be achieved by the old method.

Note that offline index methods assume that the temperature variability reconstructed over Greenland is representative of the entire NH, but this does not mean either that the amplitude or the sign is the same in the whole NH. This is, actually, the case in usual methods but not in our new method, which is one of the reasons why it represents an improvement. The reason is that the millennial scale anomaly pattern introduces its own (spatial) scaling. The details of this spatial pattern will depend on the particular climate model used to produce the climate anomaly fields, and might well improve with higher complexity and resolution. Most models agree in showing that NH temperature changes coeval with Greenland in response to northward heat transport changes caused by AMOC variations, the prevailing paradigm to explain glacial abrupt climate changes (e.g. Stouffer et al., 2006) and that this is supported by comprehensive review of spatial coverage (Voelker and Workshop Participants, 2002), but this is not an assumption of our new index method.

The different climatologies have a large impact on the development of NH ice sheets. In these areas such as North America and Fennoscandia traditional methods yield millennial scale fluctuations of very large amplitude, comparable to those recorded in Greenland. Improving the representation of millennial-scale variability by including a stadial-interstadial anomaly field leads to a strong reduction in the amplitude of millennial scale temperature fluctuations by more than 10 K in the most prominent transitions. In addition, as a result of the scaling of the orbital temperature anomaly field, the amplitude of orbital variations is enhanced, leading to colder temperatures by about 5 K in most of the LGP. Finally, the traditional method leads to a very similar amplitude of millennial scale fluctuations over the two main NH landmasses as a consequence of the nearly-symmetric temperature pattern around Greenland. In contrast, the improved millennial-scale temperature field leads to the emergence of differences between the temperature evolutions in these areas.

The lack of continuous reconstructions in NH continental areas precludes the evaluation of the temperature time series derived for these regions. However, the fact that in the traditional method the amplitude of temperature variations at sites such as the LIS and the FIS is very similar to those of the Greenland ice-core record strongly suggests that these temperature fluctuations are overestimated. If the mechanism behind millennial-scale variability are transitions between states of reduced Atlantic meridional overturning circulation (AMOC), with southward shifted deep water formation (e.g. Sarnthein et al., 1994; Alley et al., 1999b; Böhm et al., 2015; Ganopolski and Rahmstorf, 2001; Henry et al., 2016), it is difficult to conceive of a similar temperature amplitude in the centre of the LIS or the FIS as in Greenland. Proxy data actually suggest that Greenland is the location where glacial abrupt climate changes reach their maximum amplitude in

terms of temperature, decreasing farther south in the NH (Voelker and Workshop Participants, 2002). In contrast, the temperature fluctuations obtained in the new approach, with amplitudes of 30-50% of those of the Greenland ice-core record and larger values over the LIS, down and upstream of the North Atlantic, seem more realistic.

Our results show that the traditional method leads to the lowest ice volume values throughout the whole LGP. Indeed, millennial-scale climate variability enhances NH ice-volume variability on millennial timescales. This leads to an underestimation of ice volume throughout most of the LGP. Including millennial-scale patterns (in M2) yields an important increase of ice volume in all NH ice sheets, but especially in the FIS. Additionally improving the orbital and millennial scale fields through the scaling is found to increase it further. Note although sea-level records provide essential information to interpret past ice-volume variations, continuous highly-resolved sea-level reconstructions are scarce and frequently rely on an insufficient temporal control. In addition, they generally provide inferences of global sea-level changes. This complicates the evaluation of our simulated NH ice volume timeseries against the paleorecord. However, the contribution to sea level of individual ice sheets can be assessed at specific time slices such as the LGM, for which reconstructions are indeed available. Estimates of the SLE change at the LGM relative to present (see the reviews by Clark and Mix, 2002; Clark and Tarasov, 2014) range between 70 m (Tarasov et al., 2012) and 92 m (Denton and Hughes, 1981) for the LIS and between 14 m (note this case is based on modelling, see Clark and Mix (2002) and references therein) and 34 m (Denton and Hughes, 1981) for the FIS; a recently published reconstruction by Hughes et al. (2016) yields around 23 m. Thus the traditional method is well below the uncertainty range of ice-volume estimations for the LIS and its lower end for the FIS. In contrast, our new, refined method is closer to the uncertainty range for the LIS and well within it for the FIS. To summarize, even though our method is not perfect it shows a clear improvement with respect to the usual index method. In particular, the individual (FIS and LIS) and total ice volume and extent of NH ice sheets at the LGM, as well as the timing of the onset of deglaciation are clearly better captured by our new method. Interestingly, our new approach underestimates ice-volume variations on millennial timescales as indicated by sea-level records. This suggests that either the origin of the latter is not the NH or that processes not represented in our study need to be invoked to account for an important role of millennial-scale climate variability on millennial-scale ice-volume fluctuations. Variation in oceanic conditions, ignored in our study, are a likely candidate.

The climate model used to build the present-day, LGM, and interstadial fields used in this study is an intermediate complexity model with low spatial (latitude $\times$ longitude) resolution ($7.5^\circ \times 22.5^\circ$) (Montoya et al., 2005). Using a more

comprehensive and/or higher resolution model should provide both a more accurate representation of millennial-scale glacial climate variability and a more realistic forcing for the ice-sheet model. Nevertheless, we do not expect this to change our main conclusions. To the extent that orbital and millennial-scale anomaly fields are different, our new forcing method should provide a better representation of the climate of the LGP. We expect this result to be robust against the use of different climate models. The precise temperature and ice volume evolution could, nevertheless, be model dependent, and this is worth investigating with additional climate models, in particular more comprehensive ones. In the last years a rising number of state-of-the-art climate models have recently shown two different climatic regimes under glacial conditions (Peltier and Vettoretti, 2014; Zhang et al., 2014, 2017). This study opens a new research pathway for these models which could take advantage of our new forcing method to investigate their skill to provide a synthetic reconstruction of the climate variability of the last glacial cycle and apply that to investigate the evolution of NH ice sheets. One recommendation that emerges from our study is that, in case of unavailability of an interstadial simulated snapshot to force the ice-sheet model, the use of a low-pass filtered index from the ice-core record should provide a better forcing than the traditional method including the full variability.

In a similar manner, although our ice-sheet model accounts for the surface elevation change feedback on temperature and precipitation, other important climate-ice sheet feedbacks such as surface albedo changes are not represented. Note, however our goal is precisely to improve offline forcing methods, for which most of these feedbacks are inherently absent. It would nevertheless be interesting to investigate this issue further by coupling our ice-sheet model to a regional energy-moisture balance model where feedbacks such as the ice-albedo feedback, the effect of continentality and the orographic effect on precipitation are better represented.

Finally, the novelty of this work lies in the consideration of an additional climatic pattern associated with millennial-scale climate variability to reconstruct the climate variability of the last glacial-interglacial cycle for the whole NH. Our results reveal that an incorrect representation of the characteristic pattern of millennial-scale climate variability within the climate forcing not only affects NH ice-volume variations at millennial timescales, but has consequences for glacial-interglacial ice-volume changes too. Thereby our new forcing method contributes to clarify the still uncertain role of glacial abrupt climate change in past ice volume variations, thus shedding light on the evolution of the NH ice sheets. As mentioned above, one aspect that remains to be assessed is the role of the ocean; this should be in the scope of future work.

# 5

# Oceanic forcing of the Eurasian Ice Sheet on millennial time scales during the Last Glacial Period[4]

## 5.1 Introduction

The last glacial period (LGP; ca. 110-10 ka before present, BP) was marked by the existence of two types of abrupt climatic changes: Dansgaard-Oeschger (DO) and Heinrich (H) events (e.g. Alley et al., 1999b). DO-events are identified in Greenland ice-core records as regional abrupt warmings by up to 16°C (Huber et al., 2006; Kindler et al., 2014) from cold (stadial) to relatively warm (interstadial) conditions within decades (Dansgaard et al., 1993) followed by a gradual cooling interval lasting from centuries to millennia and an ultimate phase of rapid cooling back to stadial conditions (Steffensen et al., 2008). Superimposed on the millennial-scale variability associated with DO-events, an additional lower-frequency climatic cycle is identified. So-called Bond cycles are flanked by prolonged stadials ending with prominent DO-events within about 7-10 kyr (Bond et al., 1993). Preceding these, and concomitant with the culmination of the prolonged stadials, H-events are registered in North Atlantic marine sediments as layers of remarkably high concentrations of ice-rafted debris (IRD) (Heinrich, 1988) as a result of massive iceberg discharges from the Laurentide ice-sheet (LIS) (Hemming, 2004).

While significant effort has been invested in understanding the role of the LIS in glacial abrupt climate changes, the dynamics of the Eurasian Ice Sheet (EIS) during the LGP has received comparatively less attention from a modeling perspective. However, improving our understanding of its evolution and

[4] The main contents of this chapter are published in: Alvarez-Solas, J. R. Banderas, A. Robinson, and M. Montoya, 2018: Oceanic forcing of the Eurasian Ice Sheet on millennial time scales during the Last Glacial Period *Clim. Past*, submitted; online review: https://doi.org/10.5194/cp-2018-89

response to past climate changes is important for a number of reasons. First, constraining freshwater inputs into the North Atlantic Ocean is crucial for a better understanding of the driving mechanisms of glacial abrupt climate changes (Rasmussen and Thomsen, 2013), since meltwater discharge from the ice sheets surrounding the Nordic Seas is often implied as a cause of ocean instabilities. Precursor events could possibly have originated from the European and Icelandic ice sheets (Grousset et al., 2000; Scourse et al., 2000). Meltwater peaks in the Norwegian Sea as well as in the southern border of the EIS during Marine Isotopic Stage 3 (MIS 3) have been associated with H events and millennial-scale climate variability (Lekens et al., 2006; Toucanne et al., 2015). From a broader perspective, the EIS, consisting of the Fennoscandian, the British Isles and the Barents-Kara ice sheets (FIS, BIIS and BKSIS, respectively) contained a large marine-based sector at its maximum extension (Hughes et al., 2016) that was exposed to oceanic variations, and the BKSIS is often considered as an analog for the current West Antarctic ice sheet (WAIS). At the LGM both had a similar size, but while the WAIS endured the deglaciation, the BKSIS completely disappeared (Andreassen and Winsborrow, 2009). Understanding the underlying mechanisms would provide important insights into the future evolution of the WAIS (Gudlaugsson et al., 2013, 2017).

Reconstructing the EIS response to past glacial abrupt climate changes prior to the LGM has been difficult, in part because, in reaching its maximum extent, the ice sheet eroded and removed nearly all older deposits. Nevertheless, the available paleodata indicate that during MIS 3 the EIS was highly dynamic, with its advance and retreat closely linked to stadials and interstadials (Toucanne et al., 2015). In this line, records from Norway (Mangerud et al., 2003, 2010; Olsen et al., 2002), Finland (Helmens and Engels, 2010) and Sweden (Wohlfarth, 2010) indicate rapid and rythmic ice-sheet variations in western Scandinavia, with advances and retreats during stadials and interstadials, respectively. Recent records also indicate enhanced meltwater discharges during interstadials from the Svalbard-Barents Sea ice sheet and probably also from the Scandinavian ice sheet (Rasmussen and Thomsen, 2013). The resolution and quality of geophysical data across marine sectors has improved considerably in the past decade (Hughes et al. (2016) and references therein). The results confirm substantial variations of the EIS volume, with the largest uncertainties in marine sectors of the ice sheets. Strong variations in the deposition of IRD suggest high co-variability of the BIIS with changes in ocean sea surface temperature (Hall et al., 2011; Scourse et al., 2009) and variations in EIS ice streams (Becker et al., 2017). North Atlantic marine sediment records register widespread variations of IRD input throughout the LGP indicating variations of iceberg rafting from virtually all surrounding ice sheets. Sources and timing differ among different sites. A

dominant periodicity equal to that of DO-events was identified in the Irminger Sea, with the largest IRD peaks at the end of stadials originating in the Iceland and Greenland ice sheets (Kreveld et al., 2000). Strong millennial-scale iceberg rafting variability of the BIIS has been documented as well in the North Sea (Hall et al., 2011; Peck et al., 2007; Scourse et al., 2009), but enhanced IRD seems to occur both during interstadials and stadials. For the FIS, IRD records in the Norwegian Sea show the characteristic DO periodicity, with IRD discharge occurring just before interstadial transitions (Lekens et al., 2006). More recently, however, an increase in IRDs from Fennoscandia during interstadials has been reported (Dokken et al., 2013; Becker et al., 2017). Correlating IRD occurrence with temperature changes registered in Greenland remains difficult, however, because it requires an extremely well dated chronology to assess the phasing between ocean sediments and ice cores.

Progress has been achieved also in the past decade using ice-sheet models. Siegert and Dowdeswell (2004) used inverse modelling to simulate the EIS evolution during the second part of the LGP, matching the geological evidence presented by optimizing the fit with data. Forsström and Greve (2004) used subsequent versions of a three-dimensional, polythermal ice-sheet model to simulate the EIS evolution throughout the LGP. Important variations in the EIS ice volume in response to temperature and precipitation variations were simulated. Clason et al. (2014) additionally included a parameterisation of surface meltwater enhanced sliding. In both cases too much ice was simulated in the northeastern EIS. Gudlaugsson et al. (2017) used the same model but introducing a simple representation of the subglacial hydrological system, focusing on its role in the temporal evolution of the EIS. Recently, an ice-sheet model constrained by data has been used to simulate the EIS evolution throughout part of LGP (Patton et al., 2016). The model targets the most probable EIS distribution at different time slices and reproduces substantial ice-volume variations. However, all of these models suffer from limitations, such as the use of the shallow-ice approximation (SIA) and its associated lack of an explicit treatment of the oceanic forcing. Marshall and Koutnik (2006) investigated the production of icebergs from all the North American ice sheets with a parameterized calving model. They found different behaviors on millennial time-scales depending on the local glaciological and climatic characteristic, with increased iceberg production both during stadials (e.g. from Iceland) or during interstadials (e.g. from Barents Sea). Nonetheless, sub-marine melting at the grounding line has not been explicitely considered until now and its impacts on millennial-scale variability have not been investigated up to now from a modelling perspective.

Here, we investigate the response of the EIS to millennial-scale climate variability during MIS 3 using a three-dimensional ice-sheet model. To this end, a

novel offline approach is used that provides a better representation of millennial-scale climate variability (Banderas et al., 2018). In addition, for the first time, both the atmospheric and oceanic effects of millennial scale climate variability associated with glacial abrupt climate changes are considered. This facilitates the quantification of the relative contribution of surface (ablation) and dynamic processes related to ice-ocean interactions.

The paper is organized as follows: in Section 5.2 the ice-sheet model, the forcing method and the experimental setup are described. In Section 5.3 the response of the EIS to the imposed forcing is shown, the focus being the evolution of its ice volume, its impact on sea level and the mechanisms behind meltwater and ice discharge. The results are discussed in Section 5.4. Finally, the main conclusions are summarised in Section 5.5.

## 5.2 Model and experimental setup

### 5.2.1 Model

The model used in this study is the ice-sheet model GRISLI-UCM, an extension of the original model GRISLI developed by Ritz et al. (2001). GRISLI-UCM is a hybrid three-dimensional thermomechanical ice-sheet model. Inland ice flows through deformation under the Shallow Ice Approximation (SIA, Hutter, 1983). Ice shelves and ice streams are described following the Shallow Shelf Approximation (SSA, MacAyeal, 1989). Ice streams (areas of fast flow, typically faster than $10^2\ m\ a^{-1}$) are considered as dragging ice shelves, allowing for basal movement of the ice (Bueler and Brown, 2009). Basal stress under ice streams is proportional to ice velocity and to the effective pressure of ice. The effects of varying this proportionality factor on the simulated ice streams are discussed in Alvarez-Solas et al. (2011b). The locations of the ice streams are determined by the presence of basal water within areas where the sediment layer is saturated.

The criterion to activate SSA inland relies on the presence of water above 1 meter in places of soft sediments (Laske, 1997) and above 400 meters in absence of such sediments. The grounding line position dynamically evolves following the flotation criterion after the mass conservation equation is solved. Calving takes place at the-shelf front following a double criterium. First, its thickness must first fall below a threshold. ($H_{calv}$ = 150 m, in the standard setup). This is a semiempirical parameter reflecting the fact that this is the typical thickness of observed ice-shelf fronts. Second, the upstream advection must fail to maintain the ice thickness above this threshold following a semi-Lagrangian approach (Peyaud et al., 2007) to account for the fact that ice-flux divergence fosters the formation of crevasses (Levermann et al., 2012). GRISLI-UCM thus explicitly calcu-

lates grounding line migration, ice-stream and ice-shelf velocities. This allows the model to properly represent both grounded and floating ice. GRISLI-UCM uses finite differences on a staggered Cartesian grid at a 40 km resolution, corresponding to 224×208 grid points for the Northern Hemisphere domain, including the EIS, with 21 vertical levels. By default, initial topographic conditions are provided by surface and bedrock elevations built from the ETOPO1 dataset (Amante and Eakins, 2009) and ice thickness (Bamber et al., 2001). The surface mass balance is given by the sum of accumulation and ablation, both of which are calculated from monthly surface air temperatures (SATs) and monthly total precipitation. Accumulation is calculated by assuming that the fraction of solid precipitation is proportional to the fraction of the year with mean daily temperature below 2°C. The daily temperature is computed from monthly SATs assuming that the annual temperature cycle follows a cosine function. Ablation is calculated using the positive-degree-day (PDD) method (Reeh, 1989). Its main parameters are the standard deviation of daily temperature, $\sigma$, and the conversion factors from PDDs to melt for snow and ice, $f_{PDD_{snow}}$ and $f_{PDD_{ice}}$. Here, $\sigma = 5$ K, $f_{PDD_{snow}} = 0.003$ mwe $PDD^{-1}$ and $f_{PDD_{ice}} = 0.008$ mwe $PDD^{-1}$. Refreezing is considered, with a value of $C_{si} = 60\%$. GRISLI-UCM accounts for changes in elevation at each time step considering a linear atmospheric vertical profile for temperature with different lapse rates in summer and in the annual mean (0.0065 and 0.0080 K $m^{-1}$, respectively) to account for the smaller summer atmospheric vertical stability.

Basal melting inland depends on pressure and water content at the base of the ice sheet (Ritz et al., 2001) as well as on the geothermal heat flux, which is prescribed from the reconstruction by Shapiro and Ritzwoller (2004). Basal melting for floating ice is computed using a linear temperature anomaly with respect to the freezing point. The details of the implementation of the boundary conditions (SMB and oceanic basal melting) in this particular study are given below (Section 5.2.2).

### 5.2.2 Offline forcing method

SMB and oceanic basal melting are obtained through a time-varying synthetic climatology built through a novel method that is found to provide a more realistic offline forcing for ice-sheet models than classical offline methods (Banderas et al., 2018). The method follows a perturbative approach in the sense that the forcing combines the present-day climatology, obtained from observational data, together with simulated anomalies. But in contrast to usual offline forcing methods, orbital and millennial scale variabilities are not lumped in a sole anomaly pattern but differentiated. The method thus combines present-day observations, simulated Last Glacial Maximum (LGM) anomalies relative to present, scaled by

an orbital-timescale index, and simulated stadial-interstadial anomalies, scaled by a millennial-timescale index:

$$\boldsymbol{T}^{\mathrm{atm}}(t) = \boldsymbol{T}_0^{\mathrm{atm}} + (1-\alpha^\star(t))\ \boldsymbol{\Delta T}_{\mathrm{orb}}^{\mathrm{atm}} + \beta^\star(t)\,\boldsymbol{\Delta T}_{\mathrm{mil}}^{\mathrm{atm}} \tag{5.1}$$

$$\boldsymbol{P}(t) = \boldsymbol{P}_0\ \{\alpha^\star(t) + (1-\alpha^\star(t))\,\delta\boldsymbol{P}_{\mathrm{orb}}\,[(1-\beta^\star(t)) + \beta^\star(t)\delta\boldsymbol{P}_{\mathrm{mil}}]\} \tag{5.2}$$

Here, $\boldsymbol{T}^{\mathrm{atm}}(t)$ and $\boldsymbol{P}(t)$ are the SAT and precipitation fields at time $t$. $\boldsymbol{T}_0^{\mathrm{atm}}$ and $\boldsymbol{P}_0$ are the ERA-INTERIM present-day SAT and precipitation climatologies (Dee et al., 2011). $\boldsymbol{\Delta T}_{\mathrm{orb}}^{\mathrm{atm}} = \boldsymbol{T}_{\mathrm{lgm}}^{\mathrm{atm}} - \boldsymbol{T}_{\mathrm{pd}}^{\mathrm{atm}}$ and $\delta\boldsymbol{P}_{\mathrm{orb}} = \boldsymbol{P}_{\mathrm{lgm}}/\boldsymbol{P}_{\mathrm{pd}}$ are the orbital temperature anomaly and precipitation ratio relative to the present day (not shown, see Banderas et al. (2018)), respectively, obtained from previous equilibrium simulations for the preindustrial and LGM climates performed with the CLIMBER-3$\alpha$ model (Montoya and Levermann, 2008). $\boldsymbol{\Delta T}_{\mathrm{mil}}^{\mathrm{atm}} = \boldsymbol{T}_{\mathrm{is}}^{\mathrm{atm}} - \boldsymbol{T}_{\mathrm{st}}^{\mathrm{atm}}$ and $\delta\boldsymbol{P}_{\mathrm{mil}} = \boldsymbol{P}_{\mathrm{is}}/\boldsymbol{P}_{\mathrm{st}}$ are the millennial temperature anomaly and precipitation ratio, respectively, for the interstadial relative to the stadial state (Section 5.2.2). The key differences between these climate modes are that in the stadial, North Atlantic Deep Water (NADW) formation is relatively weak and takes place south of Iceland. Accordingly the sea-ice front in the North Atlantic reaches 40°N. In the interstadial state there is a northward shift and intensification of NADW formation. Northward oceanic heat transport increases, and the North Atlantic and surrounding areas warm relative to the stadial state, in particular the Nordic Seas. The simulated interstadial state is thus characterised by a more vigorous NADW formation and AMOC together with reduced sea ice in the Nordic Seas, and a temperature increase of up to 10 K in the North Atlantic relative to the stadial state, with a maximum anomaly in the Nordic Seas. Note bold symbols indicate two-dimensional spatial fields. The stadial mode in our study is represented by a climate simulation of the LGM with CLIMBER-3$\alpha$ (Montoya and Levermann, 2008). The interstadial mode is taken from a recent glacial transient simulation performed with the same model under glacial climatic conditions, but with intensified NADW formation (Banderas et al., 2015). $\alpha^\star$ and $\beta^\star$ are two indices that separately modulate the contribution of the orbital and millennial anomalies. Both were built based on two recent complementary temperature reconstructions over Greenland, one from the NGRIP ice-core record for the LGP (Kindler et al., 2014), and the other one from several ice-core records for the Holocene (Vinther et al., 2009). Their combination (hereafter, the KV reconstruction) results in a continuous temperature reconstruction for Greenland for the past 120 ka (Banderas et al., 2018). $\alpha^\star$ is obtained after applying a low-pass frequency filter ($f_c = 1/18$ ka$^{-1}$) to the original KV reconstruction based on a spectral decomposition; $\beta^\star$ is obtained following a similar procedure but retaining the high frequency signal. Both indices are tuned in such a way that the resulting synthetic temperature time series at the NGRIP site exactly matches

the KV reconstruction (this distinguishes $\alpha^\star$ and $\beta^\star$ from the raw $\alpha$ and $\beta$ indices previous to this tuning; Banderas et al. (2018)).

The net basal melting rate for floating parts $\boldsymbol{B}$ is assumed to follow a linear relation:

$$\boldsymbol{B} = \kappa \, (\boldsymbol{T}^{\mathrm{ocn}} - \boldsymbol{T}_f) \tag{5.3}$$

where $\boldsymbol{T}^{\mathrm{ocn}}$ is the oceanic temperature close to the grounding line, $\boldsymbol{T}_f$ is the temperature at the ice base, assumed to be at the freezing point, and $\kappa$ is the heat flux exchange coefficient between ocean water and ice at the ice-ocean interface. Several marine-shelf basal melting parameterizations can be found in the literature. The submarine melt rate is thought to be directly influenced by the oceanic temperature variations below the ice shelves. Accordingly, most basal melting parameterizations are built as a function of the difference between the oceanic temperature at the iceocean boundary layer and the temperature at the ice-shelf base, generally assumed to be at the freezing point. The dependence on this temperature difference can be linear (Beckmann and Goosse, 2003) or quadratic (Holland et al., 2008; Pollard and DeConto, 2012; DeConto and Pollard, 2016; Pattyn, 2017). The linear marine-shelf basal melting parameterization used in this study is the simplest case that allows testing of the ice-sheet sensitivity to past oceanic temperature changes. Nevertheless, it accounts separately for sub-ice-shelf areas near the grounding line and for purely floating ice (ice shelves). The basal melting rate for purely floating ice shelves ($\mathrm{B_{sh}}$) is given by the grounding-line basal melt $\mathrm{B_{gl}}$ scaled by a constant factor

$$B_{\mathrm{sh}} = \gamma B_{\mathrm{gl}}(t) \tag{5.4}$$

In this study, $\gamma$ is set to 0.1. Thus, we consider that the submarine melting rate for ice shelves is 10 times lower than that close to the grounding zone, which is qualitatively in agreement with observations in some Greenland glaciers (Münchow et al., 2014; Rignot and Jacobs, 2002; Wilson et al., 2017). The melt rate in the open ocean, that is considered as being beyond the continental shelf break, is prescribed to a high value (20 m $\mathrm{a}^{-1}$ ) to avoid unrealistic ice growth beyond 750 m of ocean depth, following Peyaud et al. (2007).

Following the approach described above, $\boldsymbol{T}^{\mathrm{ocn}}(t)$ is assumed to be given by an expression analogous to Eq. 5.1. Thus Eq. 5.3 can be rewritten as:

$$\boldsymbol{B} = \boldsymbol{B}_0 + \kappa \left[ (1 - \alpha^\star(t)) \, \boldsymbol{\Delta T}^{\mathrm{ocn}}_{\mathrm{orb}} + \beta^\star(t) \, \boldsymbol{\Delta T}^{\mathrm{ocn}}_{\mathrm{mil}} \right] \tag{5.5}$$

where $\boldsymbol{B}_0 = \kappa(\boldsymbol{T}^{\mathrm{ocn}}_0 - \boldsymbol{T}_f)$ represents the present-day oceanic basal melting rate.

Finally, millennial-scale sea-level variations are prescribed according to the reconstruction by Grant et al. (2012, Section 5.2.3). The specific details of the experimental setup used are described below.

### 5.2.3 Experimental setup

We herein investigate the response of the EIS to millennial-scale climate variability during MIS 3. The starting point of our experiments is a control-run ice-sheet simulation with constant bounday conditions for MIS 3 that provides a representative configuration of the EIS for that time period (Figure 5.1). To this end, $\alpha^\star$ was set to its value at 40 ka BP, that is, $\alpha^\star = \alpha^\star_{40K} = -0.1$, and $\beta^\star = 0$ to preclude millennial-scale variations. Note however these values are to a certain extent arbitrary; they are intended to provide a stable mean background state similar but not necccessarily identical to background MIS 3 conditions. Thus:

$$\boldsymbol{T}^{\mathrm{atm}}_{40K} = \boldsymbol{T}^{\mathrm{atm}}_{0} + (1 - \alpha^\star_{40K})\, \boldsymbol{\Delta T}^{\mathrm{atm}}_{\mathrm{orb}} \tag{5.6}$$

$$\boldsymbol{P}_{40K} = \boldsymbol{P}_0 \left[\alpha^\star_{40K} + (1 - \alpha^\star_{40K})\, \delta \boldsymbol{P}_{\mathrm{orb}}\right] \tag{5.7}$$

$$\boldsymbol{B}_{40K} = \boldsymbol{B}_0 + \kappa\, (1 - \alpha^\star_{40K})\, \boldsymbol{\Delta T}^{\mathrm{ocn}}_{\mathrm{orb}} \tag{5.8}$$

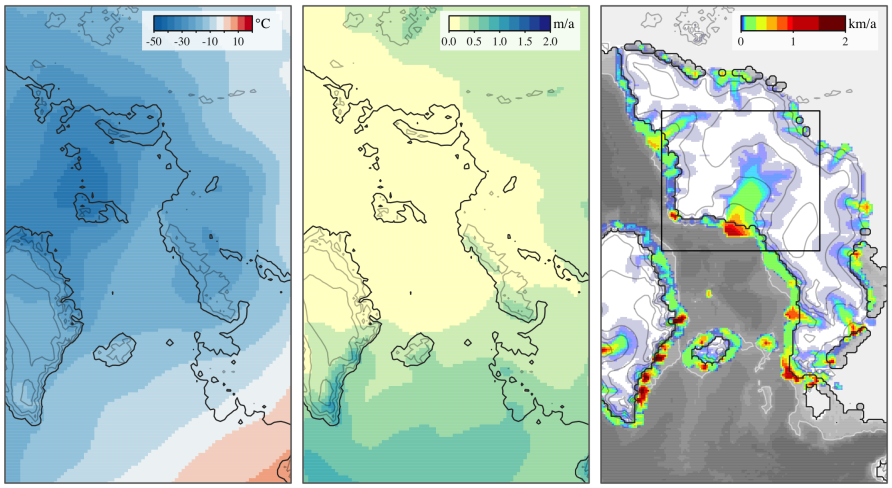


Fig. 5.1: Background climatic forcing and resulting ice sheet for the control run (CTRL). MIS 3 (∼40 ka BP) reference annual mean SAT in °C (left) and annual mean precipitation in m $a^{-1}$ (middle). Present-day countour lines with the land boundary delineated at a depth of -80 m are added for reference. Simulated MIS 3 ice sheet elevation (contours) with ice thickness contours plotted for every 500 m, the grounding line position shown by a black line, the 500 m depth contour shown by the white line, and velocities (shaded colors, in km $a^{-1}$) after the spinup was completed (right). This ice sheet represents the initial state previous to the applied perturbations. Bjørnøyrenna basin, as referenced in the text, is shown by the black rectangle.

Note that although Eq. 5.8 is formally correct and consistent with the scheme used, in contrast to the present-day SAT or precipitation the present-day rate

of oceanic basal melting cannot be determined. Thus, in practice we replace this equation by directly tuning the value of $\boldsymbol{B}_{40K}$ to obtain a reasonable ice-sheet configuration at 40 ka BP given the atmospheric forcing fields expressed by equations 5.6-5.7. To this end, a constant basal melting rate of 0.1 m $a^{-1}$ is assumed. The ice sheet was forced with the resulting climatologies for 100 kyr previous to the starting of the perturbations described below. This allows the vertical temperature profile within the ice sheet to be equilibrated with the climate. This procedure was found to facilitate the growth of European ice-sheets to an extent that satisfactorily agrees with previous reconstructions (Svendsen et al., 2004; Kleman et al., 2013).

Our forcing method allows to investigate the response of the EIS solely to millennial-scale climate variability at MIS 3 by keeping constant the orbital component of the forcing ($\alpha^\star = \alpha^\star_{40K}$) and letting $\beta^\star$ vary throughout the LGP (eqs. 5.1, 5.2 and 5.5). In order to assess the relative roles of the atmosphere and the ocean, three independent experiments have been carried out. First, an atmospheric-only forced simulation (ATM) in which the time evolution of SAT and precipitation on millennial time scales is considered, while the oceanic forcing is kept constant to MIS 3 (i.e., 40 ka BP) background climatic conditions. Thus:

$$\boldsymbol{T}^{\mathrm{atm}}(t) = \boldsymbol{T}^{\mathrm{atm}}_{40K} + \beta^\star(t)\,\boldsymbol{\Delta T}^{\mathrm{atm}}_{\mathrm{mil}} \tag{5.9}$$

$$\boldsymbol{P}(t) = \boldsymbol{P}_{40K}\left[(1-\beta^\star(t)) + \beta^\star(t)\,\delta\boldsymbol{P}_{\mathrm{mil}}\right] \tag{5.10}$$

$$\boldsymbol{B}(t) = \boldsymbol{B}_{40K} \tag{5.11}$$

Second, an oceanic-only forced simulation OCN in which the atmospheric forcing is kept constant while the oceanic basal melting is allowed to vary at millennial timescales around its background MIS 3 value:

$$\boldsymbol{T}^{\mathrm{atm}}(t) = \boldsymbol{T}^{\mathrm{atm}}_{40K} \tag{5.12}$$

$$\boldsymbol{P}(t) = \boldsymbol{P}_{40K} \tag{5.13}$$

$$\boldsymbol{B}(t) = \boldsymbol{B}_{40K} + \kappa\,\beta^\star(t)\,\boldsymbol{\Delta T}^{\mathrm{ocn}}_{\mathrm{mil}} \tag{5.14}$$

The magnitude and sign of oceanic temperature anomalies $\boldsymbol{\Delta T}^{\mathrm{ocn}}$ depends on the depth at which $\boldsymbol{T}^{\mathrm{ocn}}$ is considered. In our simulations, a large part of the NE sector of the EIS is marine based with shallow bedrock depths between 500 m and less than 100 m in several locations further south. It is therefore unclear whether this marine ice sheet should be more susceptible to changes in the surface or the subsurface of the ocean. To investigate the effect of this uncertainty, we decided to perform two different simulations considering different depths: one corresponding to the surface (OCNsrf) and the other one considering deeper (subsurface) oceanic waters by averaging temperatures within the range of 400-600 m depth (OCNsub). Therefore we hereafter distinguish between

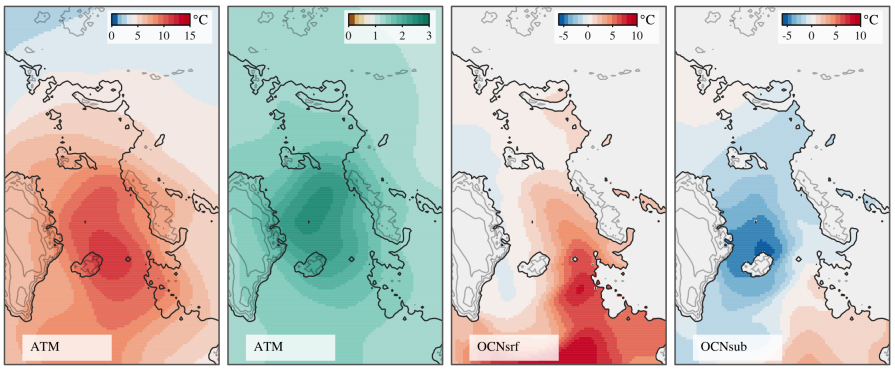


Fig. 5.2: Millennial-scale components of the boundary forcing. **a)** SAT anomalies (interstadial minus stadial) in °C. **b)** Precipitation ratio (interstadial to stadial). **c)** Anomalies of SST and **d)** subsurface ocean temperature (at 500 m depth) in °C. Present-day countour lines with the land boundary delineated at a depth of -80 m are added for reference.

$\boldsymbol{\Delta T}^{\mathrm{ocn}}_{\mathrm{mil}}$ for surface or subsurface millennial-scale temperature anomalies, respectively (Figure 5.2). The realism and convenience of aplying one or the other is adressed in section 5.4.

Finally, a simulation ALL combining both the atmospheric and the oceanic forcings:

$$\boldsymbol{T}^{\mathrm{atm}}(t) = \boldsymbol{T}^{\mathrm{atm}}_{40K} + \beta^{\star}(t)\,\boldsymbol{\Delta T}^{\mathrm{atm}}_{\mathrm{mil}} \tag{5.15}$$

$$\boldsymbol{P}(t) = \boldsymbol{P}_{40K}\,[(1-\beta^{\star}(t)\,) + \beta^{\star}(t)\,\delta\boldsymbol{P}_{\mathrm{mil}}] \tag{5.16}$$

$$\boldsymbol{B}(t) = \boldsymbol{B}_{40K} + \kappa\,\beta^{\star}(t)\,\boldsymbol{\Delta T}^{\mathrm{ocn}}_{\mathrm{mil}} \tag{5.17}$$

In all experiments $\beta^{\star}(t)$ dictates the millennial-scale variability of the forcings (Figure 5.3). Because our simulated stadial-to-interstadial transition results from an intensification of the AMOC, positive $\beta^{\star}$ values imply an increase in $\boldsymbol{T}^{\mathrm{atm}}$ relative to its background MIS 3 value (e.g., Eq. 5.15 and Figures 5.2 and 5.3). As a consequence, the atmosphere warms at interstadials relative to stadial periods, as reflected by the $\boldsymbol{\Delta T}^{\mathrm{atm}}_{\mathrm{mil}}$ millennial-scale anomaly field (Figure 5.2). Note that refreezing is not allowed to occur in our model in the current setup. If $\kappa\,\beta^{\star}\,\boldsymbol{\Delta T}^{\mathrm{ocn}}_{\mathrm{mil}} < -\boldsymbol{B}_{40K}$ (which would imply $\boldsymbol{B}(t) < 0$) we simply impose the value $\boldsymbol{B}(t) = 0$.

An ensemble of simulations for different values of $\kappa$ have been considered to evaluate the sensitivity of the EIS to the forcing. Finally, varying sea-level forcing is considered (Figure 5.3b), both alone (SL run) and in combination with the previous forcings (ALL).

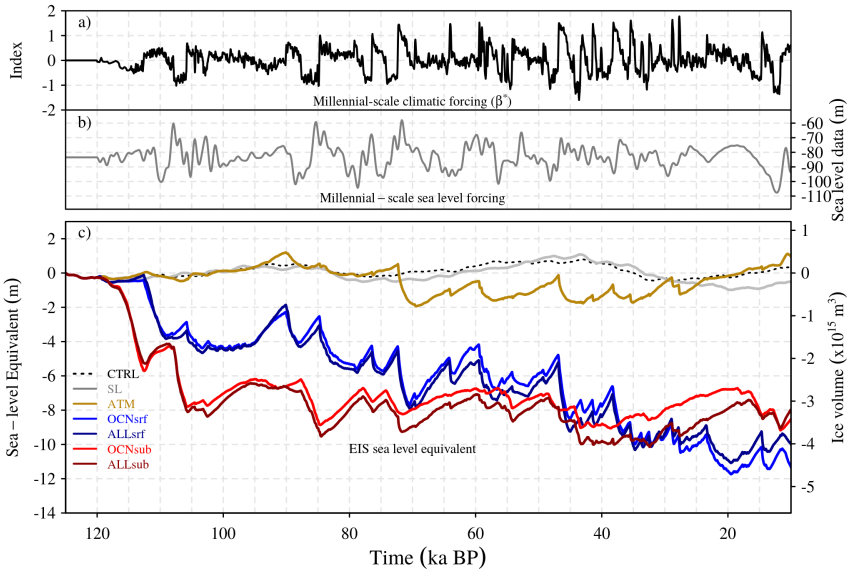


Fig. 5.3: **a)** Temporal component of the millennial-scale climatic forcing ($\beta^\star$ index). **b)** Millennial-scale sea-level forcing (Grant et al., 2012). **c)** EIS sea-level equivalent (m) related to ice volume variations ($m^3$) with respect to initial conditions for the CTRL run (black) and for the SL (gray), ATM (gold), OCNsrf (blue), OCNsub (red), ALLsrf (dark blue), and ALLsub (dark red) forcing experiments.

## 5.3 Results

Substantial differences are found in the response of the EIS to the forcing scenarios. Under constant forcing, the CTRL run shows negligible millennial-scale sea-level equivalent (SLE) variations, although a lower frequency SLE fluctuation is found as a result of internal ice-sheet variability (Figure 5.3). When the model is forced only by changes in sea level (SL run), a slight response is observed on millennial-scales. These changes appear not be sufficient to cause a substantial migration of the grounding line, thus not affecting ice velocities (not shown). In ATM, the atmospheric forcing alone causes a sequence of enhanced ablation episodes resulting in modest ice volume variations (up to 1.5 m SLE) during the most prominent stadial-interstadial transitions. In contrast, the oceanic forcing in OCNsrf induces pronounced changes in the dynamics of the EIS on millennial time scales (see below), with episodes of large volume reduction occurring during interstadials. The combination of sea level, atmospheric and oceanic forcings (ALLsrf) results in a very similar response of the EIS to that obtained in OCNsrf

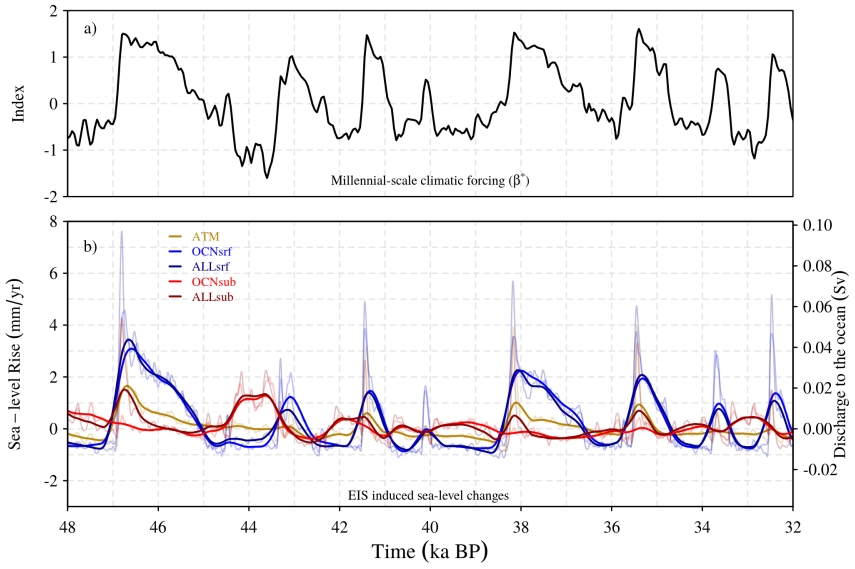


Fig. 5.4: MIS3 Period. **a)** Temporal component of the millennial-scale climatic forcing ($\beta^\star$ index), and **b)** EIS changes (mm/yr and Sv) related to ice volume variations ($m^3$) with respect to initial conditions for the CTRL run (black) and for the SL (gray) ATM (gold), OCNsrf (blue), OCNsub (red), ALLsrf (dark blue), and ALLsub (dark red) forcing experiments. Thick lines show the variables after applying a low pass filter of 100 years.

(Figure 5.3) as a consequence of the larger effect of the oceanic forcing in OCNsrf with respect to ATM. OCNsub shows an anti-phase relationship with respect to OCNsrf, with the largest reductions in ice volume occurring during prolonged stadial periods and regrowth during interstadials. This behavior can be explained by the fact that ocean waters at the subsurface warm (cool) during episodes of reduced (enhanced) convection at the Nordic Seas as a result of variations in the AMOC strength (Figure 5.2d). Thus, the out-of-phase relationship found in the dynamic response of the EIS between these two oceanic experiments results from the opposed sign of their spatial forcing patterns (Figure 5.2). When considering the forcing at the subsurface of the ocean together with the atmosphere (ALLsub), slight reductions of the EIS volume (less than 1 m of s.l.e) during interstadials are superimposed onto the previous behavior (Figure 5.3).

The magnitude of these changes in terms of sea-level rise rate and discharge, specifically for the MIS 3 period, is illustrated in Figure 5.4. The simulations forced with the surface of the ocean (OCNsrf and ALLsrf) show the largest am-

plitudes, with peaks of sea-level rise above 4 mm $yr^{-1}$ during DO-events and sustained contributions well above 1 mm $yr^{-1}$ during entire interstadial periods. In ATM, a decline of the EIS during stadial-to-interstadial transitions is still observed but presents a smaller amplitude of 1-2 mm $yr^{-1}$. The simulations in which the ice sheet is forced with the subsurface of the ocean (OCNsub and ALLsub) present a decline of their volume during stadial periods and regrowth during interstadials as a consequence of the inverted spatial pattern of temperature anomalies with respect to the surface. In OCNsub (and ALLsub) the amplitude of these changes is smaller than in OCNsrf (and ALLsrf), on the order of 0.5-1 mm $yr^{-1}$, reaching more than 1 mm $yr^{-1}$ during pronounced stadials (as ca. at 44 ka BP). The ALLsrf and ALLsub simulations show a similar or slightly larger volume loss during interstadials, as a consequence of the additional atmospheric forcing, that is superimposed onto the OCNsrf and OCNsub behaviour.

The response of the EIS has been analyzed in terms of its mass balance decomposition for the all-forcing runs (Figure 5.5). In ALLsrf the surface ocean temperature varies in phase with the atmosphere (Figure 5.2). Thus, during stadial-to-interstadial transitions the high negative values of dV/dt can be explained by the conjunction of an initial sharp increase in ablation together with pronounced increases in basal melting and calving, which allow for a large grounding line retreat in the Bjørnøyrenna basin (Figure 5.5 mid panel). The rate of ice loss by basal melting is similar to that resulting from the increase in ablation (as reflected in the surface mass balance, SMB) during the peak of a stadial-to-interstadial period. However, basal melting is much more efficient than surface mass balance in decreasing volume along the whole duration of an interstadial. This is due to the fact that ablation is restricted to the southern borders of the EIS. Thus, when the ice sheet has retreated to areas of no ablation, in spite of a slight further loss provided by the elevation feedback it rapidly equilibrates and a negative surface mass balance cannot propagate further inland. In contrast, when enhanced basal melting from higher oceanic temperatures is applied, the associated retreat can propagate further inland occupying a large proportion of the Bjørnøyrenna basin and facilitating high rates of volume loss (although similar in amplitude with respect to SMB) during the whole interstadial period. During stadial periods, both the enhanced positive mass balance and the absence of basal melting (favored by the negative oceanic anomalies) favor the regrowth of the EIS. Subsurface ocean temperatures evolve also in phase with the atmosphere in the SW part of the EIS but in anti-phase in its NE part. In other words, when forcing with the subsurface of the ocean, a slight warming (cooling) is observed around the Britain ice sheet while cooling (warming) of the Bjørnøyrenna basin is simulated during interstadial (stadial) periods (see Figure 5.2). Therefore, the ALLsub simulation presents volume declines during stadial-to-interstadial transitions due to an in-

crease in ablation and basal melting in the SW part. Subsequently, reduced basal melting in the NE part of the EIS favors regrowth of the Bjørnøyrenna basin during interstadial periods. Finally, shifting to pronounced stadial periods (as in ca. 44 ka BP) favors the penetration of warm subsurface waters that increase basal melting enough to produce an ice-sheet retreat in the NE part in spite of the enhanced positive surface mass balance (Figures 5.4 and 5.5). When considering the atmosphere and the subsurface ocean forcing together in ALLsub, these competing processes translate into a smaller amplitude of millennial-scale EIS changes as compared to the case with surface ocean forcing (ALLsrf). Furthermore, declines of the EIS can be observed both during the beginning of interstadial periods and during pronounced stadial periods in ALLsub (Figures 5.4 and 5.5).

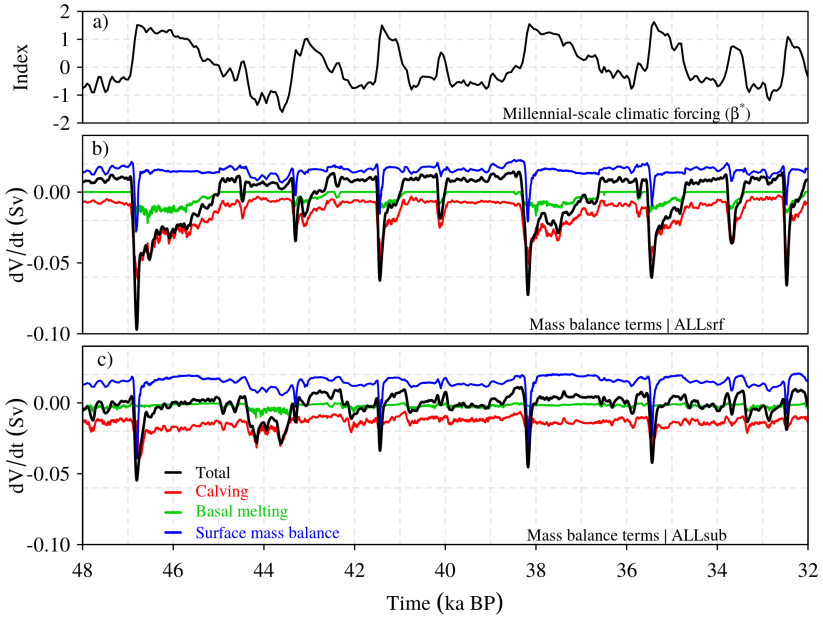


Fig. 5.5: MIS3 Period. **a)** Temporal component of the millennial-scale climatic forcing ($\beta^\star$ index), and contribution of the different terms of the EIS mass balance to ice volume variations ($m^3$) in the simulations considering all forcings, with **b)** corresponding to the surface oceanic forcing (ALLsrf) and **c)** to the subsurface oceanic forcing (ALLsub).

Focusing on the OCN and ATM simulations separately facilitates isolating the effects of the ocean on this complex pattern. To this end, the simulated ice-sheet distribution and velocities of OCNsrf, OCNsub and ATM are shown in Figure

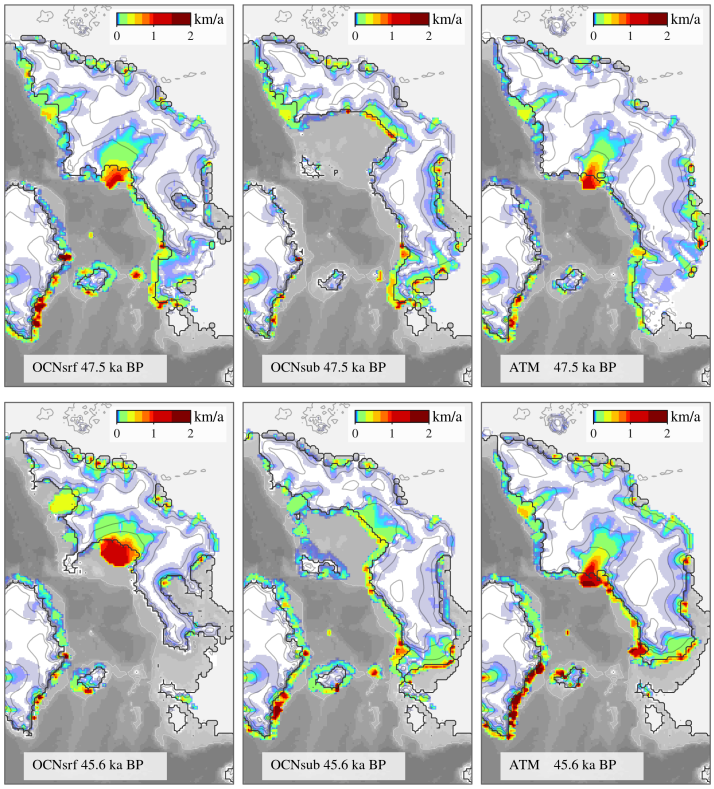


Fig. 5.6: Simulated EIS at the end of a stadial period (upper panels) and at the end of an interstadial period (lower panels) for the experiments: OCNsrf (left); OCNsub (middle) and ATM (right). Shaded colors show ice velocities (km $a^{-1}$). The ice thickness contours are plotted for every 500 m with the grounding line position shown by a black line. The 500 m depth contour is shown by the white line. The periods represented here corresponds to the stadial and intrestadial periods previous and posterior to DO 12 (ca. 47 ka BP), respectively.

5.6 for the period around DO-event 12, at ca. 47 ka BP. As expected, OCNsrf shows a widespread retreat both in the NE and the SW of the EIS from the stadial to the interstadial period (Figure 5.6, bottom left). This is accompanied by an acceleration of the Bjørnøyrenna basin due to its grounding line thinning and retreat (Figure 5.6, left panels). OCNsub presents a collapsed Bjørnøyrenna basin during the stadial period previous to DO-event 12 due to enhanced basal melting from warmer subsurface waters. The transition to the interstadial period favors a slight regrowth of this NE part of the EIS due to decreased basal melting, while its SW section slightly retreats (Figure 5.6 upper mid panel). Concerning

ATM, only in the southwestern (SW) part of the EIS is the atmospheric forcing capable of generating an important reduction in the EIS volume in response to the stadial-interstadial transition (Figure 5.6 right bottom panel). This is a result of the spatial pattern of the forcing, with the largest SAT anomalies located around the Nordic seas (Figure 5.2). Therefore, the ice volume reduction of the EIS in ATM during interstadials is due to the positive SAT anomaly, which leads to enhanced ablation in the SW part of the EIS. In turn, reduced SATs during stadials allow the regrowth of the ice sheet up to the continental margin of the Nordic seas. The more active dynamic response of the EIS in the OCN simulations can be attributed to the increase in oceanic temperatures by 2-4°C (Figure 5.2) within the margins of the ice sheet during interstadial (in the case of OCNsrf) and stadial (OCNsub case) periods, which translates into enhanced basal melting at the margins of the EIS. The SW sector of the EIS also responds to the warmer SSTs, actually with a larger reduction of ice volume than in ATM (Figure 5.6).

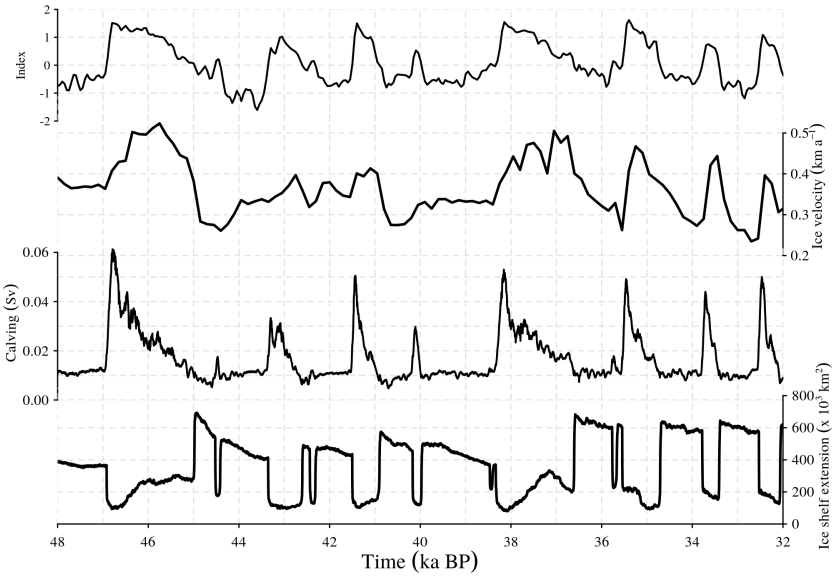


Fig. 5.7: MIS3 Period. Temporal component of the millennial-scale climatic forcing ($\beta^\star$ index), ice velocities in the Bjørnøyrenn basin (km a$^{-1}$), calving rate (Sv) and ice-shelf extension ($10^3$ $km^2$) in the OCNsrf simulation.

The spatial patterns shown in Figure 5.6 are representative of the all other stadial-to-interstadial transitions. In OCNsrf, the EIS reacts to every abrupt surface warming with a substantial ice-flow acceleration, especially in the Bjørnøyrenna basin (Figure 5.7). Ice shelves that are present during stadial periods suddenly retreat during DO-events and together with enhanced basal melting favor thinning and retreat of the grounding line that translate in large iceberg discharges up to ca. 0.06 Sv. In OCNsub, ice velocities in the Bjørnøyrenna basin increase during stadials, when enhanced basal melting erodes the grounding line and favors its retreat. Peaks in calving are recorded accordingly during pronounced stadial periods. These peaks are however of smaller amplitude than in OCNsrf. This can be explained by the fact that transitions to stadials are usually more gradual than transitions to interstadials, thus the incursion of warmer (subsurface) waters happens in this case in a smoother manner. High velocities reach their maxima at the end of the stadial and beginning of the interstadials. The latter are however not accompanied by an increase in calving due to the fact that ice shelves are expanding and thickening during this period thanks to reduced basal melting (Figure 5.8). In general, the extension of ice shelves is greatly reduced during periods of enhanced basal melting (Figures 5.7, 5.8), with no large unconfined ice shelves surviving during these episodes. Some thinner ice shelves remain, in spite of the enhanced basal melting, thanks to an increase in advection from the Bjørnøyrenna ice stream triggered by a grounding line retreat (Figure 5.6).

Note that changes in the position of the calving front are usually accompanied by a grounding line displacement (not shown). For some minor ice-shelf breakups this close relationship can be broken, but with almost no effects upstream inland. Thus we consider that the grounding line position is the best indicator for characterizing the dynamic behavior of the marine part of the EIS. Inspection of the temporal evolution of the grounding line position in OCN simulations confirms that ice dynamics control the majority of ice-volume variations in the EIS as opposed to the SMB processes involved in ATM (Figure 5.9). The migration of the grounding line through time has been characterized by means of an index ($\mu$) that weighs the proportion of non-grounded points in the region of the Bjørnøyrenna basin:

$$\mu\,(t) = \left(1 - \frac{N_g(t)}{N}\right) \cdot 100 \tag{5.18}$$

where $N_g(t)$ represents the evolution of the number of points of grounded ice within a fixed area of $N$ points in the Barents Sea region. An increase (decrease) in $\mu$ thus indicates a retreat (advance) of the grounding line. While in ATM $\mu$ barely changes (Figure 5.9), OCN runs show a large dynamic behavior of the

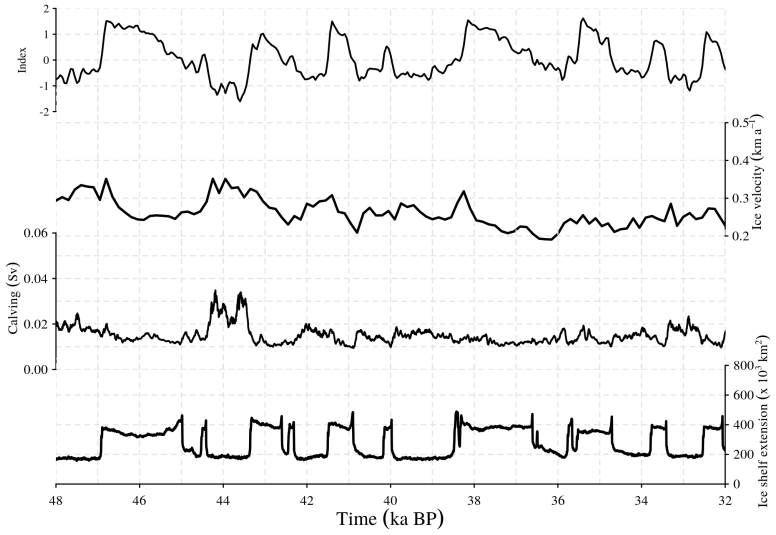


Fig. 5.8: MIS3 Period. Temporal component of the millennial-scale climatic forcing ($\beta^\star$ index), ice velocities in the Bjørnøyrenn basin ($km\ a^{-1}$), calving rate (Sv) and ice-shelf extension ($10^3\ km^2$) in the OCNsub simulation.

basin. In OCNsrf, $\mu$ reflects a synchronous evolution of the grounding line position and the oceanic forcing, with major retreats coinciding with interstadial states (Figure 5.9). Conversely, the Bjørnøyrenna basin is generally much closer to a full retreat in OCNsub during stadials due to a larger penetration of warm subsurface waters (Figure 5.2; OCNsub) compared to the surface waters (Figure 5.2;OCNsrf). However, the grounding line is able to advance and reach Svalbard during episodes of reduced basal melting at the interstadials.

The direct coupling between the oceanic forcing and the response of the Bjørnøyrenna ice stream is also evident from the relatively high negative correlation ($r \simeq -0.9$) found between $\mu$ and ice thickness in this area (Figure 5.9). In essence, in response to the grounding-line retreat (advance), acceleration (deceleration) of the flow takes place upstream in the Bjørnøyrenna ice stream, as reflected by the slightly linear positive correlation ($r \simeq 0.3$) found between $\mu$ and velocities in the channel (Figure 5.9).

As a consequence of the destabilization of the ice sheet, important ice-volume variations are observed in the NE part of the EIS during millennial-scale climatic transitions, which added to the minor contribution of the SW retreat, result in

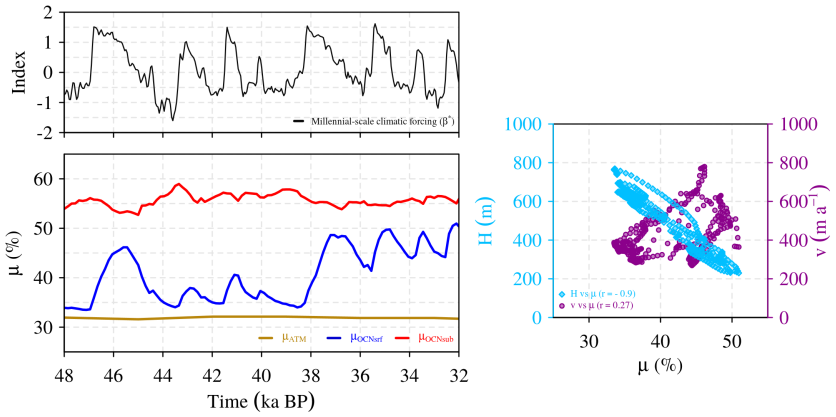


Fig. 5.9: Dynamic behavior of the EIS during millennial-scale climatic transitions for the OCNsrf, OCNsub and ATM experiments. **a)** Displacement of the grounding line in the Bjørnøyrenn basin in response to the climatic $\beta^{\star}$ forcing (gray). The evolution of the grounding line position is shown for OCNsrf (blue), OCNsub (red) and ATM (gold). The migration of the grounding line has been characterized as an index $\mu(t)$ that represents the evolution of the number of points of grounded ice $N_g\,(t)$ over a fixed area of $N$ points in the Barents Sea region. Increasing values of $\mu$ indicate grounding line retreat.**b)** OCNsrf scatter plot diagram showing the relationship between ice thickness $H$ in the region of the Bjørnøyrenna basin and $\mu$ (light blue diamonds) as well as the relationship between ice-stream velocities $v$ in the same region and $\mu$ (purple circles).

fluctuations of more than 4 m SLE in OCNsrf, up to 2.5 m in OCNsub and ca. 1 m in ATM (Figure 5.3).

In order to investigate the sensitivity of the results to the model parameters, eight additional OCN simulations, both for the surface and the subsurface, have been carried out with different $\kappa$ parameters between 1-10 $m\ a^{-1}\ K^{-1}$, i.e., bracketing our standard case of $\kappa = 5\ m\ a^{-1}\ K^{-1}$. This choice reflects the inferences based on measurements made on Antarctic ice shelves that a variation of 1 K in the effective oceanic temperature changes the melt rate by ca. 10 $m\ a^{-1}$ (Rignot and Jacobs, 2002; Shepherd et al., 2004). A robust response of the EIS is found, with a more reactive EIS response for increasing $\kappa$ values (Figures 5.10, 5.11). The sensitivity of our results to the values of the atmospheric mass balance model has also been explored. In spite of largely exploring the values of the parameters that determine the sensitivity to surface mass balance, the EIS variability induced by the ocean is always found to be of greater amplitude than the one induced by the atmosphere provided that $\kappa > 2\ m\ a^{-1}\ K^{-1}$ (Figure 5.12).

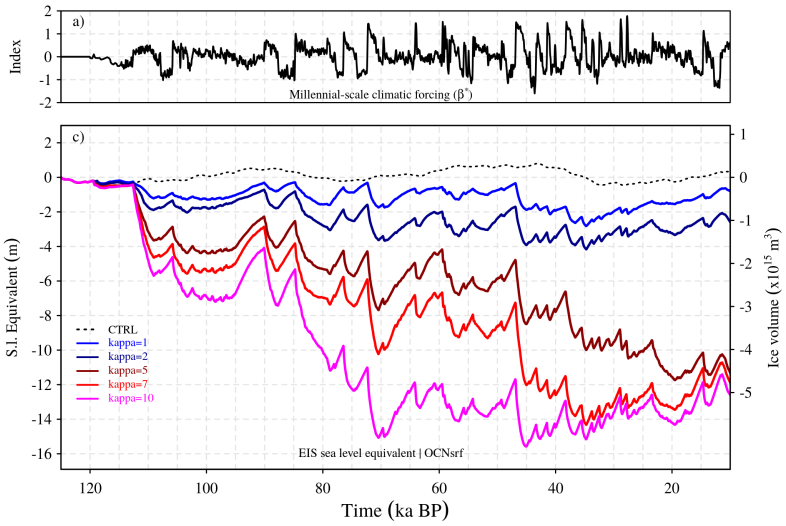


Fig. 5.10: Volume time series of the EIS for different values of the ocean heat flux coefficient corresponding to the OCNsrf forcing.

## 5.4 Discussion

Our results suggest a highly dynamic Eurasian ice sheet at millennial time-scales largely responding to changes in the ocean temperatures. Some authors present the marine based Kara-Barents complex as an analogue for present-day West Antarctic ice sheet for which bedrock topography is a major control for stability. We have shown, in this sense, that the Bjørnøyrenna basin is highly susceptible to changes in the oceanic temperatures. The timing of this response with respect to changes registered in Greenland depends, however, on whether the surface or the subsurface of the ocean is considered as the relevant forcing of the ice sheet.

Recently, IRD peaks of Fennoscandian origin reported from a high-resolution marine sediment core from the Norwegian Sea indicate the presence of more frequent IRD deposition and thus calving during interstadials than during stadials (Dokken et al., 2013). This result has been corroborated in a compilation of new and previously published data (Becker et al., 2017) clearly showing that within MIS 3, the IRD deposition increases within interstadials. The coeval deposition of carbonate-rich, sorted fine sands and near-surface warming suggests the presence of Atlantic water along the margin, and is interpreted by the authors as the effects of winnowing due to an intensified AMOC during interstadials. This

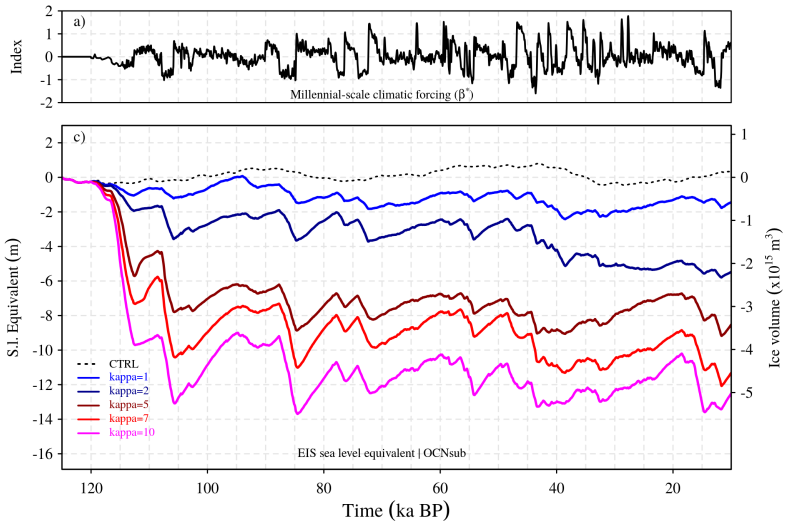


Fig. 5.11: Volume time series of the EIS for different values of the ocean heat flux coefficient corresponding to the OCNsub forcing.

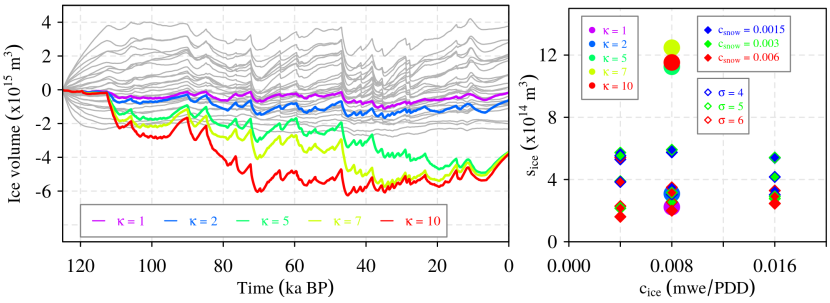


Fig. 5.12: Left: Time series of EIS volume. Gray trajectories represent the 91 realisations of perturing the PDD parameters. The sensitivity shown by different values of the ocean heat flux coefficient, $\kappa$, is included by means of the OCNsrf time series in colors. Right: Scatter plot of the amplitude of the millennial oscillations (standard deviation of the volume time series) for the PDD ensemble (diamonds) together with the OCNsrf (circles)

interpretation results in concordance with our results when considering the surface waters as the oceanic forcing. Thus, this agreement would play in favor of considering that the EIS was primarily responding to changes in the surface of the ocean.

Our results also provide a mechanism to explain the pervasive presence of IRD in the North Atlantic during MIS 3, both during stadials and interstadials, and originating both in the LIS and the EIS. During stadials, the simultaneous appearance of IRD across the wider North Atlantic Ocean can be explained through the build-up of subsurface heat in the high-latitude North Atlantic leading to increased iceberg calving in the presence of large, thick ice shelves, together with lower surface temperatures allowing for wider dispersal of icebergs (Barker et al., 2015). According to our results interstadials could lead to enhanced calving of the EIS through oceanic surface subglacial melting as a result of the warmer surface conditions and relatively shallow grounding line of this ice sheet.

The identification of IRD layers with increased calving through ice-sheet instabilities must be taken with caution, since it is based on several untested assumptions (Clark and Pisias, 2000): (i) delivery of IRD to a specific site is caused solely by iceberg calving, versus transport by sea-ice; (ii) an increase in IRD represents an increase in the iceberg flux, versus a greater amount of debris incorporated at the base of the ice sheet that delivers the icebergs, or a greater distance of iceberg transport; (iii) the amount of IRD carried by all the icebergs is similar, assuming therefore a direct relationship between IRD concentration and iceberg flux. However, the former assumptions have not been confirmed and, thus, the calving-IRD relationship might not be so direct. In addition, ocean temperatures affect melting of icebergs and thus their release of IRD. Variations in ocean temperatures can alter the IRD released by an iceberg at a certain site, causing variations in IRD deposition even for a constant amount of icebergs produced at the source.

Our experimental setup is not intended to match the paleorecord, but to provide insight into the response of the EIS to millennial-scale variability. The EIS variations simulated here represent the upper-end amplitude of potential responses during the whole glacial cycle, due to its large size. Extending the study to cover the whole LGP would require the consideration of orbital variability as part of the forcing. In this case, the EIS would likely be smaller during the mildest phase of MIS 3, thus limiting its contact with the ocean and the production of iceberg discharges.

Also, our results depend somewhat on the particular SAT and oceanic temperature anomaly patterns simulated by our climate model, the magnitudes of the resulting forcing, and the initial size of the simulated EIS. The use of different atmospheric realisations is subject to the availability of climate simulations with different models for the three climate states needed: glacial (stadial), present, and interstadial. The latter is only available for a reduced number of models. This makes the assessment of this issue difficult in the present study. Assessing the sensitivity to these features should be in the scope of future work, and illustrates

the need for carrying out new simulations of both the interstadial and the stadial states with more sophisticated climate models. Nonetheless, our results indicate that the ocean is the major driver of the EIS ice-volume changes during MIS-3. Note the temporal index used is the same for the atmosphere and the ocean and the amplitude is given by an OGCM simulation of two different oceanic states mimicking stadial and interstadial periods. We then translate those fields into ablation (through PDD, whose uncertainty has been extensively explored) and into basal melting (through a linear equation). The values of the oceanic sensitivity parameter ($\kappa$) we used here are in the range (or even below in most cases) of those suggested by data in Antarctica (Rignot et al. 2002). Note, in particular, that even from low-mid values of $\kappa$ of 2 m a $K^{-1}$ the response to the ocean begins to be of greater amplitude than that to the atmosphere, making our main conclusions robust.

Finally, our study lacks bi-directional coupling between the ice sheet, the atmosphere and the ocean. Eventually the goal is to investigate this matter with fully coupled climate-ice sheet models.

Meltwater discharge from the EIS and other ice sheets surrounding the Nordic Seas is often implied as a cause of ocean instabilities. The same would be the case for iceberg discharges. This issue is beyond the scope of this study; its assessment would require investigating the impact of these freshwater perturbations in deep water formation and the AMOC. Again, proper assessment requires the use of a coupled climate-ice sheet model.

## 5.5 Conclusions

We have investigated the response of the EIS to millennial-scale climate variability associated with DO-events through a series of simulations with a three-dimensional, hybrid ice-sheet model that represents inland ice flow under the SIA and floating ice shelves and ice streams through the SSA. The model makes use of an offline forcing method that separately accounts for orbital and millennial-scale climate variability during the LGP, improving the representation of the latter (Banderas et al., 2018). Atmospheric and ocean forcings associated with millennial-scale variability were considered both separately and together.

Separating the effects of atmospheric and oceanic forcing during the glacial period has allowed us to quantify the contribution of each to EIS variability. Atmospheric forcing during stadial-interstadial transitions has a modest effect on the ice sheet, which is a consequence of the largest SMB changes being confined to SW sector of the EIS, where the forcing is strongest. In contrast, the oceanic forcing has a larger effect, through changes in the ice dynamics in the Bjørnøyrenna basin of the EIS. Ocean warming is able to induce a retreat of grounded ice in

this part of the EIS through dynamic processes. As a consequence, significant ice-volume variations result during millennial-scale climatic transitions. Added to the smaller contribution of the SW retreat, this results in sea-level changes on the order of several meters. Sensitivity experiments for different values of the oceanic heat coefficient parameter show that this is a robust response of the model.

Our results thus support the existence of a highly dynamic EIS during the LGP. They suggest an important role of oceanic melt forcing through changes in the ocean circulation in controlling the ice-stream activity. Together with previous work (Alvarez-Solas et al., 2013), they imply that oceanic circulation changes and the associated ocean-ice sheet interactions are able to explain virtually all ice rafting events in the North Atlantic within MIS 3, from the H-events of the LIS during stadials to those of the EIS during interstadials. Additionally, our results highlight the need for stronger constraints on the local North Atlantic behavior in order to shed light on the NH ice sheet's glacial dynamics.

# 6

# Discussion

The work carried out, the goals pursued and the tools used in this thesis can be divided in two. The first goal was to investigate the origin of glacial abrupt climate changes focusing on a new mechanism consistent with proxy records. To allow simulations over long timescales an EMIC was used. The second goal was to investigate the paleo-evolution of the NH ice sheets on millennial time scales. This was pursued using an ice-sheet model that was forced offline. A new forcing method was developed and applied specifically to investigate the impact of oceanic variations in the evolution of the EIS throughout the LGP. A discussion of each of the main questions addressed is presented below, in the context of the broader scientific implications.

## Could gradual changes related to the slowly-varying conditions in the Southern Ocean (SO) promote abrupt climatic transitions during the last glacial period?

Our simulations indicate that gradual increases in atmospheric $CO_2$ levels as well as intensifications of SO winds have the potential to promote a transition to a state with intensified NADW formation and a vigorous AMOC. The AMOC strengthening occurs after a northward retreat of the Arctic sea-ice front which eventually leads to a northward shift of NADW formation sites into the Nordic Seas. The role of $CO_2$ in triggering the abrupt climatic transition is ultimately related to its radiative effect. The $CO_2$ rise leads to a global temperature increase which causes a sea-ice retreat in the Nordic seas thus enhancing heat loss to the atmosphere and reducing freshwater flux import into this region. This eventually reactivates convection in the Nordic Seas, thus leading to an AMOC

strengthening. In contrast, increasing SO wind-stress contributes to enhance the oceanic heat transport from southern latitudes to the North Atlantic through increased Ekman transport. This heat supply contributes to melt the southern margin of the North Atlantic sea-ice front, progressively favouring oceanic heat loss exchange with the atmosphere and convection in the Nordic Seas.

We have thus identified a mechanism which is consistent with proxy records by which abrupt climate change can be promoted through the idealised experiments exhibited. Up to now climate simulations focusing on abrupt climate changes have mainly been based on imposing freshwater fluctuations in the North Atlantic, as reviewed by Kageyama et al. (2010). However, the sources of these freshwater fluxes have not yet been identified. Here, we propose such freshwater flux variations could be connected with rearrangements in the Nordic Seas sea-ice extent in response to $CO_2$ and SO wind intensifications.

Our results are consistent with studies suggesting an important role of sea-ice in abrupt warming (Gildor and Tziperman, 2003; Li et al., 2005). In our case the sea-ice retreat causes the initial abrupt SAT increase in response to the onset of convection in the Nordic Seas, but it is the AMOC intensification that helps to sustain the system in the warm state. They also confirm the study by Oka et al. (2012) suggesting that if the glacial climate were close to a threshold, small perturbations leading to a reduction in the sea-ice cover could push the system across this threshold. The sea-ice cover control of NADW formation provides an explanation for the different stability of the glacial AMOC compared to the present one, and thereby the different variability of glacial and interglacial periods (Marotzke, 2012).

Our results are also in agreement with Knorr and Lohmann (2003, 2007) in showing that in a in glacial background climate slowly varying climatic conditions around the SO and/or globally are able to trigger rapid climate change. This result might seem contradictory with future projections, which suggest an increase in atmospheric $CO_2$ levels leads to North Atlantic warming and freshening, both of which weaken NADW formation. Nevertheless, in our view, the background climate, and particularly the North Atlantic sea-ice configuration, showing large differences between glacial and present day states, plays an important role in setting the climate sensitivity and its stability properties.

The comparison against paleorecords, however, is not perfect. Reconstructions indicate that the abrupt warming phase of D/O events takes place within decades (Steffensen et al., 2008). However, our simulated climatic transition evidences a two-step development in which a rapid increase of 4°C occurs in less than a decade followed by more gradual warming greater than 10°C on centennial timescales. Nevertheless, many models have shown difficulties to simulate abrupt climate changes and the scientific community has pointed out the necessity to improve

the skill of state-of-the-art models to simulate abrupt climate changes within the context of threshold-crossing processes (Valdes, 2011).

## What is the origin of Dansgaard-Oeschger variability? Does the SO play a role in glacial abrupt climate change?

According to our previous results, increased atmospheric $CO_2$ levels and enhanced SO westerlies are able to reactivate NADW formation thus causing an AMOC strengthening. In this situation, the ITCZ would shift to the NH again leading to a weakening of SH westerlies which would eventually result in decreasing upwelling and atmospheric $CO_2$ levels. This negative feedback would favour the return of the climate system back to stadial conditions through an AMOC weakening. Our transient simulations confirm that reducing atmospheric $CO_2$ levels and wind-stress over the SO allows the climate system to return into a new stadial regime. These AMOC reorganisations originate from changes in the meridional density gradient in response to the prescribed variations in atmospheric $CO_2$ concentration and SO wind-stress. The scaling relationship between the meridional density gradient and the AMOC strength was postulated long ago in conceptual models (Stommel, 1961; Rooth, 1982; Gnanadesikan, 1999) and subsequently confirmed in comprehensive ocean general circulation models (OGCMs) (e.g. Rahmstorf, 1996). Our experiments provide a plausible explanation for the driver of such changes.

Although our experimental setup consists of an externally-forced oscillation involving $CO_2$ and SO wind-stress variations, the underlying idea of this study is that $CO_2$, SO winds and the AMOC are coupled such that the proposed interhemispheric oscillation could be an internal solution of the real climate system. During prolonged stadials, a weak AMOC translates into warming of the SH at the expense of the NH. The southward shift in the atmospheric circulation patterns favors upwelling and thereby outgassing of $CO_2$. This results in gradual global warming and, eventually, in an abrupt transition from stadial to interstadial conditions associated with the resumption of NADW formation. The AMOC recovery maintains the NH in a warm phase while the SH gradually cools down following the bipolar seesaw mechanism. In this situation the atmospheric circulation patterns migrate equatorward reducing atmospheric $CO_2$ levels and SO winds and helping to revert the climate system back to the stadial state, thus starting the cycle again. The assessment of the internal nature of the mechanism presented here would require the use of a climate model accounting for an interactive carbon cycle module and a more comprehensive atmospheric component.

Our EMIC satisfactorily reproduces the phasing and timing of D/O and AIM events showing gradual warmings over Antarctica coinciding with Greenland sta-

dials as a result of AMOC reorganisations in which periods of reduced NADW formation lead to the warming of the SH at the expense of the NH. The thermal ocean bipolar seesaw hypothesis thus provides the physical basis of this interhemispheric coupling assuming that temperature anomalies originated during D/O and AIM events could simply be explained by changes in the rate of cross-equatorial ocean heat transport carried by the AMOC (Stocker and Johnsen, 2003). Under this hypothesis, the damped and gradual character of Antarctic temperature variations can be explained by the slow timescale of heat up required by a thermal reservoir located in the SO. The time scale is ultimately determined by the time needed by the meridional density gradient for triggering major AMOC reorganizations. Density changes in the South Atlantic are more gradual than in the North Atlantic where they are found to be more abrupt during transitions. The character of millennial-scale climate variability registered in proxies worldwide can therefore be interpreted as the result of an integral signal accounting for gradual changes in the SH plus the abrupt imprint provided by changes in the NH.

Our results are consistent with a wealth of records, including speleothems from East Asian Monsoon region indicating an in-phase relationship, with interstadial and stadial intervals in the North Atlantic nearly coincided with wet and dry episodes in East China, respectively (Wang et al., 2001), but an antiphase relationship with speleothem records from Brazil (Wang et al., 2007) or western Amazonia in Ecuador (Mosblech et al., 2012). Our results also reproduce proxy records from the equatorial Pacific showing a similar behavior to Antarctic temperature variability on millennial time scales, suggesting that the Antarctic climate signal was globally pervasive during the last glacial period (Barker and Knorr, 2007). This good agreement arises, in part, from the suitable representation of the simulated bipolar seesaw of the AMOC. However, in our case the AMOC reorganisations were triggered by $CO_2$ and SO wind-stress changes without using freshwater forcings (e.g. Liu et al., 2009; Menviel et al., 2014) of doubtful origin.

Our concept strongly relies on the bipolar seesaw mechanism. In this paradigm the responsible agent for slowing the propagation of the D/O signal to Antarctica is the Antarctic Circumpolar Current (ACC) which acts as a dynamic barrier that inhibits the propagation of temperature anomalies through advection or internal waves because of the absence of meridional boundaries in these latitudinal band (e.g. Schmittner et al., 2003). Advective transport across the latitudes of the ACC is only possible along the topographic ridges which are located below ca. 1500 m depth (Toggweiler and Samuels, 1995b). Therefore, the propagation of temperature anomalies in the upper 1500 m of the ocean can only be accomplished through eddy fluxes which are less efficient than wave propagation and advection

in signal transmission (McDougall and Church, 1986). Recently, however, Pedro et al. (2018) have challenged the idea that the SO is the ultimate heat reservoir in the bipolar seesaw by quantifying the change in heat content that occurs among the major ocean basins after imposing an AMOC collapse in a global coupled climate model. This study concludes that the SO only accounts for a minor part of the global increase in heat content and that the latter can be related to two main factors: first, the southward propagation of a subsurface warm anomaly through the deep western boundary current that originates from the expansion of sea ice and shutdown of convection in high-latitudes of the North Atlantic after the AMOC collapse; second, the reduction in northward advection and thermocline deepening which allows to increase the heat storage in the South Atlantic. Their simulations evidence that a large fraction of the global increase in heat content is confined into the Indian and the Pacific because temperature anomalies propagate eastward out of the South Atlantic and along continental boundaries into these basins by Kelvin and Rossby waves and eastward with the ACC flow by advection much more efficiently than they can propagate south across the ACC (which relies on eddy fluxes) into the SO (Cox, 1989; Schmittner et al., 2003). In this sense, the ultimate heat reservoir of Stocker and Johnsen (2003) would be located in the global interior ocean north of the ACC. An additional argument to consider that the heat reservoir is located in the global ocean interior is that the centennial-scale thermal inertia attributed to the SO (Knutti et al., 2004) does not fit with the millennial time scale observed for D/O and AIM events.

In relation with the discussion above, our setup is based on the assumption that $CO_2$ variations were caused by enhanced wind-driven upwelling in the SO (Anderson et al., 2009). Recent findings indicate that disruptions in the glacial biological pump could also operate in concert with wind-driven upwelling to produce millennial-scale $CO_2$ oscillations (Martínez-García et al., 2014). As suggested by Anderson et al. (2009), increased buoyancy forcing (Watson and Naveira Garabato, 2006) might actually be necessary together with the enhanced wind-stress in order to account for the upwelling intensification. The reason is that an increase in the northward Ekman transport leading to a steepening of the isopycnals would result in an increase in the baroclinicity of the ACC, leading to an intensification of the southward eddy transport that could partially offset the increased northward Ekman transport (e.g. Hallberg and Gnanadesikan, 2006). Our model only includes a parameterisation for mesoscale eddies, just as most OGCMs. Studies with eddy-permitting and eddy-resolving models indicate this eddy compensation could depend strongly on how surface buoyancy fluxes are affected, with increased surface buoyancy flux in response to increased wind-stress leading to a larger sensitivity than previously thought (Abernathey et al., 2011). This is a fundamental matter currently subject of active research

but still unaffordable for millennial-scale simulations. A shift or increase of the SO winds could also affect wind-driven mixing there. The deep SO is responsible for a large fraction of global diapycnal mixing (Watson and Naveira Garabato, 2006) that is generated almost entirely over restricted regions of rough bottom topography below the ACC through the interaction of its deep-reaching flow and its associated eddies with the seafloor (Watson et al., 2013). If the westerly winds shifted south or strengthened, the mixing of heat and freshwater into the deep ocean would most probably increase.

Antarctic ice core records have revealed that the amplitude of atmospheric $CO_2$ variations is close to 20 ppmv during the most pronounced AIM events (Ahn and Brook, 2008; Bereiter et al., 2012; Ahn and Brook, 2014) whereas in our experiments the magnitude of the $CO_2$ increase that is required to push the system into the interstadial regime is substantially larger (ca. 40 ppmv). This discrepancy can be attributed to the intrinsic nature of the CLIMBER3-model. Our results are based on the existence of an internal threshold in the model that relates to the sensitivity of the glacial AMOC to the surface oceanic wind-stress (Montoya and Levermann, 2008). The amplitude of the forcing is ultimately determined by the distance from background climatic conditions to the threshold itself and this can be model dependent. Nevertheless, following Banderas et al. (2015), a comprehensive fully coupled model has shown that gradual changes in atmospheric $CO_2$ concentration of comparable magnitude than those recorded in ice cores can trigger rapid climate shifts under intermediate glacial conditions (Zhang et al., 2017). These changes are associated with a regime of bistability of the AMOC which appears at intermediate heights of the glacial ice sheets. Our transient simulations were run under glacial background climatic conditions following the specifications of the Paleoclimate Modeling Intercomparison Project Phase II (PMIP2). This mainly includes glacial insolation values, a reduced equivalent atmospheric $CO_2$ concentration to account for the lowered concentration of greenhouse gases and the ICE-5G glacial ice sheet reconstruction (Peltier, 2004). Prescribing NH ice sheets of intermediate size in our experiments could possibly result in decreasing the distance from background climatic conditions to the intrinsic threshold which, in turn, could lead to a reduction in the amplitude of the forcing. Nevertheless, the fact that a more comprehensive model is able to qualitatively reproduce our results provides strong support for our mechanism, and furthermore to the use of EMICs to provide hints as to the problems which comprehensive and costly models should tackle from a more realistic perspective.

## How can we investigate the response of NH ice sheets on millennial time scales?

D/O events occur under glacial climatic conditions, with global ice volumes varying at intermediate levels. Thus NH ice sheets could have modulated millennial-scale climate variability during the last glacial period. Therefore having a better understanding of how NH ice sheets reacted during D/O events can shed light on the mechanisms responsible for climate variability on millennial time scales. Previous studies have forced ice sheet models offline using a synthetic time-varying climatology but its skill to reproduce millennial-scale climate variability needed to be improved. These methods often assume that the climate generated from a glacial-interglacial spatial pattern combined with a temporal index reflecting temperature variability over Greenland is representative of the entire NH. In chapter 4 (Banderas et al., 2018), we have shown how the inclusion of a spatial component representative of D/O events can improve such offline forcing methods. The reason is that the millennial-scale anomaly pattern introduces its own spatial scaling, thus contributing to generate a better representation of millennial-scale climate variability in the time-varying climatology.

The current paradigm to explain glacial abrupt climate changes involves AMOC reorganisations which eventually trigger temperature transitions of large amplitude in the Nordic Seas. Therefore, it is difficult to conceive temperature variations of similar magnitude in distant locations such as the EIS or the LIS, as would result from usual offline forcing methods. The comparison of the three different climatologies generated in this study indicates that traditional forcing methods yield millennial-scale fluctuations of very large amplitude over North America and Fennoscandia as compared to those recorded in Greenland. This eventually leads to an underestimation of ice volume throughout most of the LGP, not only at millennial but also at suborbital time scales. The inclusion of a stadial-interstadial anomaly field leads to a large reduction in the amplitude of millennial-scale temperature variations in these areas, thus generating ice volumes that are closer to the uncertainty range estimated for the LIS and well within it for the EIS.

It is important to highlight that the details of spatial patterns used in this study can be model dependent and that our method might well improve with the use of higher complexity and resolution models. This study opens a new research pathway for these models which could take advantage of our new forcing method to investigate their skill to provide a synthetic reconstruction of the climate variability of the last glacial cycle and apply that to investigate the evolution of NH ice sheets. Note that, although our ice-sheet model accounts for the surface-elevation change feedback on temperature and precipitation, other important climate-ice-sheet feedbacks such as surface albedo changes are not represented.

It would be interesting to reassess this study by coupling our ice-sheet model to a regional energy-moisture-balance model where feedbacks such as the ice-albedo feedback, the effect of continentality and the orographic effect on precipitation are better represented.

## How did the Eurasian ice sheet respond to millennial scale climate variability?

While an important effort has been made to investigate the dynamics and evolution of the LIS during the LGP, the EIS has not received much attention, in particular from a modeling perspective. However, of all NH glacial ice sheets, temperature anomalies associated with glacial abrupt climate changes were likely largest over the EIS together with the Geenland Ice Sheet. Therefore significant impacts on the EIS should be expected. Meltwater discharge from this and other ice sheets surrounding the Nordic Seas is often implied as a potential cause of ocean instabilities that lead to glacial abrupt climate changes. Thus, a better understanding of its variations during the LGP is important to understand its role in glacial abrupt climate changes. Here we investigate the response of the EIS to millennial-scale climate variability during the LGP. This issue is discussed in Chapter 5 (Alvarez-Solas et al., 2018a).

Our results indicate that the EIS shows a highly dynamic response, in phase with Greenland interstadials, when considering surface waters of the Nordic Seas as the oceanic forcing. There is increasing evidence in showing that IRD deposition of Fennoscandian origin is more frequent during interstadials than during stadials within MIS 3 (Dokken et al., 2013; Becker et al., 2017), with near-surface warming coinciding with deposition of carbonate-rich and sorted fine sands. This suggests the presence of Atlantic water along the margin of the EIS, and is interpreted by the authors as the effects of winnowing due to an intensified AMOC during interstadials.

It is important to note that the identification of IRD layers with increased calving through ice-sheet instabilities must be taken with caution, since it is based on several untested assumptions (Clark et al., 2002): (i) delivery of IRD to a specific site is exclusively caused by iceberg calving, versus sea-ice transport; (ii) an increase in IRD represents an increase in the iceberg flux, versus a greater amount of debris incorporated at the base of the ice sheet that delivers the icebergs, or a greater distance of iceberg transport; (iii) the amount of IRD carried by all the icebergs is similar, assuming therefore a direct relationship between IRD concentration and iceberg flux. However, these assumptions have not been corroborated and, thus, the relationship between IRD and calving might not be so direct. Furthermore, oceanic temperatures variations can alter the deposition

of IRD from drifting icebergs even if a given constant iceberg production ratio is considered at the source.

Our study aims to provide insight into the response of the EIS to millennial-scale variability and not to exactly match the paleorecord. Nevertheless, comparison with SLE estimates indicates that the amplitude of our simulated evolution of the EIS ice volume lies at the upper-end of potential responses during the whole glacial cycle. Extending the study to cover the whole LGP would require the consideration of orbital variability as part of the forcing. In this case, the EIS would likely be smaller during the mildest phase of MIS-3, thus limiting its contact with the ocean and the production of iceberg discharges.

Our forcing climate has been generated through the CLIMBER-3$\alpha$ model. It would be interesting to explore the response of the EIS considering different atmospheric realisations. This is obviously subject to the availability of simulations performed with different models that include the three required climate states: glacial (stadial), present, and interstadial. Our results indicate that the ocean is the major driver of the EIS ice-volume changes during MIS-3. Note that the atmosphere and the ocean vary according to the same temporal index and that the amplitude is given by an OGCM simulation which accounts for two different oceanic states that resemble stadial and interstadial conditions. We then translate those fields into ablation (through PDD, whose uncertainty has been extensively explored) and into basal melting (through a linear equation). The values of the oceanic sensitivity parameter ($\kappa$) we used here are in the range (or even below in most cases) of those suggested by data in Antarctica (Rignot and Jacobs, 2002). Note, in particular, that even from low-mid values of $\kappa$ of 2 m a $K^1$ the response to the ocean begins to be of greater amplitude than that to the atmosphere, making our main conclusions robust.

As a future goal, it would be interesting to investigate the response of the EIS to millennial-scale oceanic forcing with fully coupled climate-ice sheet models. This would give insight into the mechanism of glacial abrupt climate changes which are often thought to be the result of oceanic instabilities involving meltwater discharges from the EIS and other ice sheets surrounding the Nordic Seas.

# 7

# Conclusions and Outlook

In this thesis, the origin of glacial abrupt climate changes and their impacts on NH ice sheets have been investigated from a modelling perspective. Four complementary studies (three of them published and one under review) have been presented with the aim of providing new insight into these issues.

The novelty of the first study lies on the description of a new mechanism consistent with proxy data that allows to explain glacial abrupt climatic transitions conducted by an AMOC strengthening. Previous studies rely on experimental designs that invoke prescribed freshwater fluxes to trigger abrupt climatic transitions (e.g. Kageyama et al., 2010). However, the sources of these freshwater fluxes have not yet been identified. In this study, we describe a new mechanism by which gradual changes in atmospheric $CO_2$ levels and/or wind-stress intensification in the SO are able to promote a rapid climatic transition that resembles the abrupt warming phase of D/O events. In our experiments, increasing $CO_2$ levels and/or enhancing SO wind-stress lead to a northward migration of the Atlantic sea-ice front which eventually result in reactivating convective sites of the Nordic Seas thus promoting an AMOC strengthening and allowing the system to flip from stadial to interstadial conditions. In this study we propose that freshwater fluxes used in previous work to simulate stadial to interstadial transitions could be connected to rearrangements in the Nordic seas sea-ice extent in response to $CO_2$ and SO wind intensifications.

The second study emerges as a natural extension of Banderas et al. (2012) and focuses on simulating the return of the climate system to stadial conditions in order to investigate the mechanisms that underlie D/O cycles. Our results indicate that D/O-like transitions can be simulated as a result of AMOC reorganisations which, in turn, originates from changes in the meridional density gradient caused by variations in atmospheric $CO_2$ and SO wind-stress. Our model

satisfactorily reproduces the phasing and timing of D/O and AIM events showing gradual warmings over Antarctica coinciding with Greenland stadials and gradual Antarctic coolings coinciding with Greenland interstadials. Our results are also consistent with a wealth of records that contain the imprint of D/O and Antarctic variability, thus evidencing that the bipolar seesaw of the AMOC is satisfactorily well captured by our model.

In our third study (Banderas et al., 2018), we develop a new method to force ice-sheet models offline that provides a more realistic representation of orbital and millennial-scale climate variability and improves the transient forcing of ice sheets during the LGP. This new method is based on the consideration of an additional climatic pattern representative of D/O variability to reconstruct climate history of the last glacial-interglacial cycle. Our results indicate that traditional offline forcing methods could lead to misrepresent NH ice volume variations on both millennial and orbital time scales. These results suggest that weighting the spatial variability over time through a single index can lead to an overestimation of the response of some of the NH ice sheets during abrupt changes which can be eluded with our new method.

Our fourth study (Alvarez-Solas et al., 2018a) takes advantage of the method developed in Banderas et al. (2018) and focuses on investigating the response of the EIS, in terms of its dynamics and evolution, to glacial oceanic temperatures on millennial time scales. Our results show a highly dynamic response of the EIS to changes in oceanic temperatures on millennial time scales. In particular, we have found that the Bjørnøyrenna basin, located in the marine based Kara-Barents ice-sheet complex, is extremely sensitive to oceanic temperature variations and that the timing of its response relative to climate changes registered in Greenland depends on whether the surface or the subsurface of the ocean is considered as the relevant forcing of the ice sheet. Our results furthermore provide a mechanism to explain the pervasive signal of IRDs registered in marine sediments of the North Atlantic ocean. During stadials, the presence of IRDs can be explained through the build-up of subsurface heat in the high-latitude North Atlantic leading to increased iceberg calving in the presence of large, thick ice shelves, together with lower surface temperatures allowing for wider dispersal of icebergs (Barker and Knorr, 2007). However, increasing IRDs during interstadials could result from enhanced calving of the EIS due to subglacial melting of ice sheets in response to warmer surface oceanic conditions.

To conclude, we have used an EMIC to propose a new mechanism to explain glacial abrupt climate changes during the LGP that has obtained support from a comprehensive ESM. This highlights the usefulness of the use EMICs to open the pathway for new research lines that can be addressed with complex, more expensive ESMs. In addition, we have used an ice-sheet model to demonstrate a

substantial effect of glacial abrupt climate changes on NH ice sheets. The definite means to assess both issues will undoubtedly involve the use of coupled climate-ice-sheet models. This should be in the scope of future work.

# References


Abernathey, R., J. Marshall, and D. Ferreira, 2011: The dependence of Southern Ocean meridional overturning on wind stress. *Journal of Physical Oceanography*, **41**, 2261–2278, doi:10.1175/JPO-D-11-023.1.

Ahn, J., E. Brook, A. Schmittner, and K. Kreutz, 2012: Abrupt change in atmospheric $CO_2$ during the last ice age. *Geophysical Research Letters*, **39**, L18711, doi:10.1029/2012GL053018.

Ahn, J. and E. J. Brook, 2008: Atmospheric $co_2$ and climate on millennial time scales during the last glacial period. *Science*, **322**, 83–85.

Ahn, J. and E. J. Brook, 2014: Siple dome ice reveals two modes of millennial co 2 change during the last ice age. *Nature Communications*, **5**, 3723.

Alley, R., S. Anandakrishnan, and P. Jung, 2001: Stochastic resonance in the north atlantic. *Paleoceanography*, **16**, 190–198.

Alley, R., P. Clark, L. Keigwin, and R. Webb, 1999a: Making sense of millennial-scale climate change. *Geophysical Monograph Series*, **112**, 385–394.

Alley, R. B., 2007: Wally was right: Predictive ability of the north atlantic "conveyor belt" hypothesis for abrupt climate change. *Annu. Rev. Earth Planet. Sci.*, **35**, 241–272.

Alley, R. B., P. U. Clark, P. Huybrechts, and I. Joughin, 1999b: The deglaciation of the northern hemisphere: a global perspective. *Ann. Rev. Earth and Plan. Sci.*, **27**, 149–182, doi: 10.1146/annurev.earth.27.1.149.

Altabet, M. A., M. J. Higginson, and D. W. Murray, 2002: The effect of millennial-scale changes in arabian sea denitrification on atmospheric $co_2$. *Nature*, **415**, 159.

Alvarez-Solas, J., R. Banderas, A. Robinson, and M. Montoya, 2018a: Oceanic forcing of the eurasian ice sheet on millennial time scales during the last glacial period. **submitted**.

Alvarez-Solas, J., S. Charbit, G. Ramstein, D. Paillard, C. Dumas, C. Ritz, and D. M. Roche, 2011a: Millennial-scale oscillations in the southern ocean in response to atmospheric co 2 increase. *Global and Planetary Change*, **76**, 128–136.

Alvarez-Solas, J., M. Montoya, C. Ritz, G. Ramstein, S. Charbit, C. Dumas, K. Nisancioglu, T. Dokken, and A. Ganopolski, 2011b: Heinrich event 1: an example of dynamical ice-sheet reaction to oceanic changes. *Clim. Past*, **7**, 1297–1306, doi:10.5194/cp-7-1297-2011.

Alvarez-Solas, J., M. Montoya, and A. Robinson, 2018b: Deglacial abrupt climate changes: not simply a freshwater problem. *Geophys. Res. Lett.*, **submitted**.

Alvarez-Solas, J., A. Robinson, M. Montoya, and C. Ritz, 2013: Iceberg discharges of the last glacial period driven by oceanic circulation changes. *Proceedings of the National Academy of Sciences*, **110**, 16350–16354.

Amante, C. and B. W. Eakins, 2009: Etopo1 1 Arc-minute Global Relief Model: Procedures, Data Sources and Analysis. doi:10.7289/V5C8276M.

Anderson, R. F., S. Ali, L. I. Bradtmiller, S. H. H. Nielsen, M. Q. Fleisher, B. E. Anderson, and L. H. Burckle, 2009: Wind-driven upwelling in the Southern Ocean and the deglacial rise in atmospheric $CO_2$. *Science*, **323**, 1443 – 1448, doi:10.1126/science.1167441.

Andreassen, K. and M. Winsborrow, 2009: Signature of ice streaming in bjrnyrenna, polar north atlantic, through the pleistocene and implications for ice-stream dynamics. *Annals of Glaciology*, **50**, 1726, doi:10.3189/172756409789624238.

Asmerom, Y., V. J. Polyak, and S. J. Burns, 2010: Variable winter moisture in the southwestern united states linked to rapid glacial climate shifts. *Nature Geoscience*, **3**, 114–117.

Bamber, J. L., R. L. Layberry, and S. Gogineni, 2001: A new ice thickness and bed data set for the greenland ice sheet: 1. measurement, data reduction, and errors. *Journal of Geophysical Research: Atmospheres*, **106**, 33773–33780.

Banderas, R., J. Alvarez-Solas, and M. Montoya, 2012: Role of $CO_2$ and Southern Ocean winds in glacial abrupt climate change. *Clim. Past*, **8**, 1011–1021, doi:10.5194/cp-8-1011-2012.

Banderas, R., J. Alvarez-Solas, A. Robinson, and M. Montoya, 2015: An interhemispheric mechanism for glacial abrupt climate change. *Clim. Dyn.*, **44**, 2897–2908, doi:10.1007/s00382-014-2211-8.

Banderas, R., J. Alvarez-Solas, A. Robinson, and M. Montoya, 2018: A new approach for simulating the paleo evolution of the northern hemisphere ice sheets. *Geoscientific Model Development*, **11**, 2299–2314.

Barbante, C., J.-M. Barnola, S. Becagli, J. Beer, M. Bigler, C. Boutron, T. Blunier, E. Castellano, O. Cattani, J. Chappellaz, et al., 2006: One-to-one coupling of glacial climate variability in greenland and antarctica. *Nature*, **444**, 195–198.

Bard, E., C. Jouannic, B. Hamelin, P. Pirazzoli, M. Arnold, G. Faure, and P. Sumosusastro, 1996: Pleistocene sea levels and tectonic uplift based on dating of corals from sumba island, indonesia. *Geophysical Research Letters*, **23**, 1473–1476.

Barker, S., J. Chen, X. Gong, L. Jonkers, G. Knorr, and D. Thornalley, 2015: Icebergs not the trigger for north atlantic cold events. *Nature*, **520**, 333.

Barker, S. and G. Knorr, 2007: Antarctic climate signature in the Greenland ice core record. *Proceedings of the National Academy of Sciences*, **104**, 17278–17282, doi:10.1073/pnas.0708494104.

Bauer, E. and A. Ganopolski, 2017: Comparison of surface mass balance of ice sheets simulated by positive-degree-day method and energy balance approach. *Climate of the Past*, **13**, 819.

Becker, L. W., H. P. Sejrup, B. O. Hjelstuen, H. Haflidason, and T. M. Dokken, 2017: Ocean-ice sheet interaction along the se nordic seas margin from 35 to 15ka bp. *Marine Geology*.

Beckmann, A. and H. Goosse, 2003: A parameterization of ice shelf-ocean interaction for climate models. *Ocean Modelling*, **5**, 157–170.

Bender, M., T. Sowers, M.-L. Dickson, J. Orchardo, P. Grootes, P. A. Mayewski, and D. A. Meese, 1994: Climate correlations between greenland and antarctica during the past 100,000 years. *Nature*, **372**, 663.

Bereiter, B., D. Lüthi, M. Siegrist, S. Schüpbach, T. Stocker, and H. Fischer, 2012: Mode change of millennial $CO_2$ variability during the last glacial cycle associated with a bipolar marine carbon seesaw. *Proceedings of the National Academy of Sciences*, **109**, 9755–9760, doi:10.1073/pnas.1204069109.

Blunier, T. and E. J. Brook, 2001: Timing of millennial-scale climate change in Antarctica and Greenland during the last glacial period. *Science*, **291**, 109–11, doi:10.1038/29447.

Böhm, E., J. Lippold, M. Gutjahr, M. Frank, P. Blaser, B. Antz, J. Fohlmeister, N. Frank, M. Andersen, and M. Deininger, 2015: Strong and deep atlantic meridional overturning circulation during the last glacial cycle. *Nature*, **517**, 73–76.

Bond, G., W. Broecker, S. Johnsen, J. McManus, L. Labeyrie, J. Jouzel, G. Bonani, et al., 1993: Correlations between climate records from North Atlantic sediments and Greenland ice. *Nature*, **365**, 143–147, doi:10.1038/365143a0.

Bond, G., H. Heinrich, W. Broecker, L. Labeyrie, J. McManus, J. Andrews, S. Huon, R. Jantschik, S. Clasen, C. Simet, K. Tedesco, M. Klas, G. Bonani, and

S. Ivy, 1992: Evidence for massive discharge of icebergs into the North Atlantic ocean during the last glacial. *Nature*, **360**, 245–249, doi:10.1038/360245a0.

Bond, G. and R. Lotti, 1995: Iceberg Discharges into the North Atlantic on Millennial Time Scales During the Last Glaciation. *Science*, **267**, 1005–1010.

Bond, G., W. Showers, M. Cheseby, R. Lotti, P. Almasi, P. Priore, H. Cullen, I. Hajdas, G. Bonani, et al., 1997: A pervasive millennial-scale cycle in north atlantic holocene and glacial climates. *science*, **278**, 1257–1266.

Bonelli, S., S. Charbit, M. Kageyama, M.-N. Woillez, G. Ramstein, C. Dumas, and A. Quiquet, 2009: Investigating the evolution of major northern hemisphere ice sheets during the last glacial-interglacial cycle. *Climate of the Past*, **5**, 329–345.

Bouttes, N., D. Roche, and D. Paillard, 2011: Systematic study of the fresh water fluxes impact on the carbon cycle. *Climate of the Past Discussions*, **7**, 1363–1392, doi:10.5194/cpd–7–1363–2011.

Braun, H., M. Christl, S. Rahmstorf, A. Ganopolski, A. Mangini, C. Kubatzki, K. Roth, and B. Kromer, 2005: Possible solar origin of the 1,470-year glacial climate cycle demonstrated in a coupled model. *Nature*, **438**, 208–211.

Broecker, W., D. Peteet, and D. Rind, 1985: Does the ocean-atmosphere system have more than one stable mode of operation? *Nature*, **315**, 21–26, doi:10.1038/315021a0.

Broecker, W. S., G. Bond, M. Klas, G. Bonani, and W. Wolfli, 1990: A salt oscillator in the glacial atlantic? 1. the concept. *Paleoceanography*, **5**, 469–477, doi:10.1029/PA005i004p00469.

Brook, E. J., J. W. White, A. S. Schilla, M. L. Bender, B. Barnett, J. P. Severinghaus, K. C. Taylor, R. B. Alley, and E. J. Steig, 2005: Timing of millennial-scale climate change at siple dome, west antarctica, during the last glacial period. *Quaternary Science Reviews*, **24**, 1333–1343.

Buckley, M. W. and J. Marshall, 2016: Observations, inferences, and mechanisms of the atlantic meridional overturning circulation: A review. *Reviews of Geophysics*, **54**, 5–63.

Bueler, E. and J. Brown, 2009: Shallow shelf approximation as a sliding law in a thermomechanically coupled ice sheet model. *Journal of Geophysical Research: Earth Surface*, **114**.

Burckel, P., C. Waelbroeck, J. M. Gherardi, S. Pichat, H. Arz, J. Lippold, T. Dokken, and F. Thil, 2015: Atlantic ocean circulation changes preceded millennial tropical south america rainfall events during the last glacial. *Geophysical Research Letters*, **42**, 411–418.

Cacho, I., J. O. Grimalt, C. Pelejero, M. Canals, F. J. Sierro, J. A. Flores, and N. Shackleton, 1999: Dansgaard-oeschger and heinrich event imprints in alboran sea paleotemperatures. *Paleoceanography*, **14**, 698–705.

Ceppi, P., Y.-T. Hwang, X. Liu, D. M. Frierson, and D. L. Hartmann, 2013: The relationship between the ITCZ and the Southern Hemispheric eddy-driven jet. *J. Geophys. Res. Atmos*, **118**, doi:10.1002/jgrd.50461.

Charbit, S., C. Ritz, G. Philippon, V. Peyaud, M. Kageyama, et al., 2007: Numerical reconstructions of the northern hemisphere ice sheets through the last glacial-interglacial cycle. *Climate of the Past*, **3**, 15–37.

Charbit, S., C. Ritz, and G. Ramstein, 2002: Simulations of northern hemisphere ice-sheet retreat:: sensitivity to physical mechanisms involved during the last deglaciation. *Quaternary Science Reviews*, **21**, 243–265.

Chiang, J. and C. Bitz, 2005: Influence of high latitude ice cover on the marine Intertropical Convergence Zone. *Clim. Dyn.*, **25**, 477–496, doi:10.1007/s00382-005-0040-5.

Clark, P. U., A. S. Dyke, J. D. Shakun, A. E. Carlson, J. Clark, B. Wohlfarth, J. X. Mitrovica, S. W. Hostetler, and A. M. McCabe, 2009: The last glacial maximum. *science*, **325**, 710–714.

Clark, P. U. and A. C. Mix, 2002: Ice sheets and sea level of the last glacial maximum. *Quaternary Science Reviews*, **21**, 1–7.

Clark, P. U. and N. G. Pisias, 2000: Interpreting iceberg deposits in the deep sea. *Science*, **290**, 51–52.

Clark, P. U., N. G. Pisias, T. F. Stocker, and A. J. Weaver, 2002: The role of the thermohaline circulation in abrupt climate change. *Nature*, **415**, 863–869.

Clark, P. U. and L. Tarasov, 2014: Closing the sea level budget at the last glacial maximum. *Proceedings of the National Academy of Sciences*, **111**, 15861–15862.

Clason, C. C., P. Applegate, and P. Holmlund, 2014: Modelling late weichselian evolution of the eurasian ice sheets forced by surface meltwater-enhanced basal sliding. *Journal of Glaciology*, **60**, 29–40.

Cox, M. D., 1989: An idealized model of the world ocean. part i: The global-scale water masses. *Journal of Physical Oceanography*, **19**, 1730–1752.

Crowley, T. J., 1992: North Atlantic Deep Water cools the Southern Hemisphere. *Paleoceanography*, **7**, 489–497, doi:10.1029/92PA01058.

Cuffey, K. M., G. D. Clow, E. J. Steig, C. Buizert, T. J. Fudge, M. Koutnik, E. D. Waddington, R. B. Alley, and J. P. Severinghaus, 2016: Deglacial temperature history of west antarctica. **113**, 14249–14254, doi:10.1073/pnas.1609132113.

Curry, W. B. and D. W. Oppo, 1997: Synchronous, high-frequency oscillations in tropical sea surface temperatures and north atlantic deep water production during the last glacial cycle. *Paleoceanography*, **12**, 1–14.

Dansgaard, W., S. Johnsen, H. Clausen, D. Dahl-Jensen, N. Gundestrup, C. Hammer, C. Hvidberg, J. Steffensen, A. Sveinbjörnsdottr, J. Jouzel, et al., 1993:

Evidence for general instability of past climate from a 250-kyr ice-core record. *Nature*, **364**, 218–220, doi:10.1038/364218a0.

Dansgaard, W., S. Johnsen, H. Clausen, D. Dahl-Jensen, N. Gundestrup, C. Hammer, and H. Oeschger, 1984: North atlantic climatic oscillations revealed by deep greenland ice cores. *Climate processes and climate sensitivity*, **29**, 288–298, doi:10.1029/GM029p0288.

Deblonde, G. and W. Peltier, 1991: Simulations of continental ice sheet growth over the last glacial-interglacial cycle: Experiments with a one-level seasonal energy balance model including realistic geography. *Journal of Geophysical Research: Atmospheres*, **96**, 9189–9215.

DeConto, R. M. and D. Pollard, 2016: Contribution of antarctica to past and future sea-level rise. *Nature*, **531**, 591.

Dee, D., S. Uppala, A. Simmons, P. Berrisford, P. Poli, S. Kobayashi, U. Andrae, M. Balmaseda, G. Balsamo, P. Bauer, et al., 2011: The era-interim reanalysis: Configuration and performance of the data assimilation system. *Quarterly Journal of the Royal Meteorological Society*, **137**, 553–597.

Delworth, T. L. and M. E. Mann, 2000: Observed and simulated multidecadal variability in the northern Hemisphere. *Clim. Dyn.*, **16**, 661–676.

Denton, G., R. Anderson, J. Toggweiler, R. Edwards, J. Schaefer, and A. Putnam, 2010: The last glacial termination. *Science*, **328**, 1652, doi:10.1126/science.1184119.

Denton, G. H. and T. J. Hughes, 1981: The arctic ice sheet: an outrageous hypothesis. *The Last Great Ice Sheets. Wiley, New York*, 437–467.

Dickson, A. J., W. E. Austin, I. R. Hall, M. A. Maslin, and M. Kucera, 2008: Centennial-scale evolution of Dansgaard-Oeschger events in sediment core MD95-2006.

Dokken, T. M., K. H. Nisancioglu, C. Li, D. S. Battisti, and C. Kissel, 2013: Dansgaard-oeschger cycles: Interactions between ocean and sea ice intrinsic to the Nordic seas. *Paleoceanography*, **28**, 491–502, doi:10.1002/palo.20042.

Dubois, N., M. Kienast, S. Kienast, C. Normandeau, S. E. Calvert, T. D. Herbert, and A. Mix, 2011: Millennial-scale variations in hydrography and biogeochemistry in the eastern equatorial pacific over the last 100 kyr. *Quaternary Science Reviews*, **30**, 210–223.

Dyke, A., J. Andrews, P. Clark, J. England, G. Miller, J. Shaw, and J. Veillette, 2002: The laurentide and innuitian ice sheets during the last glacial maximum. *Quaternary Science Reviews*, **21**, 9–31.

EPICA-Project, 2004: Eight glacial cycles from an Antarctic ice core. *Nature*, **429**, 623–628, doi:10.1038/nature02599.

EPICA-Project, 2006: One-to-one coupling of glacial climate variability in Greenland and Antarctica. *Nature*, **444**, 195–198, doi:10.1038/nature05301.

Fang, Z. and J. M. Wallace, 1994: Arctic sea ice variability on a timescale of weeks and its relation to atmospheric forcing. *Journal of Climate*, **7**, 1897–1914.

Fichefet, T. and M. A. M. Maqueda, 1997: Sensitivity of a global sea ice model to the treatment of ice thermodynamics and dynamics. *J. Geophys. Res.*, **102**, 12609–12646, doi:10.1029/97JC00480.

Forsström, P.-L. and R. Greve, 2004: Simulation of the eurasian ice sheet dynamics during the last glaciation. *Global and Planetary Change*, **42**, 59–81.

Ganachaud, A. and C. Wunsch, 2002: Oceanic nutrient and oxygen transports and bounds on export production during the World Ocean Circulation Experiment. *Global Biogeochemical Cycles*, **16**, 1057.

Ganachaud, A. and C. Wunsch, 2003: Large-scale ocean heat and freshwater transports during the World Ocean Circulation Experiment. *J. Clim.*, **16**, 696–705.

Ganopolski, A. and R. Calov, 2011: The role of orbital forcing, carbon dioxide and regolith in 100 kyr glacial cycles. *Climate of the Past*, **7**, 1415–1425.

Ganopolski, A. and S. Rahmstorf, 2001: Rapid changes of glacial climate simulated in a coupled climate model. *Nature*, **409**, 153–158, doi:10.1038/35051500.

Ganopolski, A., S. Rahmstorf, V. Petoukhov, and M. Claussen, 1998: Simulation of modern and glacial climates with a coupled global model of intermediate complexity. *Nature*, **391**, 351–356.

Genty, D., D. Blamart, R. Ouahdi, M. Gilmour, A. Baker, J. Jouzel, and S. Van-Exter, 2003: Precise dating of dansgaard–oeschger climate oscillations in western europe from stalagmite data. *Nature*, **421**, 833.

Gherardi, J.-M., L. Labeyrie, S. Nave, R. Francois, J. F. McManus, and E. Cortijo, 2009: Glacial-interglacial circulation changes inferred from 231pa/230th sedimentary record in the north atlantic region. *Paleoceanography*, **24**.

Gildor, H. and E. Tziperman, 2003: Sea-ice switches and abrupt climate change. *Philosophical Transactions of the Royal Society of London*, **361**, 1935 – 1944, doi:10.1098/rsta.2003.1244.

Gnanadesikan, A., 1999: A simple predictive model for the structure of the oceanic pycnocline. *Science*, **283**, 2077–2079, doi:10.1126/science.283.5410.2077.

Goelzer, H., P. Huybrechts, M.-F. Loutre, and T. Fichefet, 2016: Impact of ice sheet meltwater fluxes on the climate evolution at the onset of the last interglacial. *Climate of the Past*, **12**, 1721–1737.

Goldstein, S. L. and S. R. Hemming, 2003: Long-lived isotopic tracers in oceanography, paleoceanography, and ice-sheet dynamics. *Treatise on geochemistry*, **6**, 625.

Gottschalk, J., D. A. Hodell, L. C. Skinner, S. J. Crowhurst, S. L. Jaccard, and C. Charles, 2015a: Past carbonate preservation events in the deep southeast

atlantic ocean (cape basin) and their implications for atlantic overturning dynamics and marine carbon cycling. *Paleoceanography and Paleoclimatology*, **33**, 643–663, doi:10.1029/2018PA003353.

Gottschalk, J., L. C. Skinner, S. Misra, C. Waelbroeck, L. Menviel, and A. Timmermann, 2015b: Abrupt changes in the southern extent of north atlantic deep water during dansgaard–oeschger events. *Nature geoscience*, **8**, 950.

Grant, K., E. Rohling, M. Bar-Matthews, A. Ayalon, M. Medina-Elizalde, C. B. Ramsey, C. Satow, and A. Roberts, 2012: Rapid coupling between ice volume and polar temperature over the past 150,000 [thinsp] years. *Nature*, **491**, 744–747.

Grootes, P. M., M. Stuiver, J. W. C. White, S. Johnsen, and J. Jouzel, 1993: Comparison of oxygen isotope records from the GISP2 and GRIP Greenland ice cores. *Nature*, **366**, 552–554, doi:10.1038/366552a0.

Grousset, F. E., C. Pujol, L. Labeyrie, G. Auffret, and A. Boelaert, 2000: Were the north atlantic heinrich events triggered by the behavior of the european ice sheets? *Geology*, **28**, 123–126.

Gudlaugsson, E., A. Humbert, K. Andreassen, C. C. Clason, T. Kleiner, and S. Beyer, 2017: Eurasian ice-sheet dynamics and sensitivity to subglacial hydrology. *Journal of Glaciology*, **63**, 556–564.

Gudlaugsson, E., A. Humbert, M. Winsborrow, and K. Andreassen, 2013: Subglacial roughness of the former barents sea ice sheet. *Journal of Geophysical Research: Earth Surface*, **118**, 2546–2556.

Gulev, S. K., M. Latif, N. Keenlyside, W. Park, and K. P. Koltermann, 2013: North atlantic ocean control on surface heat flux on multidecadal timescales. *Nature*, **499**, 464.

Hall, I. R., E. Colmenero-Hidalgo, R. Zahn, V. L. Peck, and S. Hemming, 2011: Centennial-to millennial-scale ice-ocean interactions in the subpolar northeast atlantic 18–41 kyr ago. *Paleoceanography*, **26**.

Hallberg, R. and A. Gnanadesikan, 2006: The role of eddies in determining the structure and response of the wind-driven Southern Hemisphere overturning: Results from the modeling eddies in the Southern Ocean (MESO) project. *Journal of Physical Oceanography*, **36**, 2232–2252.

Hays, J. D., J. Imbrie, and N. J. Shackleton, 1976: Variations in the earth's orbit: pacemaker of the ice ages. *Science*, **194**, 1121–1132.

Heinrich, H., 1988: Origin and consequences of cyclic ice rafting in the northeast Atlantic Ocean during the past 130,000 years. *Quaternary Research*, **29**, 142–152, doi:10.1016/0033-5894(88)90057-9.

Helmens, K. F. and S. Engels, 2010: Ice-free conditions in eastern fennoscandia during early marine isotope stage 3: lacustrine records. *Boreas*, **39**, 399–409.

Hemming, S. R., 2004: Heinrich events: Massive late Pleistocene detritus layers of the North Atlantic and their global climate imprint. *Rev. Geophys*, **42**, RG1005, doi:10.1029/2003RG000128.

Hendy, I. L. and J. P. Kennett, 2000: Dansgaard-oeschger cycles and the california current system: Planktonic foraminiferal response to rapid climate change in santa barbara basin, ocean drilling program hole 893a. *Paleoceanography*, **15**, 30–42.

Henry, L., J. F. McManus, W. B. Curry, N. L. Roberts, A. M. Piotrowski, and L. D. Keigwin, 2016: North atlantic ocean circulation and abrupt climate change during the last glaciation. *Science*, **353**, 470–474.

Hoff, U., T. L. Rasmussen, R. Stein, M. M. Ezat, and K. Fahl, 2016: Sea ice and millennial-scale climate variability in the nordic seas 90kyr ago to present. *Nature Communications*, **7**, 12247.

Holland, P. R., A. Jenkins, and D. M. Holland, 2008: The response of ice shelf basal melting to variations in ocean temperature. *Journal of Climate*, **21**, 2558–2572.

Huber, C., M. Leuenberger, R. Spahni, J. Flückiger, J. Schwander, T. Stocker, S. Johnsen, A. Landais, and J. Jouzel, 2006: Isotope calibrated Greenland temperature record over Marine Isotope Stage 3 and its relation to $CH_4$. *Earth and Planetary Science Letters*, **243**, 504–519, doi:10.1016/j.epsl.2006.01.002.

Hughes, A. L., R. Gyllencreutz, Ø. S. Lohne, J. Mangerud, and J. I. Svendsen, 2016: The last eurasian ice sheets–a chronological database and time-slice reconstruction, dated-1. *Boreas*, **45**, 1–45.

Hutter, K., 1983: *Theoretical glaciology: material science of ice and the mechanics of glaciers and ice sheets*, volume 1. Springer.

Imbrie, J., E. Boyle, S. Clemens, A. Duffy, W. Howard, G. Kukla, J. Kutzbach, D. Martinson, A. McIntyre, A. Mix, et al., 1992: On the structure and origin of major glaciation cycles 1. linear responses to milankovitch forcing. *Paleoceanography*, **7**, 701–738.

Indermühle, A., E. Monnin, B. Stauffer, T. F. Stocker, and M. Wahlen, 2000: Atmospheric $co_2$ concentration from 60 to 20 kyr bp from the taylor dome ice core, antarctica. *Geophysical Research Letters*, **27**, 735–738.

Johns, W. E., M. O. Baringer, L. M. Beal, S. Cunningham, T. Kanzow, H. L. Bryden, J. Hirschi, J. Marotzke, C. Meinen, B. Shaw, et al., 2011: Continuous, array-based estimates of atlantic ocean heat transport at 26.5 n. *Journal of Climate*, **24**, 2429–2449.

Johnsen, S. J., D. Dahl-Jensen, N. Gundestrup, J. P. Steffensen, H. B. Clausen, H. Miller, V. Masson-Delmotte, A. E. Sveinbjörnsdottir, and J. White, 2001: Oxygen isotope and palaeotemperature records from six greenland ice-core stations: Camp century, dye-3, grip, gisp2, renland and northgrip. *Journal of*

*Quaternary Science: Published for the Quaternary Research Association*, **16**, 299–307.

Kageyama, M., A. Paul, D. Roche, and C. Van Meerbeeck, 2010: Modelling glacial climatic millennial-scale variability related to changes in the atlantic meridional overturning circulation: a review. *Quaternary Science Reviews*, 2931–2956, doi:10.1016/j.quascirev.2010.05.029.

Kaspi, Y., R. Sayag, and E. Tziperman, 2004: A triple sea-ice state mechanism for the abrupt warming and synchronous ice sheet collapses during heinrich events. *Paleoceanography*, **19**, doi:10.1029/2004PA001009.

Keeling, C. D. and T. P. Whorf, 2000: The 1,800-year oceanic tidal cycle: A possible cause of rapid climate change. **97**, 3814–3819, doi:10.1073/pnas.070047197.

Keeling, R. F. and B. B. Stephens, 2001: Antarctic sea ice and the control of Pleistocene climate instability. *Paleoceanography*, **16**, 112–131, doi:10.1029/2000pa000529.

Keigwin, L. D. and E. A. Boyle, 1999: Surface and deep ocean variability in the northern sargasso sea during marine isotope stage 3. *Paleoceanography*, **14**, 164–170.

Kindler, P., M. Guillevic, M. Baumgartner, J. Schwander, A. Landais, and M. Leuenberger, 2014: Temperature reconstruction from 10 to 120 kyr b2k from the ngrip ice core. *Climate of the Past*, **10**, 887–902.

Kissel, L. C. L. L. D. T. V. A. . B. D., C., 1999: Rapid climatic variations during marine isotopic stage 3: magnetic analysis of sediments from nordic seas and north atlantic. *Earth and Planetary Science Letters*, **171(3)**, 489–502.

Kleman, J., J. Fastook, K. Ebert, J. Nilsson, and R. Caballero, 2013: Pre-lgm northern hemisphere ice sheet topography. *Climate of the Past*, **9**, 2365.

Kleppin, H., M. Jochum, B. Otto-Bliesner, C. A. Shields, and S. Yeager, 2015: Stochastic atmospheric forcing as a cause of greenland climate transitions. *Journal of Climate*, **28**, 7741–7763, doi:10.1175/JCLI-D-14-00728.1.

Knorr, G. and G. Lohmann, 2003: Southern Ocean origin for the resumption of the Atlantic thermohaline circulation during deglaciation. *Nature*, **424**, 532–536, doi:10.1038/nature01855.

Knorr, G. and G. Lohmann, 2007: Rapid transitions in the Atlantic thermohaline circulation triggered by global warming and meltwater during the last deglaciation. *Geochemistry Geophysics Geosystems*, **8**, Q12006, doi:10.1029/2007GC001604.

Knutti, R., J. Flückiger, T. Stocker, and A. Timmermann, 2004: Strong hemispheric coupling of glacial climate through freshwater discharge and ocean circulation. *Nature*, **430**, 851–856.

Krebs, U. and A. Timmermann, 2007: Tropical air-sea interactions accelerate the recovery of the Atlantic meridional overturning circulation after a major shutdown. *Journal of Climate*, **20**, 4940–4956, doi:10.1175/JCLI4296.1.

Kreveld, S. v., M. Sarnthein, H. Erlenkeuser, P. Grootes, S. Jung, M. Nadeau, U. Pflaumann, and A. Voelker, 2000: Potential links between surging ice sheets, circulation changes, and the dansgaard-oeschger cycles in the irminger sea, 60–18 kyr. *Paleoceanography*, **15**, 425–442.

Kuhlbrodt, T., A. Griesel, M. Montoya, A. Levermann, M. Hofmann, and S. Rahmstorf, 2007: On the driving processes of the Atlantic meridional overturning circulation. *Rev. Geophys.*, **45**, RG2001, doi:10.1029/2004RG000166.

Lambeck, K. and J. Chappell, 2001: Sea level change through the last glacial cycle. *Science*, **292**, 679–686.

Lambeck, K., H. Rouby, A. Purcell, Y. Sun, and M. Sambridge, 2014: Sea level and global ice volumes from the last glacial maximum to the holocene. *Proceedings of the National Academy of Sciences*, **111**, 15296–15303.

Lambeck, K., Y. Yokoyama, P. Johnston, and A. Purcell, 2000: Global ice volumes at the last glacial maximum and early lateglacial. *Earth and planetary science letters*, **181**, 513–527.

Lambeck, K., Y. Yokoyama, and T. Purcell, 2002: Into and out of the last glacial maximum: sea-level change during oxygen isotope stages 3 and 2. *Quaternary Science Reviews*, **21**, 343–360.

Lamy, F., J. Kaiser, H. Arz, D. Hebbeln, U. Ninnemann, O. Timm, A. Timmermann, and J. Toggweiler, 2007: Modulation of the bipolar seesaw in the southeast pacific during termination 1. *Earth and Planetary Science Letters*, **259**, 400–413, doi:10.1016/j.epsl.2007.04.040.

Landais, A., J. Barnola, V. Masson-Delmotte, J. Jouzel, J. Chappellaz, N. Caillon, C. Huber, M. Leuenberger, and S. Johnsen, 2004: A continuous record of temperature evolution over a sequence of Dansgaard-Oeschger events during Marine Isotopic Stage 4 (76 to 62 kyr BP). *Geophysical Research Letters*, **31**, doi:10.1029/2004GL021193.

Lang, C., M. Leuenberger, J. Schwander, and S. Johnsen, 1999: 16° C rapid temperature variation in central Greenland 70,000 years ago. *Science*, **286**, 934, doi:10.1126/science.286.5441.934.

Langebroek, P., A. Paul, and M. Schulz, 2009: Antarctic ice-sheet response to atmospheric co 2 and insolation in the middle miocene. *Climate of the Past*, **5**, 633–646.

Laske, G., 1997: A global digital map of sediment thickness. *Eos Trans. AGU*, **78**, F483.

Lea, D. W., D. K. Pak, C. L. Belanger, H. J. Spero, M. A. Hall, and N. J. Shackleton, 2006: Paleoclimate history of galapagos surface waters over the last 135,000 yr. *Quaternary Science Reviews*, **25**, 1152–1167.

Lee, S., J. Chiang, K. Matsumoto, and K. Tokos, 2011: Southern Ocean wind response to North Atlantic cooling and the rise in atmospheric $CO_2$: Modeling perspective and paleoceanography implications. *Paleoceanography*, **26**, PA1214, doi:10.1029/2010PA002004.

Lekens, W., H. Sejrup, H. Haflidason, J. Knies, and T. Richter, 2006: Meltwater and ice rafting in the southern norwegian sea between 20 and 40 calendar kyr bp: Implications for fennoscandian heinrich events. *Paleoceanography*, **21**.

Levermann, A., T. Albrecht, R. Winkelmann, M. A. Martin, M. Haseloff, and I. Joughin, 2012: Kinematic first-order calving law implies potential for abrupt ice-shelf retreat. *The Cryosphere*, **6**, 273–286.

Li, C., D. Battisti, D. Schrag, and E. Tziperman, 2005: Abrupt climate shifts in Greenland due to displacements of the sea ice edge. *Geophys. Res. Lett.*, **32**, L19702, doi:10.1029/2005GL023492.

Li, C., D. S. Battisti, and C. M. Bitz, 2010: Can North Atlantic sea ice anomalies account for Dansgaard–Oeschger climate signals? *Journal of Climate*, **23**, doi:10.1175/2010JCLI3409.1.

Liu, Z., B. Otto-Bliesner, F. He, E. Brady, R. Tomas, P. Clark, A. Carlson, J. Lynch-Stieglitz, W. Curry, E. Brook, et al., 2009: Transient simulation of last deglaciation with a new mechanism for Bolling-Allerod warming. *Science*, **325**, 310–314, doi:10.1126/science.1171041.

Lumpkin, R. and K. Speer, 2007: Global ocean meridional overturning. *Journal of Physical Oceanography*, **37**, 2550–2562.

Lynch-Stieglitz, J., 2017: The atlantic meridional overturning circulation and abrupt climate change. *Annual review of marine science*, **9**, 83–104.

Lynch-Stieglitz, J., J. F. Adkins, W. B. Curry, T. Dokken, I. R. Hall, J. C. Herguera, J. Hirschi, E. Ivanova, C. Kissel, O. Marchal, T. Marchitto, I. McCave, J. McManus, S. Mulitza, U. Ninnemann, F. Peeters, E. Yu, and R. Zahn, 2007: Atlantic meridional overturning circulation during the last glacial maximum. *Science*, **316**, 66–68.

MacAyeal, D. R., 1989: Large-scale ice flow over a viscous basal sediment: Theory and application to ice stream b, antarctica. *Journal of Geophysical Research: Solid Earth*, **94**, 4071–4087.

Mangerud, J., S. Gulliksen, and E. Larsen, 2010: 14c-dated fluctuations of the western flank of the scandinavian ice sheet 45–25 kyr bp compared with bølling–younger dryas fluctuations and dansgaard–oeschger events in greenland. *Boreas*, **39**, 328–342.

Mangerud, J., R. Løvlie, S. Gulliksen, A.-K. Hufthammer, E. Larsen, and V. Valen, 2003: Paleomagnetic correlations between scandinavian ice-sheet fluctuations and greenland dansgaard–oeschger events, 45,000–25,000 yr bp. *Quaternary Research*, **59**, 213–222.

Marchitto, T. M. and W. S. Broecker, 2006: Deep water mass geometry in the glacial atlantic ocean: A review of constraints from the paleonutrient proxy cd/ca. *Geochemistry, Geophysics, Geosystems*, **7**.

Margold, M., C. R. Stokes, and C. D. Clark, 2015: Ice streams in the laurentide ice sheet: Identification, characteristics and comparison to modern ice sheets. *Earth-Science Reviews*, **143**, 117–146.

Marotzke, J., 2012: A grip on ice-age ocean circulation. *Nature*, **485**, 180–181, doi:10.1038/485180a.

Marshall, J., A. Donohoe, D. Ferreira, and D. McGee, 2014: The oceans role in setting the mean position of the inter-tropical convergence zone. *Climate dynamics*, **42**, 1967–1979.

Marshall, J. and K. Speer, 2012: Closure of the meridional overturning circulation through southern ocean upwelling. *Nature Geoscience*, **5**, 171–180.

Marshall, S. J., T. S. James, and G. K. Clarke, 2002: North american ice sheet reconstructions at the last glacial maximum. *Quaternary Science Reviews*, **21**, 175–192.

Marshall, S. J. and M. R. Koutnik, 2006: Ice sheet action versus reaction: Distinguishing between heinrich events and dansgaard-oeschger cycles in the north atlantic. *Paleoceanography*, **21**.

Marshall, S. J., L. Tarasov, G. K. Clarke, and W. R. Peltier, 2000: Glaciological reconstruction of the laurentide ice sheet: physical processes and modelling challenges. *Canadian Journal of Earth Sciences*, **37**, 769–793.

Marsiat, I., 1994: Simulation of the northern hemisphere continental ice sheets over the last glacial-interglacial cycle: experiments with a latitude-longitude vertically integrated ice sheet model coupled to a zonally averaged climate model. *Paleoclimates*, **1**, 59–98.

Martínez-García, A., D. M. Sigman, H. Ren, R. F. Anderson, M. Straub, D. A. Hodell, S. L. Jaccard, T. I. Eglinton, and G. H. Haug, 2014: Iron fertilization of the Subantarctic Ocean during the last ice age. *Science*, **343**, 1347–1350, doi:10.1126/science.1246848.

Martrat, B., J. Grimalt, C. Lopez-Martinez, I. Cacho, F. Sierro, J. Flores, R. Zahn, M. Canals, J. Curtis, and D. Hodell, 2004: Abrupt Temperature Changes in the Western Mediterranean over the Past 250,000 Years.

Martrat, B., J. Grimalt, N. Shackleton, L. de Abreu, M. Hutterli, and T. Stocker, 2007: Four Climate Cycles of Recurring Deep and Surface Water Destabilizations on the Iberian Margin. *Science*, **317**, 502.

McCarthy, G., D. Smeed, S. Cunningham, and C. Roberts, 2017: Atlantic meridonal overturning circulation.

McCarthy, G., D. Smeed, W. Johns, E. Frajka-Williams, B. Moat, D. Rayner, M. Baringer, C. Meinen, J. Collins, and H. Bryden, 2015a: Measuring the atlantic meridional overturning circulation at 26 n. *Progress in Oceanography*, **130**, 91–111.

McCarthy, G. D., I. D. Haigh, J. J.-M. Hirschi, J. P. Grist, and D. A. Smeed, 2015b: Ocean impact on decadal atlantic climate variability revealed by sea-level observations. *Nature*, **521**, 508.

McCave, I. and I. R. Hall, 2006: Size sorting in marine muds: Processes, pitfalls, and prospects for paleoflow-speed proxies. *Geochemistry, Geophysics, Geosystems*, **7**.

McDougall, T. J. and J. A. Church, 1986: Pitfalls with the numerical representation of isopycnal diapycnal mixing. *Journal of Physical Oceanography*, **16**, 196–199.

McManus, J. F., R. Francois, J. M. Gherardi, L. D. Keigwin, and S. Brown-Leger, 2004: Collapse and rapid resumption of Atlantic meridional circulation linked to deglacial climate changes. *Nature*, **428**, 834–837.

Menviel, L., A. Timmermann, T. Friedrich, and M. England, 2014: Hindcasting the continuum of Dansgaard–Oeschger variability: mechanisms, patterns and timing. *Climate of the Past*, **10**, 63–77, doi:10.5194/cp-10-63-2014.

Menviel, L., A. Timmermann, A. Mouchet, and O. Timm, 2008: Climate and marine carbon cycle response to changes in the strength of the southern hemispheric westerlies. *Paleoceanography*, **23**, PA4201, doi:10.1029/2008PA001604.

Milne, G. A., J. X. Mitrovica, and D. P. Schrag, 2002: Estimating past continental ice volume from sea-level data. *Quaternary Science Reviews*, **21**, 361–376.

Montoya, M., A. Griesel, A. Levermann, J. Mignot, M. Hofmann, A. Ganopolski, and S. Rahmstorf, 2005: The Earth System Model of Intermediate Complexity CLIM*BER*-3$\alpha$. Part I: description and performance for present day conditions. *Clim. Dyn.*, **25**, 237–263, doi:10.1007/s00382-005-0044-1.

Montoya, M. and A. Levermann, 2008: Surface wind-stress threshold for glacial Atlantic overturning. *Geophys. Res. Lett.*, **35**, L03608, doi:10.1029/2007GL032560.

Moreno, P. I., R. Villa-Martínez, M. Cárdenas, and E. Sagredo, 2012: Deglacial changes of the southern margin of the southern westerly winds revealed by terrestrial records from sw patagonia (52s). *Quaternary Science Reviews*, **41**, 1 – 21, doi:https://doi.org/10.1016/j.quascirev.2012.02.002.

Mosblech, N. A., M. B. Bush, W. D. Gosling, D. Hodell, L. Thomas, P. van Calsteren, A. Correa-Metrio, B. G. Valencia, J. Curtis, and R. van Woesik,

2012: North Atlantic forcing of Amazonian precipitation during the last ice age. *Nature Geosci.*, **5**, 817–820, doi:10.1038/ngeo1588.

Moseley, G. E., C. Spötl, A. Svensson, H. Cheng, S. Brandstätter, and R. L. Edwards, 2014: Multi-speleothem record reveals tightly coupled climate between central europe and greenland during marine isotope stage 3. *Geology*, **42**, 1043–1046.

Münchow, A., L. Padman, and H. A. Fricker, 2014: Interannual changes of the floating ice shelf of petermann gletscher, north greenland, from 2000 to 2012. *Journal of Glaciology*, **60**, 489–499.

Munk, W. and C. Wunsch, 1998: Abyssal recipes II. *Deep-Sea Research I*, **45**, 1977–2010.

NGRIP members, 2004: High-resolution record of Northern Hemisphere climate extending into the last glacial period. *Nature*, **431**, 147–151.

Ohmura, A. and N. Reeh, 1991: New precipitation and accumulation maps for greenland. *Journal of Glaciology*, **37**, 140–148.

Oka, A., H. Hasumi, and A. Abe-Ouchi, 2012: The thermal threshold of the atlantic meridional overturning circulation and its control by wind stress forcing during glacial climate. *Geophys. Res. Lett.*, **39**, L09709, doi:10.1029/2012GL051421.

Olsen, L., H. Sveian, K. Borg, B. Bergstram, and M. Broekmans, 2002: Rapid and rhythmic ice sheet fluctuations in western scandinavia 15-40 kya–a review. *Polar Research*, **21**, 235–242.

Palter, J. B., 2015: The role of the gulf stream in european climate. *Annual review of marine science*, **7**, 113–137.

Parrenin, F., V. Masson-Delmotte, P. Köhler, D. Raynaud, D. Paillard, J. Schwander, C. Barbante, A. Landais, A. Wegner, and J. Jouzel, 2013: Synchronous change of atmospheric $CO_2$ and Antarctic temperature during the last deglacial warming. *Science*, **339**, 1060–1063, doi:10.1126/science.1226368.

Patton, H., A. Hubbard, K. Andreassen, M. Winsborrow, and A. P. Stroeven, 2016: The build-up, configuration, and dynamical sensitivity of the eurasian ice-sheet complex to late weichselian climatic and oceanic forcing. *Quaternary Science Reviews*, **153**, 97–121.

Pattyn, F., 2017: Sea-level response to melting of antarctic ice shelves on multi-centennial timescales with the fast elementary thermomechanical ice sheet model (f. etish v1. 0). *The Cryosphere*, **11**, 1851.

Peck, V., I. Hall, R. Zahn, F. Grousset, S. Hemming, and J. Scourse, 2007: The relationship of heinrich events and their european precursors over the past 60ka bp: a multi-proxy ice-rafted debris provenance study in the north east atlantic. *Quaternary Science Reviews*, **26**, 862–875.

Pedro, J. B., M. Jochum, C. Buizert, F. He, S. Barker, and S. O. Rasmussen, 2018: Beyond the bipolar seesaw: Toward a process understanding of interhemispheric coupling. *Quaternary Science Reviews*, **192**, 27–46.

Pedro, J. B., T. Van Ommen, S. Rasmussen, V. I. Morgan, J. Chappellaz, A. D. Moy, V. Masson-Delmotte, and M. Delmotte, 2011: The last deglaciation: timing the bipolar seesaw. *Climate of the Past*, **7**, 671–683.

Peltier, W., 2004: Global glacial isostasy and the surface of the ice-age Earth-The ICE-5 G(VM 2) model and GRACE. *Ann. Rev. Earth and Plan. Sci.*, **32**, 111–149, doi:10.1146/annurev.earth.32.082503.144359.

Peltier, W. and J. Andrews, 1976: Glacial-isostatic adjustmenti. the forward problem. *Geophysical Journal International*, **46**, 605–646.

Peltier, W., D. Argus, and R. Drummond, 2015: Space geodesy constrains ice age terminal deglaciation: The global ice-6g_c (vm5a) model. *Journal of Geophysical Research: Solid Earth*, **120**, 450–487.

Peltier, W. R. and S. Marshall, 1995: Coupled energy-balance/ice-sheet model simulations of the glacial cycle: A possible connection between terminations and terrigenous dust. *Journal of Geophysical Research: Atmospheres*, **100**, 14269–14289.

Peltier, W. R. and G. Vettoretti, 2014: Dansgaard-oeschger oscillations predicted in a comprehensive model of glacial climate: A kicked salt oscillator in the atlantic. *Geophysical Research Letters*, **41**, 7306–7313.

Petersen, S., D. Schrag, and P. Clark, 2013: A new mechanism for Dansgaard-Oeschger cycles. *Paleoceanography*, doi:10.1029/2012PA002364.

Peterson, L., G. Haug, K. Hughen, and U. Röhl, 2000: Rapid changes in the hydrologic cycle of the tropical atlantic during the last glacial. *Science*, **290**, 1947–1951, doi:10.1126/science.290.5498.1947.

Peterson, L. C. and G. H. Haug, 2006: Variability in the mean latitude of the atlantic intertropical convergence zone as recorded by riverine input of sediments to the cariaco basin (venezuela). *Palaeogeography, Palaeoclimatology, Palaeoecology*, **234**, 97–113.

Petit, J., J. Jouzel, D. Raynaud, N. Barkov, J.-M. Barnola, I. Basile, M. Bender, J. Chappellaz, M. Davis, G. Delaygue, M. Delmotte, V. Kotlaykov, M. Legrand, V. Lipenkov, c. Lorius, L. Pepin, C. Ritz, E. Saltzman, and M. Stievenard, 1999: Climate and atmospheric history of the past 420, 000 years from the vostok ice core, antarctica. *Nature*, **399**, 429 – 436.

Petoukhov, V., A. Ganopolski, V. Brovkin, M. Claussen, A. Eliseev, C. Kubatzki, and S. Rahmstorf, 2000: CLIMBER-2: a climate system model of intermediate complexity. Part I: model description and performance for present climate. *Clim. Dyn.*, **16**, 1–17, doi:10.1007/PL00007919.

Peyaud, V., C. Ritz, and G. Krinner, 2007: Modelling the early weichselian eurasian ice sheets: role of ice shelves and influence of ice-dammed lakes. *Climate of the Past Discussions*, **3**, 221–247.

Philippon, G., G. Ramstein, S. Charbit, M. Kageyama, C. Ritz, and C. Dumas, 2006: Evolution of the antarctic ice sheet throughout the last deglaciation: a study with a new coupled climatenorth and south hemisphere ice sheet model. *Earth and Planetary Science Letters*, **248**, 750–758.

Piotrowski, A. M., S. L. Goldstein, R. H. Sidney, R. G. Fairbanks, and D. R. Zylberberg, 2008: Oscillating glacial northern and southern deep water formation from combined neodymium and carbon isotopes. *Earth and Planetary Science Letters*, **272**, 394–405.

Pollard, D. and R. DeConto, 2012: Description of a hybrid ice sheet-shelf model, and application to antarctica. *Geoscientific Model Development*, **5**, 1273.

Putnam, A., J. Schaefer, D. Barrell, M. Vandergoes, G. Denton, M. Kaplan, R. Finkel, R. Schwartz, B. Goehring, and S. Kelley, 2010: In situ cosmogenic 10be production-rate calibration from the southern alps, new zealand. *Quaternary Geochronology*, **5**, 392 – 409, doi:https://doi.org/10.1016/j.quageo.2009.12.001.

Quiquet, A., H. Punge, C. Ritz, X. Fettweis, M. Kageyama, G. Krinner, D. Salas Y Mélia, and J. Sjolte, 2012: Large sensitivity of a greenland ice sheet model to atmospheric forcing fields. *The Cryosphere Discussions*, **6**, 1037–1083.

Quiquet, A., C. Ritz, H. Punge, and D. Salas y Mélia, 2013: Greenland ice sheet contribution to sea level rise during the last interglacial period: a modelling study driven and constrained by ice core data. *Climate of the Past*, **9**, 353–366.

Rahmstorf, S., 1996: On the freshwater forcing and transport of the Atlantic thermohaline circulation. *Clim. Dyn.*, **12**, 799–811, doi:10.1007/s003820050144.

Rahmstorf, S., 2002: Ocean circulation and climate during the past 120,000 years. *Nature*, **419**, 207–214.

Rashid, H., R. Hesse, and D. Piper, 2003: Evidence for an additional Heinrich event between H5 and H6 in the labrador sea. *Paleoceanography*, **18**, 1077, doi:10.1029/2003PA000913.

Rasmussen, T. L. and E. Thomsen, 2013: Pink marine sediments reveal rapid ice melt and arctic meltwater discharge during dansgaard-oeschger warmings. *Nature communications*, **4**, 2849.

Rasmussen, T. L., E. Thomsen, and M. Moros, 2016: North atlantic warming during dansgaard-oeschger events synchronous with antarctic warming and out-of-phase with greenland climate. *Scientific reports*, **6**, 20535.

Ravelo, A. C. and C. Hillaire-Marcel, 2007: Chapter eighteen the use of oxygen and carbon isotopes of foraminifera in paleoceanography. *Developments in Marine Geology*, **1**, 735–764.

Reeh, N., 1989: Parameterization of melt rate and surface temperature on the greenland ice sheet. *Polarforschung*, **59**, 113–128.

Rignot, E. and S. S. Jacobs, 2002: Rapid bottom melting widespread near antarctic ice sheet grounding lines. *Science*, **296**, 2020–2023.

Ritz, C., V. Rommelaere, and C. Dumas, 2001: Modeling the evolution of antarctic ice sheet over the last 420,000 years: Implications for altitude changes in the vostok region. *Journal of Geophysical Research: Atmospheres (1984–2012)*, **106**, 31943–31964.

Rohling, E. J., K. Grant, M. Bolshaw, A. Roberts, M. Siddall, C. Hemleben, and M. Kucera, 2009: Antarctic temperature and global sea level closely coupled over the past five glacial cycles. *Nature Geoscience*, **2**, 500–504.

Rooth, C., 1982: Hydrology and ocean circulation. *Progress in Oceanography*, **11**, 131–149.

Sachs, J. and S. Lehman, 1999: Subtropical North Atlantic Temperatures 60,000 to 30,000 Years Ago. *Science*, **286**, 756–759.

Salgueiro, E., A. Voelker, L. De Abreu, F. Abrantes, H. Meggers, and G. Wefer, 2010: Temperature and productivity changes off the western iberian margin during the last 150 ky. *Quaternary Science Reviews*, **29**, 680–695.

Sarnthein, M., K. Winn, S. Jung, J. Duplessy, L. Labeyrie, H. Erlenkeuser, and G. Ganssen, 1994: Changes in east Atlantic deepwater circulation over the last 30,000 years: Eight time slice reconstructions. *Paleoceanography*, **9**, 209–267.

Schewe, J. and A. Levermann, 2010: The role of meridional density differences for a wind-driven overturning circulation. *Clim. Dyn.*, **34**, 547–556, doi:10.1007/s00382-009-0572-1.

Schilt, A., M. Baumgartner, J. Schwander, D. Buiron, E. Capron, J. Chappellaz, L. Loulergue, S. Schupbach, R. Spahni, H. Fischer, and T. Stocker, 2010: Atmospheric nitrous oxide during the last 140,000 years. *Earth and Planetary Science Letters*, **300**, 33–43, doi:10.1016/j.epsl.2010.09.027.

Schmittner, A., O. Saenko, and A. Weaver, 2003: Coupling of the hemispheres in observations and simulations of glacial climate change. *Quaternary Science Reviews*, **22**, 659–671.

Schulz, H., U. von Rad, and H. Erlenkeuser, 1998: Correlation between arabian sea and greenland climate oscillations of the past 110,000 years. *Nature*, **393**, 54.

Schulz, M., 2002: On the 1470-year pacing of dansgaard-oeschger warm events. *Paleoceanography*, **17**, 4–1.

Scourse, J. D., A. I. Haapaniemi, E. Colmenero-Hidalgo, V. L. Peck, I. R. Hall, W. E. Austin, P. C. Knutz, and R. Zahn, 2009: Growth, dynamics and deglaciation of the last british–irish ice sheet: the deep-sea ice-rafted detritus record. *Quaternary Science Reviews*, **28**, 3066–3084.

Scourse, J. D., I. R. Hall, I. N. McCave, J. R. Young, and C. Sugdon, 2000: The origin of heinrich layers: evidence from h2 for european precursor events. *Earth and Planetary Science Letters*, **182**, 187–195.

Seager, R. and D. S. Battisti, 2006: *Global Circulation of the Atmosphere*, Princeton University Press., chapter Challenges to our understanding of the general circulation: abrupt climate change, in press.

Seager, R., D. S. Battisti, J. Yin, N. Gordon, N. Naik, A. C. Clement, and M. A. Cane, 2002: Is the gulf stream responsible for europe's mild winters? *Quarterly Journal of the Royal Meteorological Society*, **128**, 2563–2586.

Shackleton, N. J., M. A. Hall, and E. Vincent, 2000: Phase relationships between millennial-scale events 64,000–24,000 years ago. *Paleoceanography*, **15**, 565–569.

Shapiro, N. M. and M. H. Ritzwoller, 2004: Inferring surface heat flux distributions guided by a global seismic model: particular application to antarctica. *Earth and Planetary Science Letters*, **223**, 213–224.

Shepherd, A., D. Wingham, and E. Rignot, 2004: Warm ocean is eroding west antarctic ice sheet. *Geophysical Research Letters*, **31**.

Siegenthaler, U., E. Monnin, K. Kawamura, R. Spahni, J. Schwander, B. Stauffer, T. F. Stocker, J.-M. Barnola, and H. Fischer, 2005: Supporting evidence from the epica dronning maud land ice core for atmospheric $co_2$ changes during the past millennium. *Tellus B: Chemical and Physical Meteorology*, **57**, 51–57.

Siegert, M. J. and J. A. Dowdeswell, 2004: Numerical reconstructions of the eurasian ice sheet and climate during the late weichselian. *Quaternary Science Reviews*, **23**, 1273–1283.

Skinner, L. and H. Elderfield, 2007: Rapid fluctuations in the deep north atlantic heat budget during the last glacial period. *Paleoceanography*, **22**.

Steffensen, J., K. Andersen, M. Bigler, H. Clausen, D. Dahl-Jensen, H. Fischer, K. Goto-Azuma, M. Hansson, S. Johnsen, J. Jouzel, V. Masson-Delmotte, T. Popp, S. Rasmussen, R. Rthlisberger, U. Ruth, B. Stauffer, M. Siggaard-Andersen, A. Sveinbjrnsdóttir, A. Svensson, and J. White, 2008: High-Resolution Greenland Ice Core Data Show Abrupt Climate Change Happens in Few Years. *Science*, **321**, 680–684, doi: 10.1126/science.1157707.

Stenni, B., D. Buiron, M. Frezzotti, S. Albani, C. Barbante, E. Bard, J. Barnola, M. Baroni, M. Baumgartner, M. Bonazza, et al., 2011: Expression of the bipolar see-saw in antarctic climate records during the last deglaciation. *Nature Geoscience*, **4**, 46.

Stocker, T. F., 1998: The Seesaw Effect. *Science*, **282**, 61–62, doi:10.1126/science.282.5386.61.

Stocker, T. F., 2003: South dials north. *Nature*, **424**, 496–499, doi:10.1038/424496a.

Stocker, T. F. and S. Johnsen, 2003: A minimum thermodynamic model for the bipolar seesaw. *Paleoceanography*, **18**, PA1087, doi:10.1029/2003PA000920.

Stocker, T. F. and O. Marchal, 2000: Abrupt climate change in the computer: Is it real? *Proceedings of the National Academy of Sciences of the United States of America*, **97**, 1362, doi: 10.1073/pnas.97.4.1362.

Stommel, H., 1961: Thermohaline convection with two stable regimes of flow. *Tellus*, **13**, 224–230, doi:10.1111/j.2153-3490.1961.tb00079.x.

Stott, L., C. Poulsen, S. Lund, and R. Thunell, 2002: Super enso and global climate oscillations at millennial time scales. *Science*, **297**, 222–226.

Stouffer, R. J., J. Yin, J. M. Gregory, K. W. Dixon, M. J. Spelman, W. Hurlin, A. J. Weaver, M. Eby, G. M. Flato, H. Hasumi, A. Hu, J. H. Jungclaus, I. V. Kamenkovich, A. Levermann, M. Montoya, S. Murakami, S. Nawrath, A. Oka, W. R. Peltier, D. Y. Robitaille, A. P. Sokolov, G. Vettoretti, and S. L. Weber, 2006: Investigating the causes of the response of the thermohaline circulation to past and future climate changes. *J. Clim.*, **19**, 1365–1387.

Svendsen, J. I., H. Alexanderson, V. I. Astakhov, I. Demidov, J. A. Dowdeswell, S. Funder, V. Gataullin, M. Henriksen, C. Hjort, M. Houmark-Nielsen, et al., 2004: Late quaternary ice sheet history of northern eurasia. *Quaternary Science Reviews*, **23**, 1229–1271.

Talley, L. D., 2013: Closure of the global overturning circulation through the indian, pacific, and southern oceans: Schematics and transports. *Oceanography*, **26**, 80–97.

Tarasov, L., A. S. Dyke, R. M. Neal, and W. R. Peltier, 2012: A data-calibrated distribution of deglacial chronologies for the north american ice complex from glaciological modeling. *Earth and Planetary Science Letters*, **315**, 30–40.

Timmermann, A., S. Lorenz, S. An, A. Clement, and S. Xie, 2007: The effect of orbital forcing on the mean climate and variability of the tropical pacific. *Journal of Climate*, **20**, 4147–4159, doi: 10.1175/JCLI4240.1.

Toggweiler, J. R., 2009: Shifting westerlies. *Science*, **323**, 1434–1435, doi:10.1126/science.1169823.

Toggweiler, J. R. and D. Lea, 2010: Temperature differences between the hemispheres and ice age climate variability. *Paleoceanography*, **25**, PA2212, doi:10.1029/2009PA001758.

Toggweiler, J. R., J. L. Russell, and S. Carson, 2006: Midlatitude westerlies, atmospheric $CO_2$, and climate change during the ice ages. *Paleoceanography*, **21**, PA2005, doi:10.1029/2005PA001154.

Toggweiler, J. R. and B. Samuels, 1995a: Effect of Drake Passage on the global thermohaline circulation. *Deep-Sea Research*, **42**, 477–500, doi:10.1016/0967–0637(95)00012–U.

Toggweiler, J. R. and B. Samuels, 1995b: Effect of sea ice on the salinity of Antarctic Bottom Water. *J. Phys. Oceanogr.*, **25**, 1980–1997.

Toucanne, S., G. Soulet, N. Freslon, R. S. Jacinto, B. Dennielou, S. Zaragosi, F. Eynaud, J.-F. Bourillet, and G. Bayon, 2015: Millennial-scale fluctuations of the european ice sheet at the end of the last glacial, and their potential impact on global climate. *Quaternary Science Reviews*, **123**, 113–133.

Trenberth, K., J. Olson, and W. Large, 1989: A global ocean wind stress climatology based on ECMWF analyses. Tech. Rep. NCAR/TN-338+STR, National Center for Atmospheric Research, Boulder, Colorado, USA.

Trenberth, K. E. and J. M. Caron, 2001: Estimates of meridional atmosphere and ocean heat transport. *Clim. Dyn.*, **14**, 3433–3443.

Trenberth, K. E. and J. T. Fasullo, 2018: Applications of an updated atmospheric energetics formulation. *Journal of Climate*.

Tschumi, T., F. Joos, and P. Parekh, 2008: How important are southern hemisphere wind changes for low glacial carbon dioxide? a model study. *Paleoceanography*, **23**, PA4208, doi:10.1029/2008PA001592.

Valdes, P., 2011: Built for stability. *Nature Geoscience*, **4**, 414–416, doi:10.1038/ngeo1200.

Vellinga, M. and R. A. Wood, 2002: Global climatic impacts of a collapse of the Atlantic thermohaline circulation. *Climatic Change*, **54**, 251–267, doi:10.1023/A:1016168827653.

Vettoretti, G. and W. R. Peltier, 2016: Thermohaline instability and the formation of glacial north atlantic super polynyas at the onset of dansgaard-oeschger warming events. *Geophysical Research Letters*, **43**, 5336–5344, doi:10.1002/2016GL068891.

Vettoretti, G. and W. R. Peltier, 2018: Fast physics and slow physics in the nonlinear dansgaardoeschger relaxation oscillation. *Journal of Climate*, **31**, 3423–3449, doi:10.1175/JCLI-D-17-0559.1.

Vinther, B. M., S. L. Buchardt, H. B. Clausen, D. Dahl-Jensen, S. J. Johnsen, D. Fisher, R. Koerner, D. Raynaud, V. Lipenkov, K. Andersen, et al., 2009: Holocene thinning of the greenland ice sheet. *Nature*, **461**, 385–388.

Voelker, A. and Workshop Participants, 2002: Global distribution of centennial-scale records for marine isotope stage (MIS) 3: a database. *Quaternary Science Reviews*, **21**, 1185–1212, doi:10.1016/S0277–3791(01)00139–1.

Waelbroeck, C., L. Labeyrie, E. Michel, J. C. Duplessy, J. McManus, K. Lambeck, E. Balbon, and M. Labracherie, 2002: Sea-level and deep water temperature changes derived from benthic foraminifera isotopic records. *Quaternary Science Reviews*, **21**, 295–305.

WAIS Divide Project Members, 2015: Precise interpolar phasing of abrupt climate change during the last ice age. *Nature*, **520**, 661–665.

Wang, X., A. Auler, R. Edwards, H. Cheng, E. Ito, Y. Wang, X. Kong, and M. Solheid, 2007: Millennial-scale precipitation changes in southern Brazil over the past 90,000 years. *Geophys. Res. Lett.*, **34**, L23701, doi:10.1029/2007GL031149.

Wang, Y., H. Cheng, R. Edwards, Z. An, J. Wu, C. Shen, and J. Dorale, 2001: A high-resolution absolute-dated late Pleistocene monsoon record from Hulu Cave, China. *Science*, **294**, 2345, doi:10.1126/science.1064618.

Watanabe, O., J. Jouzel, S. Johnsen, F. Parrenin, H. Shoji, and N. Yoshida, 2003: Homogeneous climate variability across east antarctica over the past three glacial cycles. *Nature*, **422**, 509.

Watson, A. J., J. R. Ledwell, M.-J. Messias, B. A. King, N. Mackay, M. P. Meredith, B. Mills, and A. C. N. Garabato, 2013: Rapid cross-density ocean mixing at mid-depths in the Drake Passage measured by tracer release. *Nature*, **501**, 408–411, doi:10.1038/nature12432.

Watson, A. J. and A. C. Naveira Garabato, 2006: The role of Southern Ocean mixing and upwelling in glacial-interglacial atmospheric $CO_2$ change. *Tellus B*, **58**, 73–87, doi:10.1111/j.1600-0889.2005.00167.x.

Weaver, A. J., M. Eby, M. Kienast, and O. A. Saenko, 2007: Response of the atlantic meridional overturning circulation to increasing atmospheric co 2: Sensitivity to mean climate state. *Geophys. Res. Lett.*, **34**, L05708, doi:10.1029/2006GL028756.

Weaver, A. J., O. A. Saenko, P. U. Clark, and J. X. Mitrovica, 2003: Meltwater pulse 1A from Antarctica as a Trigger of the Bølling-Allerød Warm Interval. *Science*, **299**, 1709–1713, doi:10.1126/science.1081002.

Wilson, N., F. Straneo, and P. Heimbach, 2017: Satellite-derived submarine melt rates and mass balance (2011–2015) for greenland's largest remaining ice tongues. *The Cryosphere*, **11**, 2773.

Wohlfarth, B., 2010: Ice-free conditions in sweden during marine oxygen isotope stage 3? *Boreas*, **39**, 377–398.

Yamamoto, A., J. B. Palter, M. S. Lozier, M. S. Bourqui, and S. J. Leadbetter, 2015: Ocean versus atmosphere control on western european wintertime temperature variability. *Climate dynamics*, **45**, 3593–3607.

Yokoyama, Y., K. Lambeck, P. De Deckker, P. Johnston, and L. K. Fifield, 2000: Timing of the last glacial maximum from observed sea-level minima. *Nature*, **406**, 713–716.

Zhang, X., G. Knorr, G. Lohmann, and S. Barker, 2017: Abrupt north atlantic circulation changes in response to gradual $co_2$ forcing in a glacial climate state. *Nature Geoscience*, **10**, 518.

Zhang, X., G. Lohmann, G. Knorr, and C. Purcell, 2014: Abrupt glacial climate shifts controlled by ice sheet changes. *Nature*, **512**, 290–294.

Zweck, C. and P. Huybrechts, 2005: Modeling of the northern hemisphere ice sheets during the last glacial cycle and glaciological sensitivity. *Journal of Geophysical Research: Atmospheres*, **110**.